THE KINETICS OF SILICA REDUCTION

THE KINETICS OF SILICA REDUCTION
BY CARBON-SATURATED IRON

by

SUDHIR KUMAR SHARMA, B.Sc.,B.Tech.

A Thesis
Submitted to the Faculty of Graduate Studies
in Partial Fulfilment of the Requirements
for the Degree
Master of Engineering

McMaster University
April 1965

MASTER OF ENGINEERING (1965)
(Metallurgical Engineering)

McMASTER UNIVERSITY
Hamilton, Ontario

TITLE: The Kinetics of Silica Reduction by Carbon Saturated Iron

AUTHOR: Sudhir Kumar Sharma B.Sc. (Agra University)
B.Tech.(Indian Institute of Technology, Bombay)

SUPERVISOR: Professor R. G. Ward

NUMBER OF PAGES (vii), 122

Scope and Contents

In this thesis an attempt has been made to resolve the existing ambiguity regarding the nature of silica reduction reaction, that is, to determine whether the reaction is chemically controlled or transport controlled. A review of the research work on the kinetics of silica reduction has been presented, leading to a postulated reaction mechanism. The experiments were performed in a critically designed apparatus in which the reduction of solid silica by carbon-saturated iron was studied in the temperature range of 1300 to 1600°C. The rate of evolution of carbon monoxide due to the reaction was measured. The results are in accord with a transport control mechanism in which the diffusion of oxygen in the iron was assumed to be the rate limiting factor.

ACKNOWLEDGEMENTS

The author is greatly indebted to his research supervisor, Dr. R. G. Ward for suggesting the problem and for his continuing guidance and encouragement throughout the course of the work.

In addition, the author would like to thank Dr. A. McLean and Dr. L. A. Baker for their keen interest in the research and helpful and stimulating discussions, and Mr. H. Neumeyer for help with the chemical analyses.

Thanks are also due to the graduate students of the Metallurgical Engineering Department for their assistance on many aspects of the problem.

The financial assistance of American Iron & Steel Institute (in form of grant-in-aid to Dr. R. G. Ward) and the award of a University Scholarship to the author is gratefully acknowledged.

TABLE OF CONTENTS

TABLE OF TABLES

TABLE OF FIGURES

CHAPTER I

INTRODUCTION

1.1 The Kinetic Approach

The principles of thermodynamics and chemical kinetics are the tools which are used in the analysis of a process or a reaction. The knowledge of pertinent thermodynamic properties is indispensible, not only for defining the equilibrium state of the reaction, but also for determining the necessary driving force required to attain equilibrium. In defining the equilibrium state of a reaction by thermodynamic principles, it is not required to have the knowledge of the mechanism of the process. Thus thermodynamics neither gives an insight into the mechanism of the process nor does it tell about the conditions which are likely to govern the rate of the process. However, in a kinetic analysis, a knowledge of detailed reaction mechanism is necessary in order to identify the factors which could control the reaction rates. Thus the kinetic approach gives a detailed picture of the nature of the process.

In most of the metallurgical systems of interest, the reactions taking place are heterogeneous in nature. Heterogeneous reactions, generally occurring at a surface or at a phase-boundary of the two different phases, involve several steps in sequence. The methods of chemical kinetics consist in isolating and identifying the slowest step, the rate of which is essentially the rate of overall reaction.

In steelmaking systems, the temperatures are high enough so that chemical reaction within a phase is not likely to be the controlling step. In such a case transport of the chemical species to and from the reaction site i.e. phase boundary, may become the controlling factor. Consequently the transport of one of the components to and from the phase boundary may be the rate determining step. Darken's[5] concept of "local equilibrium" and Wagner's[6] principle of "virtual maximum rate" have been successfully employed in this type of analysis.

Before starting a kinetic investigation it is necessary to have accurate knowledge of the thermodynamic and thermochemical properties of the system concerned. This is essential for calculating the quantities like driving force of a reaction or the interfacial equilibrium contents of various components or so forth. Inaccuracies in these data may lead to wrong interpretation of kinetic results.

1.2 Silica-Reduction Reaction

The reduction of silica by carbon in blast-furnace slag metal system is described by the following overall reaction*

$$SiO_{2\,(slag)} + 2C_{(gr)} = \underline{Si} + 2CO_{(g)} \qquad (1)$$

The thermodynamics of this reaction has been studied to greater extent

---

* The subscripts in parentheses (slag), (gr) and (g) indicate components in slag, graphite and gas phases respectively. The underlined symbol refers to the species dissolved in liquid iron.

under laboratory conditions. As is well known, the reaction (1) is notoriously slow and at 1600°C, the reduction of silica may not proceed half-way to equilibrium in eight hours.[13]

Fulton and Chipman[14] first attempted to investigate the kinetics of the silica reduction. The slow rate of the reaction and a high activation energy of about 130kcal per mole, led them to believe that the silica reduction was chemically controlled, the slow step being in the breaking of Si-O bonds. In a written discussion on this paper of Fulton and Chipman, Schuhmann[19] indicated that observed slowness of the reaction could be due to the transport of oxygen across a boundary layer in the liquid metal. Some of the recent work by Turkdogan et al,[20] Rawling and Elliott[21], Simkovich and co-authors[24], indicate the possibility of transport control for silica reduction. The first two authors explain their results on the basis of oxygen diffusion control. But Simkovich et al assumed the transport of silicon in the metal as the slow step, though the results are not in good agreement with the theoretical predictions. Grimble, Ward and Williams[23] have shown that at least 50% of the silicon in the reaction (1) taking place in graphite crucibles is reduced electrochemically.

Thus there seem to be diverse opinions about the mechanism of the silica reduction reaction.

1.3 The Scope of Present Work

As the silica reduction reaction is of considerable importance in iron and steel industry, it was decided to investigate the reaction in order to find the nature of controlling mechanism. The experiments have been limited to the reduction of pure solid silica by carbon-saturated iron. The possibility of electrochemical transfer has been eliminated by the use of non-conducting silica crucibles. A reaction mechanism has been postulated and the diffusion of oxygen has been regarded the slow step in the overall reaction. The good agreement between the experimental activation energy and theoretically calculated one, seems to suggest that silica reduction is controlled by the transport of oxygen in the metal.

CHAPTER II

THEORETICAL CONSIDERATIONS

2.1 Theories of Rate Process

As early as 1889, Arrhenius[1], while studying the inversion of cane sugar in the presence of acids, found the influence of temperature on the rate of the reaction. He proposed the relationship between the reaction rate constant, k, and the temperature in the form of equation (2)

$$\ln k = \ln A - \frac{E}{RT} \qquad (2)$$

where E is the heat or energy of activation and A is a constant, called collision number or frequency factor and both are practically independent of the temperature. This relationship, better known as the Arrhenius equation could be written in the more familiar form

$$k = A \exp\left(-\frac{E}{RT}\right) \qquad (3)$$

Arrhenius suggested an existence of equilibrium between passive and active molecules, only the latter ones taking part in the reaction. The Arrhenius equation, for most of the chemical processes very well represents the dependence of the specific rate constant on the temperature.

The activation energy, E, in the Arrhenius equation, represents the energy required by the molecules in initial state to take part in the reaction. The fraction $\exp\left(-\frac{E}{RT}\right)$ is proportional to the number of molecules possessing energy E, in excess of the initial energy. Thus the number of molecules reacting per unit time is proportional to the number of molecules in the activated state.

The concept of activation energy is best illustrated by a energy vs reaction coordinate plot[4]. In Figure 1 the energies of the reactants, products and activated states are shown. Though the final energy of the products is lower than that of reactants, an activation energy is required to surmount the peak or energy barrier in the curve. Only the molecules of reactants possessing an excess energy E would react to form the products.

The factor A represents the number of collisions between the reacting molecules and hence the name "collision theory". Eyring and co-workers[2] showed that at least for bimolecular gaseous reactions A is equal to the number of collisions Z, between the reacting molecules. To explain some of the slower reactions, which were expected to be faster according to the simple collision theory, a probability factor P was introduced and the equation (3) was modified to

$$k = P\,Z \exp\left(-\frac{E}{RT}\right) \qquad (4)$$

The factor P represented the deviation from the ideal behaviour of the simple collision theory.

Application of the collision theory to reversible reactions exposed its weakness. This required inclusion of an entropy term in the factor P which is not explicitly indicated by the collision theory.[2]

The theory of "absolute reaction rates" proposed and developed by Polanyi[3] and Eyring and co-workers[2] could more satisfactorily account for A and E, than the collision theory. This theory also known as "activated complex" theory has been successfully applied by Eyring et al[2] to many rate processes viz, chemical reactions, diffusion, viscous flow, etc.

The theory supposes formation of an "activated complex" from the reactants at the peak in the Figure 1. The activated complex is regarded as an ordinary molecule having all the thermodynamic properties and is in equilibrium with reactants. But the activated complex must lead to the formation of products only. On this basis Eyring et al[2] showed that the absolute reaction rate constant is given by

$$k = \frac{k'T}{h} \exp\left(\frac{\Delta S^{\ddagger}}{R}\right) \exp\left(-\frac{\Delta H^{\ddagger}}{RT}\right) \qquad (5)$$

where k' is Boltzmann constant, h is Planck's, and $\Delta S^{\ddagger}$ and $\Delta H^{\ddagger}$ are entropy and enthalpy change for the formation of activated complex. This rate constant given by equation (5) has a better explanation for A than given by equation (3).

These theories seek to explain the observed reaction rates theoretically. However, the reaction rate theory cannot be applied indiscriminately to the overall reaction. The overall reaction might consist of several steps in sequence. A step which is slowest of all, can be isolated and considered responsible for the slow rate of overall reaction[4].

2.2 General Rate Equation

Classical kinetic theory had been mainly concerned with the homogeneous reactions taking place in a single phase, either a gas or a liquid. The slag-metal reactions are in a sense heterogeneous because the reactants come from different phases and react at a common phase boundary. However the principles used in analyzing the phase boundary reactions are the same as those used for homogeneous reactions. The driving force for the overall reaction is the difference in free energies between the final and initial states.

Consider the reaction

$$A + B = C + D \qquad (6)$$

The rate of forward reaction will be proportional to the activities of A and B. Assuming the reversibility of the reaction, the rate of reverse reaction will be proportional to the activities of C and D.

Hence the rate, $\dot{n}$ (moles per sec.), of the overall reaction will be given by

$$\dot{n} = k_1 a_A a_B - k_2 a_C a_D \qquad (7)$$

If the activity coefficients are constant, we can replace the activities by concentration terms. Hence,

$$\dot{n} = k_1' C_A C_B - k_2' C_C C_D \qquad (8)$$

At equilibrium the two rates are equal but opposite so that

$$\frac{k_1'}{k_2'} = K = \frac{C_C^{eq.} \cdot C_D^{eq.}}{C_A^{eq.} \cdot C_B^{eq.}} \qquad (9)$$

where K is the equilibrium constant for the overall reaction and $C^{eq.}$ represents the concentrations at the equilibrium.

Eliminating k'_2 in the equation (3) and writing Q for $\frac{C_C C_D}{C_A C_B}$, the rate is given by

$$\dot{n} = k'_1 C_A C_B \left(1 - \frac{Q}{K}\right) \qquad (10)$$

where Q is called activity or concentration quotient. When the system is considerably displaced from equilibrium $\frac{Q}{K} \ll 1$ and hence could be neglected in the equation (10). The equation (10) thus reduces to

$$\dot{n} \approx k'_1 C_A C_B. \qquad (11)$$

In the above treatment it has been assumed that the activity coefficients do not vary over a concentration range. Thus the rate constants k'_1 and k'_2 derived from the measurements of concentration will not be exact unless the activity coefficient terms are included in above equations.

2.3 Reaction Path and Rate Determining Step in Slag-Metal Reaction

In general the path followed by a slag-metal reaction may consist of series of consecutive steps such as follows.

(1) Transport of reactants from bulk phases to the slag-metal interface

(2) Adsorption of the reactants on the interface

(3) Reaction at the interface

(4) Desorption of the products

(5) Transport of the desorbed products from the interface to the bulk phases.

The steps (1) and (5) involve diffusion and (2) to (4) may be regarded as the reaction process. Though these steps must take place consecutively, it is possible that one of them is considerably slower than others and consequently determines the rate of overall reaction. Wagner[6] thus defines the virtual maximum rate of the reaction as the rate which would be observed if all the preceding and succeeding steps were in equilibrium. Consequently it is assumed that all the steps except the slow one, are in a state of local equilibrium.[5]

Wagner[6] pointed two limiting cases:

(a) Transport Control: -- Equilibrium is attained at the interface and hence the rate of the process is determined by the diffusion of one or more reactants to and from the interface.

(b) Chemical Reactions Control: -- Difference between the concentration at the interface and the bulk phases are insignificant and hence the rate of the process is controlled by the rate of the interface reaction.

These two cases are diagrammatically represented by Figures 2(a) and (b). The two cases are briefly discussed here.

(a) Transport Control: -- The transport of the chemical species in a reaction to and from the slag-metal interface is not only effected by the molecular diffusion but also by convection due to the fluid motion. The flux $j_i \left(\frac{\text{moles}}{\text{cm}^2\ \text{sec.}}\right)$ of a certain species i in the liquid phase in x-direction is given by

$$j_i = \frac{\dot{n}_i}{A} = -D_i\left(\frac{\partial C_i}{\partial x}\right) + C_i U_x \tag{12}$$

where $\dot{n}_i$ is the rate of transfer of 'i' in moles.sec^{-1}, A is the interface area in cm^2, D_i is the diffusivity in cm^{2}sec^{-1}, C_i is the concentration in moles.cm^{-3} and U_x is the resolved flow velocity in the x-direction. The first term in equation (12) is obtained by Fick's first law for molecular diffusion across a plane and the second term accounts for the transport by the fluid motion.

The concentration gradient is mostly significant near the interface in a boundary layer through which diffusion occurs. The thickness of the boundary layer could be calculated from mass transfer principles for a simpler case like the flow of liquid along a flat wall where the flow conditions are known[7]. Wagner[6] defines an effective boundary layer thickness as the value which would result in the same flux of the species if the molecular diffusion were the only process operating.

The thickness is given by the equation (13)

$$\delta_i = \frac{C_i - C_i^*}{(\partial C_i/\partial x)_{x=0}} \tag{13}$$

where C_i^* and C_i are the concentrations of the species 'i' at the interface and in the bulk respectively. Since $U_x = 0$ at $x = 0$, the rate of transfer of 'i' is obtained by combining the equations (12) and (13).

Thus

$$\frac{\dot{n}_i}{A} = \frac{D_i}{\delta_i}(C_i^* - C_i) \tag{14}$$

The ratio D/δ has the units of cm.sec^{-1} and is called the diffusion or transport rate constant.

The experimental activation energy for transport controlled processes is generally low[33]. In the equation (14), the temperature dependent terms are D, δ and C_i^* and all of these contribute to the temperature coefficient of the observed rate constant.

In addition, if the activity coefficients are not unity, these would also appear in equation (14) and would affect the experimental activation energy. A theoretical calculation of the activation energy is possible if the temperature dependence of various terms is known. Riddiford[9] has shown that 'δ' also varies exponentially with temperature as does D. Hence the ratio D/δ has an exponential temperature dependence.

Examples of transport controlled processes are afforded by the work of Parlee, Seagle and Schuhmann[10] and Pehlke and Elliott[11]. The former studied the rates of evolution and absorption of CO from low carbon iron melts contained in an alumina crucible. It was concluded that the rates were controlled by the diffusion of oxygen through a boundary layer in the iron. Pehlke and Elliott studied the kinetics of nitrogen absorption and desorption in liquid iron. In the absence of oxygen (<0.01%), the rates were thought to be controlled by transport in the metal boundary layer. The presence of oxygen (< 0.04%) caused mixed control.

(b) Chemical Reaction Control

For the processes controlled by a chemical reaction at the interface the rate is given by the type of equation (10) in Section 2.2. Eyring[8] has discussed in great details many chemically controlled, homogeneous and heterogeneous reactions. However, for the heterogeneous reactions, the reaction rates are considerably affected by interface structure. Adsorption of reactants and desorption of products may be rate limiting, if the surface reaction is rapid enough. Generally it is believed that in steel making systems, for most of the reactions, the chemistry cannot be rate controlling[12]. This inference is based on the fact that the rates calculated on the basis of absolute reaction rate theory are faster than the observed rates and the values of the experimental activation energies are lower than that expected for chemically controlled reactions. Richardson[12] in a theoretical analysis of the results of Fulton and Chipman's[14] work on silica reduction from blast furnace type slags, found that theoretical (reaction control) and experimental rates were comparable (of the order of 10^{-6} gm. mole. cm^{-2}. sec^{-1}). In this extreme case chemistry might be rate controlling. Philbrook and Kirkbride[15] measured the rate of FeO reduction by carbon saturated iron. Comparing this experimental rate of 10^{-6} gm. mole. $cm.^{-2}$ $sec.^{-1}$ at 0.03 mole fraction of FeO, with his theoretical rate of 10^{3} gm. mole. $cm.^{-2}$ $sec.^{-1}$, Richardson[12] concluded that FeO reduction must be transport controlled. Wagner[6] explained the same results of Philbrook and Kirkbride[15] assuming the diffusion of iron ions across a boundary layer in the slag as the rate controlling step.

Apart from the two rate controlling processes (transport control and chemical control) discussed above, the nucleation and growth of a new phase may also affect the rate.[4] The formation of CO bubbles in the open hearth is an example of a nucleation and growth process. Homogeneous nucleation of CO bubbles in the steel requires a high degree of supersaturation. Körber and Oelsen[17] found that under laboratory conditions bubble formation in steel did not occur until the degree of supersaturation was more than 10 atm. Darken[5] has discussed the nucleation of CO bubbles with reference to Brower and Larsen's[16] observation. He believes that since homogeneous nucleation of CO bubbles will be extremely difficult in view of high degree of supersaturation required in the bath, the bubbles must be nucleated in the crevices of the open hearth where already a thin film of gas exists. These subsequently grow by the diffusion of carbon and oxygen from the metal to them.

It has been shown[6,18,33] that the slag-metal interfacial area and the effective boundary layer thickness are influenced by the gas evolution. Higher rates of gas evolution tend to decrease the diffusion thickness and increase the interfacial area. This would result in an increase in the apparent order of reaction.[5,6]

2.4 Slag-Metal Reactions

Kinetics of different slag-metal reactions have been studied by various authors. The slag-metal reactions in general involve simultaneous transfer of elements across the interface with or without evolution of carbon monoxide. The experimental data have been explained on the basis of the theories already discussed in earlier sections of this chapter.

One of the important reactions in slag-metal systems is the reduction of silica from the slag by carbon-saturated iron in the blast-furnace hearth. This reaction in the laboratory has been studied by reacting blast furnace type slags with carbon-saturated iron contained in a graphite crucible.[14,20,21,26] In some cases solid silica has also been used.[24,25]

Fulton and Chipman[14] first studied the kinetics of silica reduction. They reacted a slag of the composition 45% SiO_2, 38% CaO, 17% Al_2O_3 with carbon-saturated iron in atmosphere of carbon monoxide. The slag and metal were stirred in a manner such that the slag metal interface remained mostly undisturbed. They treated the rate data assuming the following overall reaction

$$SiO_{2(slag)} + 2C_{(gr)} = \underline{Si} + 2CO_{(g)} \qquad (15)$$

The effect of stirring on the rate was only slight and bubbling of CO through the metal did not affect the rate of silicon transfer. The reaction (15) was believed to be chemically controlled on the basis of high activation energy of 130 kcal per mole and the slow rate of transfer, of order of 10^{-6} gm. moles. $cm.^{-2}$ $sec.^{-1}$.

Schuhmann[19], in a written discussion of the above paper, pointed out the possibility of transport control. The reaction mechanism for silica reduction, suggested by Schuhmann, was analogous to that for alumina reduction from the work of Parlee et al[10].

The overall reaction is supposed to take place in the following steps:

(I) Decomposition of silica at the slag-metal interface according to equation (16)

$$SiO_{2(slag)} = \underline{Si} + 2\underline{O} \qquad (16)$$

(II) Transport of oxygen from the slag-metal interface to gas metal interface by

(a) diffusion across metal boundary layer at slag-metal interface,

(b) convection within the liquid metal,

(c) diffusion across the boundary layer at metal-gas interface

(III) Reaction of carbon and oxygen at gas-metal interface

$$\underline{C} + \underline{O} = CO_{(g)} \qquad (17)$$

(IV) Dissolution of carbon at graphite-metal interface

$$C_{(gr)} = \underline{C} \qquad (18)$$

On the basis of oxygen transport as the rate limiting step, Schuhmann[19] calculated the rate using equation (19)

$$\frac{dn_{SiO_2}}{dt} = \frac{1}{2} \frac{A\ D_o}{\delta_o} (C_o^* - C_o) \qquad (19)$$

This equation predicted a rate of 0.002% to 0.2% Si per hr. compared to the observed rate of approximately 0.03% Si per hr. Thus the theoretical estimate seems consistent with the experimental results of Fulton and Chipman[14].

Turkdogan et al[20] studied the kinetics of silica reduction from CaO-SiO_2 and BaO-CaO-SiO_2 slags. In these experiments, 5 gm. of metal was held in a graphite holder, which was immersed in a large slag bath. Both the metal and slag were heated separately and at the required temperature of 1600°C, were brought into contact. The experimental set up was such as to allow bubbling of carbon monoxide at one atmosphere pressure at the slag-metal interface. The results were interpreted on the basis of interfacial reaction as the rate controlling step. The following is the reaction mechanism proposed by Turkdogan et al[20]:

(1) Adsorption of silica at slag-metal interface

$$SiO_{2(slag)} + \square \rightleftharpoons \square_{SiO_2} \qquad (20)$$

where $\square$ and $\square_{SiO_2}$ are the vacant and occupied sites at the interface.

(2) Since the silicon potential of the slag is higher than that of metal, silica adsorbed at the interface is disorbed into the metal by dissociating into silicon and oxygen which then dissolve in the metal, thus

$$\square_{SiO_2} = \underline{Si} + 2\underline{O} + \square \qquad (21)$$

(3) Diffusion of Silicon and oxygen into the bulk of metal.

(4) Reaction of carbon and oxygen at gas-metal interface

$$\underline{C} + \underline{O} = CO_{(g)} \qquad (22)$$

In some of their experiments a lower rate of silicon transfer was observed even with similar experimental conditions as in others.

The authors believe that for these experiments the transport of oxygen from slag-metal interface through a boundary layer in the metal could be rate controlling. Though this interpretation for slow transfer of silicon in the metal is in keeping with Schuhmann's[19] explanation of Fulton and Chipman's[14] results, the thickness of the effective boundary layer estimated is very small, of the order of 0.0005 cm.

Rawling and Elliott[21] investigated the silicon transfer from blast furnace type slags in an experimental system, not different from that of Fulton and Chipman[14]. The investigation was carried out with two types of experiments. In one, the only reducing agent present was graphite and the overall reaction was described by equation (15). In the secondtype of experiments graphite saturated ferrosilicon-iron concentrations cells were set up so that the reduction of silica in slag could occur as described by the equation (15) or by a reaction of electrochemical nature.

From the results of first type of experiments, it was concluded that diffusion of oxygen in the metal could be rate determining. These results are in agreement with those of Turkdogan et al[20].

The results from the second type of experiment showed no or little change of silica concentration in the slag. At the same time the silicon concentration of iron increased while that of ferrosilicon decreased correspondingly. Since no CO bubbles were observed bursting at the slag-gas interface, it was concluded that the transfer of silicon occurred by the following electrochemical reaction in which no CO evolution is necessary.

$$Si(Fe\text{-}Si) = Si^{4+} + 4e \quad (23)$$

$$Si^{4+}_{(slag)} + 4e = Si(Fe) \quad (24)$$

Grimble, Ward and Williams[23] studied the electrochemical nature of silicon transfer. The overall silica reduction reaction could take place in the following steps:

An anodic reaction occurring at slag-graphite interface

$$2C + 2(O^{2-}) - 4e = 2CO_{(g)} \quad (25)$$

and a cathodic reaction at the slag-metal interface

$$Si^{4+} + 4e = \underline{Si} \quad (26)$$

The electron transfer takes place through the graphite crucible and the reaction can occur at two different sites. From their results, Grimble et al found that 50% of the silica is reduced electrochemically and the rest by chemical reaction at 1450°C.

The electrochemical nature of sulfur transfer has been demonstrated by King and Ramachandran[34]. It was shown that the simultaneous transfer of other elements like Si, Mn etc. also takes place by an electrochemical mechanism.

In a recent study Simkovich, Li and McCabe[24] examined the rate of dissolution of alumina and silica rods in carbon saturated iron. The rods were either rotated at previously set speeds or were kept stationary. The concentration of aluminum and silicon in the melt was measured as a function of time. The experimental results indicated that in the case of alumina the rate of dissolution is controlled by transport of aluminum away from the alumina-metal interface. The fact that diffusivity of Al observed at 1500°C was higher than that at 1600°C, could not be explained. However for silica dissolution the results seem to be inconclusive, but still the mechanism of mass transport control is believed by the authors.

2.5 Postulation of Reaction Mechanism for Silica Reduction in the Present Investigation

(i) The reduction of silica from slags by carbon saturated iron is represented by the following overall reaction

$$SiO_{2(slag)} + 2C_{(gr)} = \underline{Si} + 2CO_{(g)} \qquad (27)$$

As discussed earlier, there are various mechanisms put forward to explain the results. It is seen that reduction of silica could also take place by electrochemical reaction. If a graphite crucible is used, this possibility always exists. Hence to suppress the electrochemical reaction, a silica crucible was used. Carbon saturated-iron was melted in the silica crucible and allowed to react with the silica of the crucible walls. The rate of reaction at a fixed temperature was calculated by measuring the rate of CO evolution. Stoichiometrically the volume of CO evolved should be equivalent to the silicon transferred to the iron according to the reaction (27). The experiments in principle were similar to those of Parlee et al[10] who studied the reduction of alumina by carbon-saturated iron from an alumina crucible. However, the experimental technique was entirely different from that of Parlee et al[10].

(ii) Reaction Mechanism

The suggestion of a probable reaction mechanism is mainly based on the observation of other workers reported in the section 2.4.

As the reduction from solid silica is studied the transport of species in silica is eliminated. Hence following reaction path is possible.

(1) Dissociation of silica network at the silica metal interface according to reaction

$$SiO_2 = \underline{Si} + 2\underline{O} \qquad (28)$$

(2) Transport of silicon away from the interface into the bulk metal.

(3) Transport of oxygen from silica-metal interface by

  (a) Diffusion across a boundary layer in the liquid metal

  (b) Convection within the liquid metal

  (c) Diffusion of oxygen to metal-gas (CO) interface

(4) Diffusion of carbon to gas-metal interface.

(5) Reaction of carbon and oxygen at the gas bubble to form carbon monoxide

$$\underline{C} + \underline{O} = CO \qquad (29)$$

It is assumed that the reactions (28) and (29) are in a state of local equilibrium. It is interesting to consider the formation of carbon monoxide bubbles. Turkdogan et al[20] believe that CO bubbles are produced near to the slag-metal-crucible line of contact and consequently no major stirring of the melt is expected in their system. In the case of Simkovich et al's[24] work the reaction is occurring between solid silica and the melt. From equation (28) it is evident that reaction must occur at silica-metal (S/M) interface, reaction (29) could, however occur at either S/M interface or gas-metal interface. Since there is abundance of carbon near S/M interface and there is no positive reason to rule out the possibility of nucleation at this interface, the reaction (29) may possibly take place at S/M interface. On this line of argument Simkovich et al[24] believe that CO bubbles are forming at S/M interface. Fulton and Chipman[14] had found no effect of bubbling of CO through the melt on the rate of silicon transfer. It seems justified, in that case, to assume that nucleation and growth of CO bubbles are not the rate controlling factors.

Of the steps listed above only 2, 3(a), 3(c) and (4) could be rate limiting. Considering these steps separately, step (4) could not be rate limiting owing to large concentration of carbon in the melt. Silicon diffusion (step 2) in the bulk metal could be discarded on the basis of the results of Simkovich et al[24]. Also this would predict a higher silicon flux than experimentally observed[22]. Thus the diffusion of oxygen from the S/M interface to the bulk metal or from bulk metal to the gas metal interface could be rate controlling. The latter seems improbable as the bubbling of CO through the metal does not affect the rate[14].

2.6 (i) Rate Equation for Silicon Transfer if Oxygen Diffusion is Rate-Limiting

In general there are three criteria for identifying the actual rate controlling step in an overall reaction[22].

(1) Comparison of the experimental rate with the theoretically calculated rates.

(2) Comparison of theoretical and experimental activation energy.

(3) Determination of reaction order.

Though these are helpful in analyzing the reaction mechanism, they do not lead to an unambiguous determination of the rate limiting step. For example, the last one is a weaker criterion and is affected by stirring, gas evolution[6] etc.

For the present case let us evaluate a rate equation based on oxygen transport control. The flux of oxygen from S/M interface to the metal is given by equation (30)[19]

$$\dot{n}_o = \frac{AD_o}{\delta} (Co - C'_o) \qquad (30)$$

where $\dot{n}_o$ = Rate of oxygen transfer in moles. sec.$^{-1}$

A = Area of silica-metal interface in cm^2

δ = Effective boundary layer thickness for oxygen in cm.

Co and C'_o = Oxygen concentration at the silica-metal interface and in bulk metal respectively in moles. cm^{-3}.

The values of Co and C'_o are governed by the silica dissociation (equation 28) and carbon-oxygen reactions (equation 29) and are calculated as follows:

For silica dissociation, the equilibrium constant is

$$SiO_2 = \underline{Si} + 2\underline{O}$$

$$K_{Si} = \frac{a_{Si}\, a_o^2}{a_{SiO_2}} \qquad (31)$$

In our case $a_{SiO_2} = 1$ for the reduction of pure solid silica. For silicon and oxygen in solution in iron, the reference state selected is the infinitely dilute solution such that activity coefficient $f_i = 1$ as $\%i \rightarrow 0$ [35]. Hence substituting for the activities in equation (31) we get

$$K_{Si} = (\%Si \times f_{Si})(\%O \times f_o)^2 \qquad (32)$$

or

$$(\%O) = \frac{K_{Si}^{1/2}}{f_o(\%Si\ f_{Si})^{1/2}} \qquad (33)$$

Equation (33) gives the value of oxygen content at the interface in equilibrium with Si and SiO_2.

For carbon monoxide formation

$$\underline{C} + \underline{O} = CO_{(g)}$$

$$K_{CO} = \frac{P_{CO}}{a_C\, a'_O} \qquad (34)$$

or

$$(\%O)' = \frac{a'_o}{f'_o} = \frac{P_{CO}}{K_{C-O}\, a_c\, f'_o} \qquad (35)$$

Value of K_{C-O} is known from Fuwa and Chipman's data[27].

The weight-percent could be converted to mole per cm^3 by using the equation (36)

$$\text{Moles. cm}^{-3} = \frac{\text{weight percent}}{100} \frac{\rho}{M} \qquad (36)$$

where ρ is density of iron and M is the molecular weight of the dissolved species.

From the known thermodynamic data on Si-O[28,29,30] and C-O[27] reactions in iron it is found that C_o is about ten times larger than C'_o and hence to a good approximation can be ignored in comparison to C_o. Thus the rate equation (30) becomes

$$\dot{n}_o = \frac{AD_o}{\delta} C_o = \frac{AD_o}{\delta} \frac{(\%O)}{100} \frac{\rho}{16} \qquad (37)$$

Since the molar rate of oxygen transfer is twice that of silicon, $\dot{n}_o = 2\dot{n}_{Si}$.

Hence $$\dot{n}_{Si} = \frac{1}{2} \frac{AD_o}{\delta} \frac{(\%O)}{100} \frac{\rho}{16} \qquad (38)$$

Converting the molar concentration to weight percent by using the relation

$$n_{Si} = C_{Si} V = \frac{\%Si}{100} \frac{\rho}{28 \cdot 09} V \qquad (39)$$

where V is the volume of melt in cm^3. Substituting in (38) the value of n_{Si} from equation (39)

$$\frac{d\%Si}{dt} \frac{1}{100} \frac{\rho}{28 \cdot 09} V = \frac{1}{2} \frac{AD_o}{\delta} \frac{(\%O)}{100} \frac{\rho}{16}$$

or $$\frac{d\%Si}{dt} = \frac{28 \cdot 09}{32} \frac{A}{V} \frac{D_o}{\delta} (\%O) \qquad (40)$$

The oxygen concentration (%O) at the interface is given by equation (33) in terms of silicon content. Hence equation (40) becomes

$$\frac{d\%Si}{dt} = \frac{28\cdot 09}{32}\,\frac{A}{V}\,\frac{D_o}{\delta}\,\frac{K_{Si}^{1/2}}{(\%Si)^{1/2}\; f_o f_{Si}^{1/2}} \qquad (41)$$

This relation (41) involves the product $f_o f_{Si}^{1/2}$. The presence of carbon in iron increases the activity coefficient of silicon (f_{Si}) and decreases that of oxygen (f_o), and hence $f_o f_{Si}^{1/2}$ can be approximately taken as one[20,33].

Thus we can write equation (41) finally as

$$\frac{d\%Si}{dt} = \frac{28\cdot 09}{32}\,\frac{A}{V}\,\frac{D_o}{\delta}\,\frac{K_{Si}^{1/2}}{(\%Si)^{1/2}} \qquad (42)$$

This shows that the rate of silicon transfer $\left(\frac{d\%Si}{dt}\right)$ is proportional to $\frac{1}{(\%Si)^{1/2}}$. Also, at a constant temperature the quantity $\frac{D_o}{\delta}K_{Si}^{1/2}$ is constant and could be called the specific rate constant, k., for silicon transfer.

$$k = \frac{D_o}{\delta}K_{Si}^{1/2} = \frac{\left(\frac{d\%Si}{dt}\right)(\%Si)^{1/2}}{\frac{28\cdot 09}{32}\,\frac{A}{V}} \qquad (43)$$

2.6 (ii) Theoretical Activation Energy

If the silica reduction reaction is controlled by the transport of oxygen, the specific rate constant is given by equation (43). The activation energy for the process could be obtained from the Arrhenius plot of the rate constant as a function of temperature. In the expression for k in equation (43) it is seen that D_o, δ and K_{Si} are all temperature dependent terms. Hence a theoretical calculation for the temperature coefficient of k could be made if these for D_o, δ and K_{Si} are known.

It is well known that the diffusivity D varies exponentially with temperature according to the relation[31]

$$D = A(D) \exp\left(-\frac{E_D}{RT}\right) \qquad (44)$$

where A(D) is the frequency factor and E_D is the activation energy for diffusion. Riddiford[9] has shown that effective boundary layer thickness, δ, has also a similar temperature dependence, so that the following relation is valid,

$$\frac{D}{\delta} = A\left(\frac{D}{\delta}\right) \exp\left(-\frac{E(D|\delta)}{RT}\right) \qquad (45)$$

where $A(D/\delta)$ is the frequency factor and $E(D/\delta)$ is the temperature coefficient or activation energy of D/δ.

Riddiford[9] has given following relations for the evaluation of $E(D/\delta)$.

$$E(D/\delta) = \frac{4E_D + E_\gamma}{6} \quad \text{(for laminar flow)} \qquad (46)$$

$$= \frac{2(E_D + E_\gamma)}{3} \quad \text{(for turbulent flow)} \qquad (47)$$

Here E_D is the activation energy for diffusion and E_γ is that for kinematic viscous flow. As E_D and E_γ are of the same order of magnitude[9], it follows from equations (46) and (47) that the value of $E(D/\delta)$ lies approximately between 0.8 E_D and 13 E_D.

The diffusivity of oxygen in carbon-saturated iron is not known. But from the values of D and E_D available for silicon, carbon and manganese[32] D_0 is estimated to be 10^{-5} cm.^{2}sec^{-1} at 1600°C, and

E_{D_O} approximately 8 to 10 kcal per mole. Hence $E\left(\frac{D_O}{\delta}\right)$ will be of the order of 6 to 13 kcal per mole.

The temperature dependence of K_{Si} is given by $\Delta G^\circ = -RT\ln K_{Si}$ where ΔG° is the standard free energy change for the reaction (28). Thus k could be written as

$$k = A\left(\frac{D_o}{\delta}\right) \exp\left(-\frac{E\left(\frac{D_o}{\delta}\right)}{RT}\right) \exp\left(-\frac{\Delta G^\circ}{2RT}\right) \qquad (48)$$

Since $\Delta G^\circ = \Delta H^\circ - T\Delta S^\circ$

$$k = A\left(\frac{D_o}{\delta}\right) \exp\left(\frac{\Delta S^\circ}{2R}\right) \exp\left\{-\frac{E\left(\frac{D_o}{\delta}\right) + \frac{\Delta H^\circ}{2}}{RT}\right\} \qquad (49)$$

Taking logarithms

$$\ln k = \ln A\left(\frac{D_o}{\delta}\right) + \frac{\Delta S^\circ}{2R} - \frac{E\left(\frac{D_o}{\delta}\right) + \frac{\Delta H^\circ}{2}}{RT} \qquad (50)$$

A plot of lnk vs $1/T$ will yield a straight line with a slope equal to $-\frac{E(D_o/\delta) + \frac{\Delta H^\circ}{2}}{R}$. Hence the experimental activation energy calculated from above rate constant, k, will be equal to $\left(E(D_o/\delta) + \frac{\Delta H^\circ}{2}\right)$. Since the standard free energy change for reaction (28) is

$$\Delta G^\circ = 142000 - 55.62T \qquad \text{(See Appendix I)}$$

Hence $\frac{\Delta H^\circ}{2} = \frac{142000}{2} = 71000$ cal/mole.

As shown earlier $E(D_0/\delta) \approx 6 - 13$ kcal/mole so that experimental activation energy will be approximately 77 to 84 kcal/mole. If the experimental results for silicon transfer obey the rate equation (42) and if the activation energy has the value as predicted from above considerations, it will be an evidence of oxygen transport control.

CHAPTER III

EXPERIMENTAL APPARTUS AND TECHNIQUE

3.1 Experimental Apparatus

The experimental apparatus consisted of the following:

(1) Heating Furnaces
  (i) Crusilite furnace with temperature controller
  (ii) High Frequency induction furnace
(2) Reaction vessel
(3) Capillary tube for measurement of gas volume

3.2 (i) The Crusilite Furnace

For first set of experiments this silicon carbide resistor furnace was used. The furnace is schematically shown in figure 3(a). This rectangular box type furnace had over-all outside dimensions 14½" x 14½" x 16½" and was mounted on a movable dexion stand. The furnace chamber was filled with K-28 type fireclay bricks. The bricks in the centre were cut as shown in the figure 3(a), so as to provide a tubular space of 4" diameter around the vertical axis.

The heating element was a one piece tubular construction and had a helical heating zone about six inches long. This gave an almost constant maximum temperature, ±5°C, over a zone length of two and a half inches. The crusilite (silicon-carbide) element was mounted vertically in the furnace and was supported at the bottom. A mullite tube of two inches internal diameter was placed vertically inside the cylindrical element, taking care not to touch the heating element. The space between the maximum temperature zone and the bottom of the tube was filled with a refractory brick. This brick also acted as a support for the reaction vessel.

3.2 (ii) The Power Supply and Temperature Controller

A 230 volts, single phase power supply was used for heating the furnace. The voltage was stepped down by using a variac. A saturable core reactor (3 KVA, 25 Amps.) was connected in series with the furnace element. This was used in combination with a digital set point type temperature controller, and a magnetic amplifier. The working principle of the controller is as follows: The required temperature is set on the three digit set point drum and this in turn selects a corresponding voltage on the potentiometer in the controller. This voltage is compared with an external signal from a Pt/Pt-13% Rh thermocouple in the furnace. The resulting voltage difference is fed to the magnetic amplifier which acts as a power amplifier to boost the low level input signal from the temperature controller to a high level output d-c voltage to activate the saturable core reactor. Thus it controls the power in the furnace circuit and provides a continuous stepless electrical control. If the temperature in the furnace rises above the required temperature set on the controller, the power is proportionately reduced in the circuit.

The temperature of the furnace was kept constant with a maximum fluctuation of ±5°C. Mostly a control within ±3°C was achieved.

Two Pt/Pt - 13% Rh thermocouples were inserted inside the working tube such that their welded ends were in the maximum temperature zone. One of these was connected to the temperature controller and the other to a precision potentiometer. Thus the temperature in the furnace was continuously checked by measuring the e.m.f. of the second thermocouple.

3.3 High Frequency Induction Heating

In the second set of experiments a high frequency induction was used. This provided fair amount of stirring in the melt which was lacking in the first set of experiments. It is on these experiments that most of the interpretation of the results is based.

A 450 kilocycles, 10KW Toccotron induction generator was used as the source of power. The induction coil was a water-cooled copper tubing of 1/4 inch diameter. This was wound to form a cylindrical heating zone three inches long with an inside diameter of approximately 2 1/4 inches. The induction coil surrounded a two inch i.d. Vycor tube, packed with refractory bricks. The refractory block was drilled in the centre to provide one inch diameter cylindrical cavity. The reaction vessel was kept in this cylindrical cavity as shown in the figure 3(b). The arrangement of the apparatus is shown pictorially in figure 4.

Temperature Measurement: - The temperature of the melt was continuously measured by a two-colour pyrometer. For this, the melt was sighted through a prism kept on the optically flat surface at the top of reaction vessel. Thus the temperature measurement was continuous, providing for precise temperature control. The two-colour pyrometer used was a Milletron Thermoscope with a temperature range of 800-1300/1300-1800°C and a recorder output of 100 mv.

The obvious advantage of using a two-colour pyrometer was that no correction was required for the variation in the emissivity of of radiating surface. The pyrometer was calibrated against a Pt/Pt-13% Rh immersion thermocouple with a silica sheathing. A calibration curve was plotted in the temperature range 1300-1650°C.

The temperature of the melt was controlled manually with a variac to within ±10°C of the required temperature and sometimes a control of ±5°C was achieved.

3.4 The Reaction Vessel

Initially an "U" shaped reaction vessel made of vitreous silica was used; it is shown in figure 5(a). This silica reaction vessel was lowered in the Crusilite furnace such that the length CD was in the maximum temperature zone. The tube ABCD had 12.5 cm internal diameter and was bent to give an "U" shape. At D, it was joined to a 4 mm i.d., silica tube which was bent at right angles at E. The portion EF was in the plane of ABCDE and was horizontal.

The end F of the thinner tube was joined with a plastic tubing to capillary tube for measuring the rate of evolution of carbon monoxide. The molten carbon saturated iron was contained in both the limbs of the vessel. Only in the limb AB, the slag was added to the molten iron.

Using this type of reaction vessel, the reduction of silica from the blast furnace type slags was to be investigated. In this type of setup, it was assumed that the silica from the slag will decompose at the slag-metal interface to form silicon and oxygen. The oxygen and carbon would subsequently diffuse to the free melt surface in the limb CD to form carbon monoxide. Accordingly all the CO due to the reaction should have formed in the limb CD and measured in the capillary tube.

In actual practice, carbon monoxide bubbles were seen bursting out of the slag surface. This was further confirmed by calculating the mass balance for carbon in the melt. More carbon was lost than the corresponding volume of carbon monoxide measured from the limb CD. This necessitated a change in the design of reaction vessel, to allow the reaction of carbon saturated iron with the silica walls of the vessel to be investigated. The reduction of silica from the walls turned out to be appreciable.

Hence it was decided to study the reduction of silicon from solid silica. This also avoided the complicated set up required for adding the slag to gas tight system.

The modified reaction vessel, hereafter called silica crucible, is shown in figure 5(b). It consisted of a silica tube A, 25 cm long and with a hemispherical bottom. Silica tubes of two different diameters viz., 12.5 and 17 mm i.d. were employed to get different silica-metal interfacial area for the same mass of the melt.

The silica crucible, A, was connected to a Vycor (96% SiO_2)

tube C with the help of a teflon union, B. The top of the Vycor tube C, was closed by sealing an optically flat glass plate with plastic cement. A right prism, D, was placed on this glass window for observing the melt surface. Two small tubes 4 mm i.d. were joined to the tube C' as shown in the figure 5(b). One of these small tubes was connected to the capillary tube for gas volume measurement and the other was used as an inlet to provide CO atmosphere in the reaction vessel. This inlet tube was chain clamped during the run.

The teflon union provided an effective seal for joining the tubes A and C. There was no leakage of CO through the joint and the volume of CO evolved due to the reaction was measured accurately by the capillary tube.

3.5 Capillary Tube for Measurement of Gas Volume

The rate of CO evolution and its total volume were measured with the help of an ingenious device. This is shown in figure 6. It consisted of a 2 mm bore pyrex glass capillary tube, 110 cm long and was mounted on a meter scale. About 5 cm, from one end, was joined a small capillary tube with a stopcock and a small reservoir for holding mercury as shown in figure 6. By turning the stopcock knob swiftly, a small pellet of mercury could be dropped in the main capillary tube. The zero of the meter scale was adjusted such that front end of the mercury pellet always nearly coincided with it.

This end of the capillary tube was joined to the reaction vessel tube with a plastic tubing. The oncoming gas pushed the mercury pellet, and its position could be read on the meter scale at any time.

The position of the mercury pellet was recorded at minute intervals.

As soon as one mercury pellet crossed the 100 cm mark on the scale, another was dropped in the capillary from the reservoir. Thus the volume measurement was continuous. By plotting the curves, volume of CO against time, the rate of CO evolution could be calculated by taking tangents at any time on the curve.

3.6 Experimental Technique

(i) *Preparation of Carbon-Saturated Iron:* - The carbon-saturated iron was prepared separately by melting pure Armco ingot iron (composition 0.015%C, 0.028% Mn, 0.005% P, 0.025% S and 0.003% Si) in a graphite crucible in an induction furnace. After melting, the iron was held in the graphite crucible for about half an hour for carbon saturation. The iron was saturated with carbon at about 1450°C and cast in a steel mold to give 9 mm diameter rods. About 500 gm of carbon-saturated iron was prepared at a time. Subsequent analysis showed about 4.6-4.8%C in different lots of iron. The carbon content of iron used in any run was predetermined.

(ii) *Chemical Analysis:* - As indicated earlier no samples of the metal were taken during a run. The solidified metal was analysed for carbon and silicon after each run. The carbon was determined by combustion method and silicon, gravimetrically by perchloric acid method.[37]

(iii) *Experimental Procedure:* - The procedure for a typical run was as follows. A predetermined amount of carbon-saturated iron was weighed on a chemical balance and transferred to the silica tube. For the tubes of diameter 12.5 mm, generally 25 gm of metal was used for a deeper bath and a small amount of 5 gm for a shallow bath. In the case of 17 mm diameter tube, the amounts taken were 35 and 10 gm respectively for a deeper and shallower bath.

The silica tube was joined to the other tube with a teflon union as discussed earlier. This was then joined to the capillary tube (figure 4). Before starting the run, the whole system i.e. reaction vessel and capillary tube, was evacuated with a mechanical pump for about half an hour. And later the evacuated system was filled with C.P. grade, 99.9% pure, CO gas. This was required so as to prevent oxidation and decarburizing of iron during heating period. The heating period ranged from 4 to 4-1/2 hours in the Crusilite furnace and 1/2 to 1 hour in induction furnace.

Once the reaction tube was filled with carbon monoxide the farther end of the capillary tube was opened to atmosphere, thus keeping atmospheric pressure in the chamber. During the heating period, the gas in the chamber expanded and was allowed to come out. If a mercury pellet was introduced in the capillary, it was pushed ahead by the expanding gas. When the iron was about to melt, it was observed that the movement of the mercury drop stopped, indicating no further expansion of the gas. The mercury drop remained stationary till all the iron had melted (1130 to 1200°C). The zero time was counted as soon as all the iron was molten. Initially the volume of the gas evolved, was very small. The temperature of the melt was raised quickly to the required temperature viz., 1300°C to start with. A record of time and volume of the gas evolved prior to the required temperature was maintained.

As soon as the melt temperature was 1300°C, the position of the mercury pellet was noted at a fixed interval of one minute. This interval was reduced to half a minute at higher temperatures. The volume of the gas was recorded in terms of centimeters as the area of x-section of the capillary was constant. The values could be converted to volume units by multiplying with the x-sectional area.

The position of the meter scale was such that whenever a small droplet of mercury was inserted through the stopcock, the front end of the pellet coincided with the zero of meter scale. Hence this end was taken as the reference point for taking the reading on meter scale. With little practice a pellet about 1/2 - 1 cm long could be introduced into the capillary. Thus when the front end of a mercury pellet reached 100 cm mark on the scale, another was introduced in the capillary at the zero mark. The procedure was repeated every time one pellet crossed 100 cm mark. This gave continuous measurement of the volume of gas evolved due to the reaction at any temperature. At the same time the rate of gas evolution was also known, which is the measure of the rate of silicon transfer to the metal. The rate of CO evolution was higher at the beginning of the run and it fell gradually with increase in time. This decrease was not linear with respect to time.

Usually a run lasted for about 50 to 70 minutes at each temperature. The same melt was used for all the subsequent temperatures. At the end of a run, the power was increased and the temperature was increased by about 50°C. During this interval of the increase in temperature, the time and volume of CO were continuously noted. As soon as the required temperature was attained the observations were taken as described earlier. In this way the volume and rate of CO evolution were measured at temperatures from 1300 to 1600°C at an interval of 50°C. At the end of entire run, the melt was cooled down in CO atmosphere. The samples were drilled from the solidified melt and analysed for carbon and silicon.

Thus one silica tube lasted for only one run and each time a new silica tube was used.

3.6 (iv) Effect of Carbon Activity: - The carbon concentration of the melt decreases as the reaction proceeds. Because of this, and the increased solubility of carbon in iron with increase in temperature, the melt does not remain saturated with carbon. In some experiments, it was decided to keep the activity of carbon constant by saturating the melt with graphite at all the temperatures and to study the effect on the rate of CO evolution. This was done either by allowing a small lump of graphite to float on the melt surface or by entrapping a graphite block at the bottom of the silica tube.

3.7 Gas Analysis

The gas evolved due to the reaction was analysed, nearly at the end of a run by gas chromatographic method. It consisted of more than 92% of CO and the rest being oxygen and nitrogen in the same ratio as in air. This suggested that air rushed in the sampling tube after sampling, due to slight pressure differential. There was no trace of CO_2 in the sampled gas. The analysis was done to see if any cracking of CO occurred, and if so, the observed rate of gas evolution would be faulty. If at all any cracking occurred it was very negligible and was beyond the limits of detection.

CHAPTER IV

EXPERIMENTAL RESULTS

4.1 Introduction

The results of the investigation of silicon transfer from solid silica to molten iron are presented in this section. The experiments are classified in three groups.

(1) Silicon transfer to unstirred high carbon iron.

(2) Silicon transfer to induction stirred high carbon iron.

(3) Silicon transfer to induction stirred graphite-saturated iron.

The iron under (1) and (2) contained more than 4.6% carbon to start with. Though the carbon content of the iron during a run remained more than 3.8 - 4.0%, the carbon saturation was not maintained at higher temperatures.

The results from the above experiments were used to determine the dependence of the rate of transfer on silica-metal interfacial area.

The specific rate constants were calculated from the observed rates as a function of temperature. The activation energy is calculated from the Arrhenius plot of these rate constants, in order to identify the rate controlling step in the silica reduction reaction.

4.2 The Rate Curves

(i) The volume of the carbon monoxide evolved as a result of the silica reduction was measured as a function of time in each of the experiments. The volume was measured at minute intervals for temperatures up to 1500°C. But at 1550 and 1600°C the rate of evolution was faster and the volume was measured at half minute intervals. As the area of cross-section of the capillary was a constant factor, the volume is recorded in the units of length i.e. the distance travelled by the mercury pellet. To get the volume in cubic centimeters, the length is multiplied by cross-sectional area (0.033 cm^2) of the capillary. For measuring the cross-sectional area, accurately weighed amount of mercury was introduced in the capillary tube and the length of the mercury thread was noted. This was repeated with several different amounts of mercury. The average of mass (M) to length (l) ratio was taken to calculate the area of cross-section which is equal to $M/l\rho$, ρ being the density of mercury.

The volume of carbon monoxide observed is tabulated in tables I(a), I(b) and I(c), and shown graphically in figures 7 to 22. In the tables I(a), I(b), and I(c), the volume is recorded only at ten minute intervals.

In the figures 7 and 8, all the points at minute intervals are plotted to justify drawing of a smooth curve passing through almost all the points. In the rest of the rate curves these points are not shown.

(ii) Determination of the rate: - The figures 7 to 22 show that the rate curves are non-linear. To determine the rate of gas evolution at any instant, a tangent was drawn to the curve. The slope of the tangent represents the rate, $\frac{dv}{dt}$ at that instant. These tangents are shown in figure 8 and were drawn using a plane mirror. This method of drawing the tangents to the curve was fairly accurate and the errors in the calculated rate were within ±3-5%. In general a number of tangents, from as few as four to as many as ten, were drawn over the entire curve. The corresponding volume was also noted.

(iii) <u>Calculation of Silicon Flux</u>: - By the stoichiometry of the overall reaction (15) the equivalent amount of silicon transferred was calculated from the volume of carbon monoxide. Since

2 x 22400 ml CO at S.T.P. ≡ 28.09 gm silicon.

$$\text{Hence v ml CO at S.T.P.} \equiv \frac{28.09}{44800} \text{ v gm silicon}$$

$$= 6.270 \times 10^{-4} \text{ v gm Si.} \qquad (51)$$

From equation (51), the silicon content of iron is given by

$$\%\text{Si} = (6.270 \times 10^{-4} \text{ v}) \frac{100}{W} \qquad (52)$$

where W is the mass of iron in gm.

$$\text{Thus} \qquad \frac{d\%\text{Si}}{dt} = (6.27 \times 10^{-4} \times \frac{100}{W}) \frac{dv}{dt} \qquad (53)$$

As the volume of carbon monoxide was measured at room temperature and atmospheric pressure, the same was converted to standard temperature and pressure conditions (0°C and 760 mm) by equation (54)

$$v_{\text{S.T.P.}} = \frac{273}{760} \frac{Pv}{T} = 0.3592 \frac{Pv}{T} \qquad (54)$$

where P is the atmospheric pressure in mm (Hg), T the room temperature in °K and v is the observed volume in ml.

The equivalence between the volume of carbon monoxide and the silicon content of the melt was checked by analyzing the solidified iron after the run. In table V, the final silicon and carbon contents of the melt are shown. The amount of silicon calculated from the CO volume is also shown. These agree very well. The carbon loss is equivalent to CO volume observed. In some cases however more carbon was lost than the corresponding silicon and carbon monoxide.

The pressure in the reaction vessel was assumed to be atmospheric. However when a mercury pellet is dropped in the capillary tube a small pressure differential is produced across the mercury pellet. The magnitude of this pressure differential was obtained by attaching a manometer between the reaction vessel and the capillary tube. The manometer showed the pressure in the vessel 2 to 3 mm (Hg) in excess of the atmospheric pressure. It being a small quantity, no correction was considered necessary for the pressure.

4.3 The Dependence of the Rate on the Silica-Metal Interfacial Area

As is obvious the reduction of silica takes place all along the area of contact of iron with the silica. Therefore the rate of silicon transfer must be proportional to the silica-metal interfacial area. This direct proportionality between the silica-metal interfacial area and the rate, was distinctly established for the stirred melts in runs 13, 14, 15 and 16. In figure 23, the rate of CO evolution is plotted as a functionof S/M area. A straight line passing through these points and origin clearly indicates one to one correspondence between the rate and contact area.

For the unstirred melts, (runs 6 to 12) the rate is not proportional to the area. Figure 23 also shows the results from unstirred melts. A line drawn through the points does not pass through the origin but has an intercept on the ordinate axis, giving a definite rate even at zero contact area.

4.4 Specific Rate Constants

In Chapter II, a reaction mechanism for silica reduction was postulated based on the transport of oxygen as the rate limiting step. The rate of the overall reaction, controlled by oxygen diffusion is given in terms of oxygen flux equation (30) of chapter II. This equation was further modified to equation (42) to calculate the rate of silicon transfer. The rate equation (42) is

$$\frac{d\%Si}{dt} = \frac{28.09}{32}\,\frac{A}{V}\,\frac{D_o}{\delta}\,\frac{K_{Si}^{1/2}}{\sqrt{\%Si}}$$

From this equation, the specific rate constant k was defined as

$$k = \frac{D_o K_{Si}^{1/2}}{\delta} = \frac{\left(\frac{d\%Si}{dt}\right)(\%Si)^{1/2}}{\frac{28.09}{32}\,\frac{A}{V}}$$

where $\frac{d\%Si}{dt}$ = Rate of silicon transfer in %Si/min.

$\%Si$ = Silicon content of iron in percent.

A = Silica-Metal (S/M) interfacial area in cm^2.

V = Volume of the iron in cm^3.

D_o = Diffusivity of oxygen in iron in cm^2/min.

δ = Effective boundary layer thickness in cm.

and K_{Si} = Equilibrium constant for silica dissociation (equation 28).

The quantities on the right hand side of the above expression are experimentally known and hence the rate constants could be calculated for different temperatures at which the runs were performed.

The values of $\frac{d\%Si}{dt}$ and %Si were calculated using equations (52) and (53) from the values of v and $\frac{dv}{dt}$, obtained from the rate curves. Thus the value of the product $\left(\frac{d\%Si}{dt}\right)(\%Si)^{1/2}$ is given by equation (55)

$$\left(\frac{d\%Si}{dt}\right)(\%Si)^{1/2} = \left(6.27 \times 10^{-4} \times \frac{100}{W}\right)^{3/2} \frac{dv}{dt}\, v^{1/2} \qquad (55)$$

For a run at constant temperature, the other quantities remaining constant, the product $\frac{dv}{dt} v^{1/2}$ should be constant. As this was found to vary slightly with time, a mean of all the values was taken. For runs at higher temperatures, this product decreased with time but a mean value could be used for calculating the specific rate constant without introducing appreciable errors.

In table III, the values of $\frac{dv}{dt} v^{1/2}$, $\left(\frac{d\%Si}{dt}\right)(\%Si)^{1/2}$ and the specific rate constant, k, are shown for each of the runs.

The same table also shows the ratio V/A. The volume, V, of the melt was calculated using the relation $V = W/\rho$ where W is the mass of the iron and ρ the density of the melt. The density of carbon saturated iron at different temperatures was computed from the data of Lucas[38] and a correction was applied for the silicon content using the relation given by Turkdogan et al[20]. An average value of the density was employed between the temperatures 1300 to 1600°C and for a mean silicon concentration of 0.5%. Use of the average density did not introduce errors in k by more than 5%.

4.5 The Activation Energy

The activation energy for the process was determined from the Arrhenius plots of the specific rate constants. In the figures 24 to 26, the logarithm of the rate constants are plotted against the reciprocal of the temperature. The slope of this line is a measure of the activation energy of the process:

$$\text{Slope} = -\frac{Q}{2.303R} = -\frac{Q}{4.575} \qquad (56)$$

where Q is the activation energy (cals/mole) and R is the universal gas constant and is equal to 1.987 $\text{cals.mole}^{-1}\ {}^{\circ}\text{K}^{-1}$. The values of the experimental activation energy are shown in table IV.

4.6 The Thickness of Effective Boundary Layer

Using the expression (57) for the rate constant, the effective boundary layer thickness for oxygen diffusion was calculated:

$$\delta = \frac{D_o}{k} K_{Si}^{1/2} \qquad (57)$$

where K_{Si} is the equilibrium constant for silica dissociation, k is the rate constant and D_o the diffusivity of oxygen at corresponding temperature. At 1600°C the values of δ are tabulated in table IV. The diffusivity of oxygen in the carbon saturated iron is not known but it could be estimated from the work of Parlee et al[10], and from Saito and co-workers[32] measurement on silicon diffusivity. The value of D_o at 1600°C is taken to be 10^{-5} cm^2/sec in the present calculations. The value of effective boundary layer obtained here, is smaller than Darken's[4] value of 0.003 cm in a vigorously boiling open hearth bath.

4.7 Observation of Gas Bubbles on the Silica Wall

During the course of one experiment, the refractory bricks surrounding the reaction vessel, were removed to allow the direct observation of the melt in the transparent silica vessel.

It was observed that carbon monoxide bubbles nucleate and grow on the silica wall. The photographs of these bubbles are shown in figures 29 and 30. As these bubbles could grow and some attained a large diameter of approximately 5-8 mm, they were believed to be very flat and thin. There was a tendency for the bubbles to slide along the walls and escape to the gas atmosphere above the melt. On observing the top surface of the melt through a right prism, no indication of bubble formation on the silica wall could be obtained.

As soon as a large bubble escaped the melt, small bubbles nucleated on the walls and these grew very rapidly. The formation of gas bubbles on the silica walls reduced the contact time between the melt and silica. Because of this, the effective silica-metal interfacial area was reduced considerably.

To estimate the effective area and approximate residence time of bubbles on the silica surface movie photographs were taken. In the figure 30, the consecutive frames have been printed.

These photographs in figures 29(a), 29(b) and 30 were taken by viewing the image of the transparent silica vessel in a plane mirrored glass kept slightly inclined to the horizontal plane. By this technique, one side of the crucible wall and the bottom of crucible could be observed directly through the mirror. The darker portion in these photographs represent the gas bubbles. A detailed discussion of the bubbles is given in section 5.4 of next chapter.

CHAPTER V

DISCUSSION OF THE RESULTS

5.1 Rate Constants

The rate constants calculated for all the experiments have been shown in table III and plotted graphically in figures 24, 25, 26 and 27. An error of ±15% is estimated in the calculated values of the rate constants. This error is the result of errors involved in the measurement of various quantities. The errors in the derived functions are calculated using a technique suggested by Mickley et al[36].

(i) Rate constants for unstirred melts: - In the runs 6 to 12, the melt was not stirred. For these runs it has been shown in previous chapter that the rate is not proportional to the silica-metal interfacial area (figure 23). Consequently the rate constants, calculated on the basis of S/M interfacial area are not in agreement with each other. The rate constants for runs 7 and 10 (A = 2.65 cm^2) are six to eight times higher than those for runs 6, 9, 11 (A = 11.8 cm^2) and 12 (13.6 cm^2). For the runs 6, 11 and 12 where the S/M interfacial area was nearly same, the rate constants are also similar.

The non-proportionality of the rate to the area of contact and such a large difference in the rate constants could be ascribed to changes in the stirring conditions in the melt. Since the gas bubbles are produced at the S/M interface, the effective interface area is reduced. If the melt is stirred by some method, the gas bubbles will be regularly swept away from the interface thus providing similar effective area in different runs. In the absence of external stirring, the bubbles in the larger melt (runs 6, 9, 11 and 12) would tend to remain at the interface for longer time than those in smaller melts (runs 7 and 12). This will give larger effective area in the latter case than the former. Thus the rate of CO evolution will be higher for a smaller melt.

Another factor which could affect the rate of gas evolution, is the geometrical factor. For smaller melts, the shape of melt was that of a hemisphere, whereas for larger melts, the shape was that of a cylinder with a hemispherical bottom.

In view of considerable difference in the geometry of the melts and in the stirring conditions, the two rate constants are not comparable.

5.1 (ii) Rate Constants for Stirred Melts: - In the runs 13, 14, 15 and 16, the melt was inductively stirred. Different S/M interfacial areas were obtained by varying the amount of iron and these were 4.54 cm^2 (run 14), 13.6 cm^2 (runs 13 and 16) and 17.90 cm^2 (run 15). From table III and figure 25, it is seen that the rate constants at different temperatures for all the runs agree very well within the experimental error. This shows that the stirring provided an effective area proportional to or equal to the total area. It could also be concluded that the difference in the rate constants for unstirred melts is only because of ill-defined and dissimilar conditions of the melt.

From the figure 25 it is observed that the points at 1300 to 1400°C do not lie on the line passing through the high temperature points. It is possible to plot a best fitting curve through all the points between 1300 and 1600°C. This curve is convex upwards with the slope becoming less negative at higher temperatures. Thus the rate constants at 1300, 1350 and 1400°C are lower than expected.

In calculating, the rate constants according to the equation (42), in Chapter II the bulk oxygen content is neglected in comparison to the interfacial oxygen content. However at lower temperatures the interfacial oxygen content C_o is only 3 to 4 times greater than bulk oxygen C'_o and hence the latter cannot be neglected. For temperatures higher than 1450°C, $C_o \approx 10\ C'_o$ and the bulk oxygen can be ignored in the calculation of the rate constants. On taking into account the bulk oxygen content at lower temperatures and recalculating the rate constants, we find that there is no substantial increase in the magnitude of the rate constants.

The observed non-linearity of the Arrhenius plot for these runs could be due to several factors listed below:

(1) Effect of the activity of carbon which is varying during the run; $a_c \approx 0.9$ to 1 in the beginning of run at 1300°C and at the end of the run at 1600°C $a_c \approx 0.5$.

(2) Change in the stirring conditions due to higher power input at higher temperatures and due to greater rate of gas evolution.

(3) Possibility of a different rate controlling mechanism at lower temperatures.

(4) Errors in the activity coefficients used.

Comparing the above results with those of runs 17 and 18 in which activity of carbon was maintained unity, it is seen that the rate constants are of the same order of magnitude in the temperature range 1500 - 1600°C. But at 1400 - 1450°C, the rate constants for graphite saturated runs are higher than those for unsaturated runs (13 to 16). Also, the Arrhenius plot is linear for carbon saturated runs for the entire range of temperatures from 1400 to 1600°C. This implies that there is no effect of carbon activity on the rate constants at temperatures 1500-1600°C (as $a_c \approx 0.5$ for unsaturated runs as compared to $a_c = 1$ for saturated runs). There is no reason why the carbon activity should affect the rate constants at lower temperatures. Hence possibly the variation in carbon activity is not the cause of lower values of rate constants in these runs.

The effect of enhanced stirring at higher temperatures would be to increase the rate of silicon transfer. Simultaneously, this would reduce the effective silica-metal interfacial area and the boundary layer thickness[6,18,33] because of greater rate of gas evolution. The effect of reduced effective area would be to give lower rate constants at higher temperatures. This could in part explain the slight curvature (convex upwards) of the Arrhenius plots.

The possibility of a different rate controlling mechanism at lower temperatures also exists. From the results of the present experiments, it is not possible to verify and single out one particular factor which would lead to lower rates at lower temperatures.

5.1 (iii) Rate Constants for Carbon Saturated Runs: - In the runs 17, 18, 20 and 21, the iron was kept saturated with graphite at all the temperatures. For runs 17 and 18, the carbon saturation was maintained by allowing a small lump of graphite to float on the melt surface. In case of the runs 20 and 21, the graphite block was trapped near the bottom of silica crucible between the walls. Thus the graphite block was surrounded by the molten iron during the run.

The results from the individual pairs are in good agreement. The rate constants for runs 17 and 18 are 1.9 times greater than those for runs 20 and 21. The Arrhenius plot for these runs is shown in Figure 26. The conditions in the runs 17 and 18 and in previous runs are very similar. As discussed in 5.2 (ii) the rate constants are similar at higher temperatures for these two sets (i.e. runs 17 and 18 and 13 to 16).

When the graphite block is immersed in the melt, the stirring pattern and power input at any temperature are different than in its absence. The graphite block will have a tendency to absorb more power from the inductive field. Consequently it will reduce the velocity of flow in the melt. It was also observed for these runs that graphite had precipitated at the bottom of the silica crucible. It is not possible to determine the conditions of the melt below the graphite block. But in any case the effective area and the rate of stirring should be lower when the graphite is immersed in the melt. This has consequence of reducing the silicon flux and the rate constants for the runs 20 and 21. Though the rate constants are different, the Arrhenius plots are parallel straight lines.

5.1 (iv) Long Time Run: - In run 19 the experiment was carried out at 1464°C for a longer period of 200 minutes as compared to 40-50 minutes period at each temperature in other runs. The rate constant from this run is about 1.5 times to those in runs 13 to 16 at corresponding temperature. It was seen that the product $\frac{d\%Si}{dt}(\%Si)^{1/2}$ in the equation (43) did not remain constant for the entire period. If a mean value of this product is taken for first fifty minute period, the rate constant obtained is 4.28×10^{-4} cm/min which is comparable to those from runs 13 to 16. Since the mean of the product $\frac{d\%Si}{dt}(\%Si)^{1/2}$ increases for a longer time, the value of rate constant is higher. It seems that the effect of longer time would be to raise the lines in the Arrhenius plot.

5.2 Activation Energy

The activation energies for the process calculated from the Arrhenius plots of the rate constants are shown in the table IV. The Arrhenius plots are shown in figures 24, 25, 26 and 27. The standard method of least squares[39] was employed to determine the slope of the statistical line through the points.[39] The maximum error in each point is also shown in these figures.

For the unstirred melts, the activation energy curve is shown in the figure 24. Though the rate constants for different runs are not the same, they have similar temperature coefficient. For these runs an activation energy of 39.6 kcal per mole is obtained.

For the stirred melts the Arrhenius plot is curved (figure 25), with a lower slope at higher temperatures and vice versa. The high temperature points yield an activation energy of 84.6 kcal per mole. The slope of the line which could be drawn through lower temperature points corresponds to a value of approximately 120 kcal per mole.

For the carbon saturated runs (figure 26) an activation energy of 74.9 kcal per mole is obtained.

Thus the activation energy for silica reduction in the present experimental conditions lie in a range of 75 to 90 kcal per mole (at higher temperatures). This value compares very well with the theoretically predicted activation energy of 77-85 kcal per mole, if the rate controlling step in the silica reduction were the transport of oxygen in the liquid iron. This agreement may be regarded as one evidence for the oxygen transport control for silica reduction.

Fulton and Chipman[14] observed an activation energy of 130 kcal per mole for the silica reduction. On the basis of high value of 130 kcal, they assumed the reaction to be chemically controlled. In view of the present analysis and those of other workers[12,22], a high value of 100-120 kcal and above could be explained for transport controlled processes also.

5.3 Apparent Reaction Order

Though the term order of reaction has not much significance for heterogeneous reactions, it may sometimes be helpful in identifying the rate limiting mechanism in an overall reaction. According to the equation (42) in Chapter II, the rate of silicon transfer $\left(\frac{d\%Si}{dt}\right)$ is proportional to $\frac{1}{(\%Si)^{1/2}}$ at a fixed temperature and mass of the metal.

This relationship was obtained on the assumption that silica reduction reaction is controlled by the oxygen diffusion in the metal. Hence it could be said that order of reaction is 1/2 with respect to $\frac{1}{\%Si}$. The plot of $\frac{d\%Si}{dt}$ vs. %Si on a logarithmic scale will be straight line with a slope of - 1/2. In figure 28, this is shown for run 21. The slope of the lines vary from -0.47 to -0.73 at temperature 1370 to 1505°C. But at 1560 and 1600°C the slope is approximately -1.8.

The observation of higher order at 1560 and 1600°C could be attributed to greater rate of gas evolution which decreases the effective boundary layer thickness. Philbrook and Kirkbride[15] in their study of the rate of reduction of iron oxide in a slag by graphite saturated iron found that rate is proportional to the square of iron oxide concentration in the slag. By chemical kinetics the rate should be proportional to iron oxide concentration. Wagner[6] explained this second order dependence by assuming the reaction to be transport controlled (see chapter II). Consequently following relation between the rate and the boundary layer thickness was assumed

$$\delta_{Fe''} = b \left(\frac{\dot{n}}{A}\right)^{-\beta} \tag{58}$$

where b and β are constants and A is the interfacial area. The rate of transfer $\dot{n}$, will be given by

$$\dot{n} = \frac{A\ D_{Fe''}\ C_{Fe''}}{\delta_{Fe''}} \tag{59}$$

Substituting in equation (59) the value of $\delta_{Fe''}$ from equation (58) we get

$$\frac{\dot{n}}{A} = \left(\frac{D_{Fe''}\ C_{Fe''}}{b}\right)^{1/1-\beta} \qquad (60)$$

and if $\beta = 1/2$, $$\frac{\dot{n}}{A} = \left(\frac{D_{Fe''}\ C_{Fe''}}{b}\right)^{2} \qquad (61)$$

which is in accordance with the experimental observation. In our case, taking a slightly higher value of β, between 1/2 and 3/4, the relationship $\frac{d\%Si}{dt} \propto \frac{1}{\%Si^{1.5}}$ could be explained. This seems quite justified in view of the fact that CO bubbles are produced at S/M interface which at higher temperatures affect the boundary layer thickness and effective area significantly.

5.4 Formation of Gas Bubbles at Silica-Metal Interface

(i) Size: - From the photographs of the gas bubbles in figures 29(a) and 29(b) it is clear that at any instant the effective S/M interfacial area is much less than the nominal area. Since these photographs represent the projection of the crucible on a plane surface, exact calculations of the area covered by the gas bubbles is difficult. However an approximate estimate could be made from these photographs.

In a region where only smaller bubbles of the size 0.7 - 1.0 mm diameter are present (i.e. during the initial stages of growth of bubbles) approximately 50 - 60% of S/M area is occupied by the bubbles. Hence the effective S/M area during the initial stage is 40 - 50% of the nominal area. But when these bubbles grow and attain a larger size of about 6-8 mm, the effective interfacial area is reduced to 10-20% that of nominal area.

(ii) Rate of Growth of the Bubbles: - In the figure 30, the consecutive frames from a series of motion pictures taken at a speed of 24 frames per second are shown. A total of sixty-six consecutive frames, corresponding to a time interval of 2.75 sec. are reproduced here. From these pictures rapidity of the growth of these bubbles can be readily estimated.

In frame 1, a big bubble is seen at the bottom of the crucible, this bubble has escaped in the next frame. At the same site, the melt comes into contact with silica and very small bubbles could be seen, nucleating at the same site. These small bubbles (size < 1/2 mm) are seen clearly in the frames 5, 6 and 7. The growth rate is estimated to be nearly $\frac{1}{2} \times \frac{24}{4} = 3$ mm/sec. Later these bubbles coalesce with each other and become larger. After one second (i.e. 24th frame, counting from first frame), the diameter of the bubbles, growing on the above-mentioned site, has increased to 2.5 - 4.0 mm. Observing these frames up to 2 second, we see that bubbles have moved up along the silica wall and others are continuing to grow. In the frames 37 to 39 a big bubble (8-9 mm) at the right-hand side has escaped and all over again small bubbles are forming. The above-mentioned bubble was present since frame 1, hence it nearly took 1.6 sec. or more before escaping from the interface.

On the left-hand side of these pictures, bigger bubbles of 6 to 7 mm have grown within two seconds. One of these bubbles leaves the melt in the frame 55 i.e. after 2.3 sec. Another of these escapes in the frame 60 i.e. after 2.5 sec. (The bubbles leaving the site have been arrow marked.) One of the bubbles (indicated by a double arrow) has not left the melt till frame 66. It was found that this bubble attained a size of 9-10 mm before escaping the melt at the end of 4 sec. From this description it would seem probable that the gas bubbles escape on an average after 3 seconds from the beginning of their formation.

(iii) Shape of the Gas Bubbles: - These bubbles have an appearance of thin, flat film, rather than a spherical shape. This would imply that the contact angle between the silica, liquid iron and CO gas is very large. This observation is in conformity with those of Simkovich et al[24] who report a contact angle of 170-175° for silica, liquid iron and CO gas.

(iv) Thickness of the Effective Boundary Layer: - The boundary layer thickness for oxygen diffusion in the metal, shown in table IV, has been calculated on the basis of nominal S/M interfacial area. From the above discussion it is definite that the effective area is much less than the nominal S/M area. Also, it would be reasonable to suppose on the preceding observations, that the effective S/M area is approximately 20-25% that of nominal area.

The average value of the effective boundary layer thickness (δ), from the table IV is 0.0023 cm at 1600°C. Since only 25% of the total area is effective, the value of δ (equation 43) changes to 0.00058 cm. This indicates extreme shortness of the diffusion path.

The thickness of the diffusion path derived from the work of Turkdogan et al[20] and Rawling and Elliott[21], is 0.00055 and 0.0003 cm respectively. These compare well with the present observation.

5.5 The Controlling Mechanism

(i) Chemical Control: - The overall silica reduction reaction is

$$SiO_{2(crist.)} + 2\underline{C} = \underline{Si} + 2CO_{(g)} \tag{62}$$

It, being a three phase reaction can only occur along a curve or a line, and is unlikely to represent the actual reaction path. If the chemistry of this reaction were the rate controlling mechanism, the flux of silicon transfer will be given by

$$\dot{n}_{Si} = A\{k_1 a_{SiO_2} a_C^2 - k_2 a_{Si}\, p_{CO}^2\} \tag{63}$$

where $\dot{n}_{Si}$ = Rate of silicon transfer in moles/sec

k_1 and k_2 = Rate constants for the forward and reverse reactions in moles/cm^{2}sec.

and A = The S/M interfacial area in cm^2.

Since $a_{SiO_2} = 1$ and $p_{CO} = 1$ atm. for the present case, the equation (63) becomes

$$\dot{n}_{Si} = A\{k_1 a_c^2 - k_2 a_{Si}\} \tag{64}$$

At equilibrium $\dot{n}_{Si} = 0$ and hence

$$K = \frac{k_1}{k_2} = \left(\frac{a_{Si}}{a_C^2}\right)^{eq.} \tag{65}$$

where K is the equilibrium constant of the reaction (62).

This type of rate equation was initially employed to explain the results. Though the observation could fit in the equation (64) quite well, the ratio of k_1 and k_2 did not equal the equilibrium constant. There being a large difference between the theoretical and observed value of K, this model of chemical control was given up.

(ii) Transport Control: - Based on the observation of other workers[20,21,24], a possible reaction path for silica reduction was postulated in the Chapter II. The most probable rate controlling step was suggested to be the diffusion of oxygen in the metal. The present data have been explained on the basis of oxygen diffusion in the metal. The experimental and theoretical activation energies are in good agreement. The reaction order with respect to silicon concentration in the metal, is also as per theory except at higher temperatures where a high rate of CO evolution could give rise to a higher order dependence.

The formation of gas bubbles at the silica-metal interface definitely establishes it to be the reaction site. This might lead one to suspect that the diffusion of silicon could be the rate controlling step. The possibility of carbon diffusion to the reaction site from the bulk metal as the rate determining factor, could be discarded as there is high carbon content in the melt. Rawling[22] showed that if silicon or carbon diffusion were the rate controlling factor, the silicon flux would be 9×10^{-3} and 3×10^{-2} moles per sec. respectively at 1600°C as against the experimentally observed value of 2×10^{-6} moles per sec. This value is nearly of the same order as 6×10^{-7} moles per sec. calculated on the basis of oxygen diffusion.

Tiberg[25] observed the formation of gas bubbles at the silica-melt interface. However the carbon content of the melt was 0.8% and the effect of pressure on the rate of the reaction was investigated. It was found that the rate of dissolution of silica varied with pressure according to the relation $u = kp^{-0.55}$ where u is the rate of solution in μ/min, k the rate constant and p the pressure in atmospheres. This dependence of the reaction rate on the pressure would not be expected if the CO formation were the slowest stage in the overall reaction. Similarly if the chemistry of silica dissociation reaction were the rate controlling step, the above-mentioned relationship could not be obtained. On this basis Tiberg[25] concluded that the diffusion of silicon and oxygen away from the interface controlled the overall reaction.

Turkdogan et al[20] and Grimble[26] have reported the formation of silicon monoxide (SiO) in the region of the crucible. But it was not possible to determine whether SiO formation takes part in the main reaction.

In the presence of CO at the interface silica could be reduced according to equation (66)

$$SiO_{2\,(s)} + CO_{(g)} = SiO_{(g)} + CO_{2\,(g)} \qquad (66)$$

This would mean that the gas bubbles observed at the interface consist of CO, CO_2 and SiO. In the present work, the analysis of the evolved gas did not show any trace of CO_2. If the above reaction takes place at the gas bubble and silica interface then SiO and CO_2 must diffuse through gas to the molten iron surface where they would give off their oxygen, SiO being dissolved in iron and CO_2 being reduced to CO. If this type of reaction is controlling the process, the rate of the reaction would decrease with the growing size of bubble as the diffusion path for SiO from the interface to molten iron increases[25].

Moreover by thermodynamic calculations the equilibrium constant, for the reaction (66), is found to be approximately 1.08×10^{-6} at 1600°C (See Appendix I). This small value of equilibrium constant suggests that at 1600°C and below this reaction proceeds to a very small extent. Hence SiO formation does not seem to play a major role.

CONCLUSIONS

1) During the reduction of solid silica by carbon saturated iron in the present system, silicon is transferred to the metal and carbon monoxide is evolved. The reaction is visualised to take place by the following mechanism:
   - (a) Dissociation of silica network at the silica-metal interface;
   - (b) Transport of silicon into the bulk metal;
   - (c) Transport of oxygen from silica-metal interface to the bulk metal across a thin boundary layer in the metal;
   - (d) Reaction of carbon and oxygen at the gas bubble surface to form carbon monoxide.
2) Between 1300 to 1600°C the results are compatible with the oxygen transport control for the reaction.
3) There seems to be no effect of carbon activity on the rates at higher temperatures (1450 to 1600°C).
4) For high carbon runs, at lower temperatures (1300 to 1400°C), the rate constants are lower, consequently the Arrhenius plot in the temperature range 1300 to 1600°C is a curve, the slope of which is less negative at higher temperatures. It has not been possible to determine if this is due to a different rate controlling mechanism for the silica reduction or some other factor.
5) The activation energy for the silica reduction is in the range 75-90 kcal/mole at high temperatures which agrees well with the theoretically predicted value.

6) The thickness of the effective boundary layer for oxygen diffusion is calculated to be 0.00058 cm. This value, though very small, is in line with those of Turkdogan et al[20] and Rawling and Elliott[21].

7) The observation of gas bubbles at the silica-metal interface leads to the following definitive conclusions:

   (a) The reaction site is the silica-metal interface. Hence the reaction rate depends on the S/M interface area.

   (b) This is analogous to the carbon boil in an open hearth furnace. It could be concluded that CO bubbles in an acid open hearth are formed by the same mechanism as in here. Extending the reasoning, it could be said that for silica saturated slags the CO formation during the reduction could occur at the slag-metal interface.

8) Finally, on the basis of the evidence of activation energy and reaction order, the silica reduction reaction is believed to be transport controlled; the diffusion of oxygen in the liquid iron being the rate limiting step.

TABLE I(a) Unstirred Melt

Time-Volume of Carbon Monoxide Measurements

Area of Cross Section of Capillary Tube = 0.033 cm^2

Run No. & Temp.	Time Min.	Volume in cms.	Run No. & Temp.	Time Min.	Volume in cms.
1 to 5	Preliminary Runs		6 - IV 1445°C	230	2018.5
6				260	2190.5
6 - I 1290°C	60	306.8		270	2348.2
	70	360.0		280	2490
	80	407.5		289	2608.5
	90	452.4		300	2742.8
	100	492.5		308	2835.0
6 - II 1345°C	120	638.4	7		
	130	727.0	7 - I 1290°C	0	0
	140	800.0		10	62.6
	150	881.0		20	120.6
	160	954.5		30	170.3
6 - III 1385°C	180	1178.0		40	219.6
	190	1305.4		50	262.9
	200½	1428.5		60	310.2
	210	1531.0		70	358.7
	220	1634.5		80	401.2
	225	1682.8		90	444.1

Table I(a) continued

Run No. & Temp.	Time Min.	Volume in cms.	Run No. & Temp.	Time Min.	Volume in cms.
7 - II 1347°C	100	519.7	7 - IV 1448°C	332	2505.0
	120	689.0		340	2625.0
	130	766.3		350	2771.8
	140	827.7		360	2912.8
	150	883.1		370	3051.7
	160	940.7		380	3187.3
	170	992.4		390	3321.1
	180	1040.1		400	3453.0
7 - III 1398°C	192	1152.2		410	3581.0
	200	1238.8		420	3706.2
	210	1348.6	8	FAILURE	
	220	1451.8	9 - I 1285°C	0	0
	230	1556.0		10	74.3
	240	1650.9		20	143.2
	250	1743.1		30	202.5
	260	1834.9		40	238.3
	270	1921.2		50	317.0
	280	2005.4	9 - II 1332°C	67	491.0
	290	2089.4		70	532.3
	300	2172.2		80	648.1
	310	2250.6		90	761.8

Table I(a) continued

Run No. & Temp.	Time Min.	Volume in cms.	Run No. & Temp.	Time Min.	Volume in cms.
9 - II (cont'd)	100	871.4	10 - II 1351°C	96	369.4
	110	964.8		100	392.5
	120	1063.0		110	446.8
9 - III 1388°C	167	1656.5		120	497.1
	170	1698.5		130	548.0
	180	1869.3		140	595.1
	190	2042.5		150	643.4
	200	2202.6		160	688.9
	210	2383.4		170	734.7
	220	2439.8	10 - III 1402°C	210	1015.6
	230	2681.8		220	1103.2
	240	2823.2		230	1185.4
10				240	1265.2
10 - I 1302°C	0	0		250	1345.5
	10	43.6		260	1418.8
	20	81.7		270	1491.9
	30	119.7		280	1566.6
	40	154.6	10 - IV 1451°C	323	2033.7
	50	188.7		330	2118.2
	60	224.6		340	2238.8
	70	257.0		350	2352.7
	75	271.3		360	2462.7

Table I(a) continued

Run No. & Temp.	Time Min.	Volume in cms.	Run No. & Temp.	Time Min.	Volume in cms.
10 - IV (cont'd)	370	2570.6	11 - III (cont'd)	200	1991.5
	380½	2679.2		210	2141.6
	390	2777.5		220	2286.4
	400	2879.2		230	2424.0
11 - I 1302°C	0	0	11 - IV 1454°C	290	3368.8
	10	71.0		300½	3577.1
	20	130.8		310	3753.1
	30	183.8		320	3933.9
	40	232.6		330	4106.5
	50	284.7		335	4190.0
	60	334.0	12 - I 1301°C	0	0
11 - II 1353°C	85	554.7		10	74.6
	90	610.3		20	136.7
	100	718.7		30	210.0
	110	819.6		40	274.0
	120	918.4		50	336.0
	130½	1018.1		60	388.4
	140	1103.0		70	444.5
11 - III 1403°C	178	1640.3	12 - II 1352°C	80	529.4
	180	1673.8		90	646.5
	190	1834.4		100	750.0

Table I(a) continued

Run No. & Temp.	Time Min.	Volume in cms.
12 - II (cont'd)	110	851.0
	120	945.8
	130	1040.2
	140	1139.0
	150	1214.5
12 - III 1402°C	174	1534.1
	180	1632.9
	190	1795.3
	200	1959.0
	210	2113.8
	220	2258.4
	230	2399.0
	235	2470.3
12 - IV 1454°C	275	3226.0
	280	3348.3
	290	3588.4
	300	3818.0
	310	4026.8
	320	4230.0
	330	4424.8
	334	4495.5

Table I(b)

Stirred Melt

Run No. & Temp.	Time Min.	Volume in cms.
13 - I 1402°C	0	0
	10	202.0
	20	393.5
	30	549.0
	40	726.0
	50	872.6
13 - II 1459°C	59	1143.4
	60	1181.0
	69	1535.5
	80	1951.4
	90	2268.7
	100	2613.8
	110	2968.9
13 - III 1521°C	117	3437.1
	120	3696.0
	125	4125.0
	130	4547.0
	135	4942.0
	140	5335.8
	145	5683.8

Table I(b) continued

Run No. & Temp.	Time Min.	Volume in cms.	Run No. & Temp.	Time Min.	Volume in cms.
13 - IV 1555°C	152	6352.5	14 - I (cont'd)	40	232.0
	155½	6853.5		42	248.0
	160	7450.8		44	257.4
	165	7994.5	14 - II 1453°C	60	309.5
	170	8494.0		65	379.4
	175	8936.8		70	440.4
	180	9356.0		74½	490.0
	185	9737.0		80	561.0
13 - V 1600°C	191	10425.0		85	626.0
	195	11047.0		90	678.0
	200	11701.5		95	749.5
	205	12240.0		100	800.0
	210	12670.8		105	867.0
	215	13071.0	14 - III 1510°C	110	959.8
	220	13413.5		115	1064.0
	225	13748.0		120	1151.0
	230	14059.0		125	1240.5
14 - I 1386°C	23	120.0		130	1334.8
	25	136.0		135	1420.5
	30	172.8		141	1532.0
	34	200.4		150	1677.9
	37	225.2		160	1846.0

Table I(b) continued

Run No. & Temp.	Time Min.	Volume in cms.	Run No. & Temp.	Time Min.	Volume in cms.
14 - IV 1555°C	165	2000.0	15 - II 1363°C	45	336.2
	170	2129.1		51	453.6
	180	2413.6		60	596.0
	190	2677.8		70	749.0
	200	2938.0		80	886.0
	210	3172.2		90	1004.0
	220	3395.0		95	1065.7
14 - V 1606°C	225	3576.7	15 - III 1402°C	100	1184.5
	230	3791.0		110	1430.6
	240	4196.5		120	1665.7
	250	4569.0		130	1898.0
	260	4917.5		140	2126.0
	269	5204.5		150	2349.1
	280	5596.0	15 - IV 1453°C	155	2544.0
	290	5896.0		160	2809.5
15 - I 1306°C	0	0		170	3397.8
	5	54.5		180	3789.8
	10	101.5		190	4265.5
	15	154.5		195	4482.0
	20	171.7	15 - V 1498°C	200	4838.0
	25	192.2		210	5600.0
	30	219.5		220	6379.4
	35	244.6		230	7114.0
	40	273.6			

Table I(b) continued

Run No. & Temp.	Time Min.	Volume in cms.	Run No. & Temp.	Time Min.	Volume in cms.
15 - VI 1550°C	240	8089.0	16 - II 1466°C	55½	1367.0
	245	8698.0		60	1546.8
	250	9255.0		65	1723.5
	255	9868.0		70	1945.6
	260	10381.0		80	2386.0
	265	10890.0		85	2579.4
	270	11393.0		90	2763.9
15 - VII 1600°C	275	12174.5		95	2943.0
	280	13005.0		100	3129.0
	285	13720.5		105	3304.0
	290	14412.0	16 - III 1500°C	110	35438.0
	295	15079.0		120	4113.5
	300	15623.0		130	4666.4
	305	16079.0		140	5193.1
	310	16701.0		150	5719.0
	312	16995.0		155	65956.3
16 - I 1404°C	0	0	16 - IV 1560°C	165	6714.5
	10	379.5		170	7193.8
	20	639.6		180	7995.1
	30	828.1		190	8713.6
	40	1022.8		195	9061.0
	50	1192.8			

Table I(c) Carbon Saturated Melt

Run No. & Temp.	Time Min.	Volume in cms.	Run No. & Temp.	Time Min.	Volume in cms.
16 - V 1603°C	202	9761.8	17 - III 1550°C	108	6752.5
	205	10143.0		110	6914.0
	210	10780.0		120	8276.0
	215	11376.0		130	9286.5
	220	11879.0		140	10134.5
	225	12322.0		150	10833.5
	230	12698.0	17 - IV 1622°C	157	11591.0
	235	13043.5		160	12136.0
	240	13351.8		165	13083.0
17 - I 1425°C	0	0		170	13928.0
	10	1030.0		175	14688.0
	20	1491.0		180	15366.0
	30	1854.0		185	16046.0
	35	2056.7		190	16652.5
17 - II 1687°C	40	2386.7	18 - I Unsteady Temperature	0	0
	50½	3274.0		10	289.3
	60	3958.0		20	481.5
	70	4612.0		30½	624.5
	80½	5132.8		40	758.5
	90	5555.0	18 - II 1396°C	50	995.0
	100	5980.0		60	1225.6

Table I(c) continued

Run No. & Temp.	Time Min.	Volume in cms.	Run No. & Temp.	Time Min.	Volume in cms.
18 - II (cont'd)	70	1518.0	18 - VI (cont'd)	265	13258.9
	80	1806.4		270	13789.0
	90	2050.6		275	14302.5
	95	2164.9		280	14843.0
18 - III 1459°C	110	2999.0	19 1464°C	0	0
	120	3478.0		10	750.0
	130	3995.0		20	1474.6
	140	4458.8		30	1940.8
	150	4955.6		40	2493.6
18 - IV 1504°C	160	5677.0		50	3031.8
	170	6339.0		60	3530.8
	180	6834.0		70	4000.5
	190	7271.8		80	4456.5
	200	7705.5		90½	4937.2
18 - V 1560°C	210	8379.5		100	5364.8
	220	9157.5		110	5805.1
	230	9946.0		120	6247.5
	240	10651.0		130	6698.9
18 - VI 1600°C	250	11555.0		140	7094.8
	255	12116.5		150	7456.6
	260	12726.5		160	7818.5

Table I(c) continued

Run No. & Temp.	Time Min.	Volume in cms.	Run No. & Temp.	Time Min.	Volume in cms.
19 (cont'd)	170	8191.2	20 - III (cont'd)	150	5143.2
	180	8530.5		160	5493.4
	190	8894.0	20 - IV 1555°C	166	5795.8
	200	9240.3		171	6085.8
20 - I 1300°C	0	0		180	6570.8
	10	354.5		190	7076.3
	20	605.0		200	7570.4
	31	823.5		210	8051.0
	40	975.0	20 - V 1600°C	220	8814.5
	45	1057.6		225	9303.5
20 - II 1453°C	55	1470.0		230	9755.8
	60	1653.8		235	10184.5
	70	2010.5		240	10584.6
	80	2334.5		245	10979.0
	90	2637.8		250	11358.0
	100	2944.8		255	11770.8
	105	3186.7		260	12163.5
20 - III 1498°C	111	3460.0	21 - I 1370°C	0	0
	120	3892.0		10	286.7
	130½	4350.8		20	471.6
	140	4761.5		30	635.5

Table I(c) continued

Run No. & Temp.	Time Min.	Volume in cms.
21 - I (cont'd)	40	782.2
	50	913.5
21 - II 1447°C	62	1318.2
	70	1604.5
	80	1943.5
	90	2268.8
	100	2565.8
	110	2851.7
21 - III 1505°C	120	3411.0
	130	3923.5
	140	4428.8
	150	4828.5
	160	5253.0
	170	5625.4
21 - IV 1561°C	180	6278.2
	190	6938.9
	200	7483.4
	210	7934.0
	220	8365.0
	230	8828.4
21 - V 1600°C	241	9567.0
	245	9835.0
	250	10182.2
	255	10523.5
	260	10819.8
	265	11090.5
	270	11354.0
	275	11663.5
	280	11879.0
	285	12155.0
	290	12417.0

TABLE II — Experimental constants

Run No.	Mass of the C-saturated Iron W gms.	Initial Carbon content of the iron %	Internal Diameter of the Silica Vessel cons.	Silica-Melt Interfacial Area A - cm^2	Average Density of the melt ρ gms/cm^3	Average Volume of the melt $V = \frac{W}{\rho}$ cm^3	V/A cm.	Ambient Conditions	
								Atmospheric Pressure mm(Hg)	Average Room Temperature °C
6 (I-IV)	25.940	4.64	1.25	11.80	6.96	3.5830	0.3036	739.0	26
7 (I-IV)	5.00	4.64	1.30	2.65	6.96	0.7184	0.2705	752.0	27
9 (I-III)	25.00	4.64	1.25	11.80	6.96	3.591	0.3043	750.0	26
10(I-IV)	5.00	4.64	1.30	2.65	6.96	0.7184	0.2705	752.0	25
11(I-IV)	25.00	4.64	1.25	11.80	6.96	3.591	0.3043	746.0	24
12(I-IV)	35.00	4.50	1.70	13.60	6.78	5.162	0.3795	759.5	22
13(I-V)	35.00	4.50	1.70	13.60	6.78	5.162	0.3795	757.0	23
14(I-V)	10.00	4.50	1.70	4.54	6.78	1.474	0.3246	751.0	25
15(I-VII)	60.00	4.50	1.70	17.90	6.78	8.849	0.4943	761.0	21
16(I-V)	35.00	4.50	1.70	13.60	6.78	5.162	0.3795	749.0	24
17(I-V)	35.00	carbon saturated during the entire run	1.70	13.60	6.78	5.162	0.3795	759.0	25
18(I-VI)	35.00		1.70	13.60	6.78	5.162	0.3795	758.5	25
19	35.00	4.50	1.70	13.60	6.78	5.162	0.3795	762.0	24
20(I-V)	35.00	carbon saturated during the entire run	1.70	15.50	6.78	5.162	0.3330	752.0	26
21(I-V)	35.00		1.70	15.50	6.78	5.162	0.3330	747.5	25

TABLE III — Specific Rate Constant

Run No.	Temperature °C	Mean $\frac{dv}{dt} v^{1/2}$ $cm^3/min\ cm^{3/2}$	factor for converting the v to STP	$10^3 \times \frac{d[\%Si]}{dt}[\%Si]^{1/2}$ 1/min.	$\frac{32}{28\ 09} \frac{V}{A}$ cm.	Specific Rate Constant $k \times 10^4$ cm/min.	5 + log k	$1/T \times 10^4\ °K^{-1}$
6-I	1290	0.5508		0.05804		0.2006	0.3023	6.398
6-II	1345	1.204	0.8875	0.1268	0.3458	0.4365	0.6420	6.181
6-III	1385	2.622		0.2763		0.9552	0.9801	6.031
6-IV	1445	4.326		0.4558		1.577	1.1979	5.821
7-I	1290	0.3748		0.4494		1.384	1.1402	6.398
7-II	1347	1.128	0.9003	1.352		4.165	1.6196	6.172
7-III	1398	2.280		2.734	0.3081	8.424	1.9255	5.984
7-IV	1448	4.218		4.520		13.920	2.1436	5.870
9-I	1285	0.4770		0.05128		0.1777	0.2497	6.428
9-II	1332	1.783	0.9009	0.1916	0.3466	0.6642	0.8223	6.230
9-III	1388	4.4430		0.4776		1.6553	1.2188	6.020
10-I	1302	0.2472		0.2939		0.9055	0.9568	6.349
10-II	1351	0.687		0.8017	0.3081	2.486	1.3956	6.157

Table III continued

Run No.	Temperature °C	Mean $\frac{dv}{dt}v^{1/2}$ $cm^3/min\ cm^{3/2}$	factor for converting the v to STP	$10^3 \times \frac{d[\%Si]}{dt}[\%Si]^{1/2}$	$\frac{32}{28\ 09}\frac{V}{A}$ cm.	Specific Rate Constant $k \times 10^4$ cm/min.	5 + log k	$1/T \times 10^4\ °K^{-1}$
10-III	1402	1.6848	0.8952	2.0034		6.172	1.7904	5.970
10-IV	1451	3.222		3.8314		11.75	2.0701	5.800
11-I	1302	0.4005		0.04310		0.1493	0.1741	6.350
11-II	1353	1.623	0.9022	0.1746		0.6051	0.7819	6.150
11-III	1403	4.092		0.4404	0.3466	1.526	1.1835	5.966
11-IV	1454	6.696		0.7207		2.497	1.3974	5.791
12-I	1301	0.5640		0.04226		0.1826	0.2615	6.353
12-II	1352	1.722	0.9245	0.12903	0.4322	0.5575	0.7463	6.153
12-III	1402	4.177		0.3129		1.352	1.1309	5.969
12-IV	1454	8.154		0.6109		2.640	1.4216	5.791
13-I	1402	2.176		0.1451		0.6270	0.7973	5.97
13-II	1459	9.378	0.9186	0.6256		2.703	1.4319	5.773
13-III	1521	32.538		2.170	0.4322	9.379	1.9721	5.574
13-IV	1555	54.780		3.655		15.79	2.1984	5.470

Table III continued

Run No.	Temperature °C	Mean $\frac{dv}{dt} v^{1/2}$ $cm^3/min\ cm^{3/2}$	factor for converting the v to Stp	$10^3 \times \frac{d[\%Si]}{dt}[\%Si]^{1/2}$	$\frac{32}{28\ 09\ cm} \frac{V}{A}$	Specific Rate Constant $k \times 10^4$ cm/min.	5 + log k	$1/T \times 10^4\ °K^{-1}$
13-V	1600	67.020		4.471		19.32	2.2860	5.339
14-I	1386	0.5322		0.2246		0.8300	0.9190	6.027
14-II	1453	1.782	0.8987	0.7530		2.785	1.4448	5.794
14-III	1510	3.888		1.644	0.3697	6.077	1.7837	5.608
14-IV	1555	8.016		3.389		12.53	2.0979	5.471
14-V	1606	14.952		6.323		23.37	2.3688	5.322
15-I	1306	0.4644		0.0140		0.07915	1.8985	6.333
15-II	1363	2.308		0.0698		0.3934	0.5948	6.112
15-III	1402	5.304		0.161		0.9041	0.9562	5.969
15-IV	1453	17.250	0.9297	0.522	0.5630	2.940	1.4683	5.794
15-V	1498	35.634		1.079		6.073	1.7834	5.646
15-VI	1550	51.480		1.558		8.775	1.9432	5.486
15-VII	1600	107.580		3.257		18.340	2.2633	5.339

Table III continued

Run No.	Temperature °C	Mean $\frac{dv}{dt} v^{1/2}$ $cm^3/min\ cm^{3/2}$	factor for converting the v to STP	$10^3 \times \frac{d[\%Si]}{dt}[\%Si]^{1/2}$	$\frac{32}{28\ 09}\ \frac{V}{A}$ cm	Specific Rate Constant $k \times 10^4$ cm/min.	5 + log k	$1/T \times 10^4\ °K^{-1}$
16-I	1404	3.388	0.9058	0.2210	0.4322	0.9560	0.9805	5.963
16-II	1466	11.856		0.774		3.346	1.5245	5.750
16-III	1500	21.822		1.425		6.158	1.7895	5.640
16-IV	1560	42.825		2.797		12.09	2.0822	5.450
16-V	1603	63.049		4.117		17.79	2.2502	5.330
17-I	1425	10.116	0.9148	0.6707	0.4322	2.898	1.4621	5.889
17-II	1487	24.210		1.605		6.936	1.8411	5.681
17-III	1550	57.948		3.842		16.600	2.2202	5.486
17-IV	1622	107.610		7.134		30.830	2.4890	5.277
18-II	1396	6.6804	0.9142	0.4420	0.4322	1.912	1.2814	5.991
18-III	1459	18.516		1.226		5.298	1.7242	5.774
18-IV	1504	25.284		1.685		7.282	1.8622	5.628
18-V	1560	46.140		3.055		13.210	2.1209	5.456

Table III contiaued

Run No.	Temperature °C	Mean $\frac{dv}{dt} v^{1/2}$ $cm^3/min\ cm^{3/2}$	factor for converting the v to STP	$10^3 \times \frac{d[\%Si]}{dt}[\%Si]^{1/2}$	$\frac{32}{28\ 09} \frac{V}{A}$ cm	Specific Rate Constant $k \times 10^4$ cm/min.	5 + log k	$1/T \times 10^4 °K^{-1}$
18-VI	1600	76.560		5.071		21.910	2.3406	5.339
19	1464	18.624	0.9213	1.246	0.4322	0.5389	1.7315	5.754
20-I	1380	3.144		0.2045		0.7756	0.8896	6.050
20-II	1453	9.078	0.9034	0.5906	0.3793	2.240	1.3502	5.794
20-III	1498	16.665		1.083		4.109	1.6138	5.646
20-IV	1555	25.762		1.676		6.357	1.8033	5.471
20-V	1600	50.984		3.316		12.57	2.0993	5.339
21-I	1370	2.265		0.1466		0.5560	0.7451	6.086
21-II	1447	8.730	0.9008	0.5654	0.3793	2.144	1.3312	5.813
21-III	1505	18.162		1.176		4.460	1.6493	5.624
21-IV	1561	27.318		1.769		6.709	1.8267	5.453
21-V	1600	38.556		2.493		9.455	1.9756	5.339

TABLE IV — Activation Energy

Condition of the Melt	Slope of the line in Arrhenius Plot	Activation Energy E kcal/mole	Thickness of Effective Boundary Layer δ cm at 1600°C
1) Unstirred (Runs 6,11&12)	−1.958	89.6	0.0024
2) Stirred (Runs 13,14,15,16)	−1.850	84.6	0.0018
3) Carbon Saturated and Stirred			
i) Runs 17&18	−1.632	74.7	0.0016
ii) Runs 20&21	−1.638	74.9	0.0033

TABLE V — Chemical Analysis

Run No.	Carbon Content % Initial	Carbon Content % Final	Final Silicon in iron %	Volume of CO evolved at STP CC	% Silicon in the iron calculated from CO Volume
15	4.50	4.05	0.598	522	0.545
16	4.50	3.88	0.750	400	0.716
17	carbon saturated during the run		0.972	514	0.919

REFERENCES

1. Arrhenius, S.: On the reaction velocity of the inversion of sucrose in acids, Zeit. Physik. Chem., 4, 226 (1889).
2. Glasstone, S., Laidler, K. J. and Eyring, H.: The Theory of Rate Processes, McGraw-Hill Book Co., Inc., New York 1941.
3. Polanyi, M.: The Transition State in Chemical Reactions, J. Chem. Soc., 629 (1937).
4. Darken, L. S. and W. R. Gurry: Physical Chemistry of Metals, McGraw-Hill Co., Inc., New York 1953, Chapter 19, 465.
5. Darken, L. S.: The Physical Chemistry of Steel Making, J. F. Elliott, Ed., p. 101, Technology Press and Wiley 1958.
6. Wagner, C.: The Physical Chemistry of Steel Making, J. F. Elliott, Ed., p. 237, Technology Press and Wiley 1958.
7. Eckert, E. R. G.: Introduction to the Transfer of Heat and Mass, McGraw-Hill Book Co., Inc., New York 1950.
8. See Reference 2, Chapter VII, p. 369.
9. Riddiford, A. C.: The Temperature Coefficient of Heterogeneous Reactions. J. of Physical Chem., 56, 746 (1952).
10. Parlee, N. A., S. R. Seagle, and R. Schuhmann, Jr.: Rate of the Carbon-Oxygen Reaction in Liquid Iron, Trans. A.I.M.E. 212, 132 (1958).
11. Pehlke, R. D., and J. F. Elliott: Solubility of Nitrogen in Liquid Iron Alloys: II. Kinetics, Trans. A.I.M.E. 227, 844 (1963).
12. Richardson, F. D.: Rates of Slag/Metal Reactions and Steel Making Processes, Iron and Coal, 1103 (1961).

13. Fulton, J. C. and J. Chipman: Slag-Metal-Graphite Reactions and the Activity of Silica in Lime-Alumina-Silica Slags. Trans. A.I.M.E., 200, 1136 (1954).

14. Fulton, J. C. and J. Chipman: Kinetic Factors in the Reduction of Silica from Blast Furnace Type Slags. Trans. A.I.M.E. 215, 888 (1959).

15. Philbrook, W. O., and L. D. Kirkbride: Rate of FeO Reduction from a $CaO-SiO_2-Al_2O_3$ slag by Carbon Saturated Iron. Trans. A.I.M.E. 206, 351 (1956).

16. Brower, T. E., and B. M. Larsen: Oxygen in Liquid Open-Hearth Steel. Trans. A.I.M.E. 172, 164 (1947).

17. Körber, F. and W. Oelsen: Mitt. Kaiser-Wilhelm-Inst. Eisenforsch Düsseldorf, 17, 39 (1935).

18. King, T. B.: Oxygen Steelmaking Processes. A.I.M.E. Proc. O.H. Conf. 42, 250 (1959).

19. Schuhmann, Jr., R.: Discussion to Ref. 14, Iron and Steel Division, Trans. A.I.M.E. 218, 1130 (1960).

20. Turkdogan, E. T., P. Grieveson and J. F. Beisler: Kinetic and Equilibrium Considerations for Silicon Reaction between Silicate Melts and Graphite-Saturated Iron. Part II: Reaction Kinetics of Silica Reduction. Trans. A.I.M.E. 227, 1265 (1963).

21. Rawling, J. R. and J. F. Elliott: The Reduction of Silica in Blast Furnace Slag-Metal Systems. To be published in Trans. A.I.M.E.

22. Rawling, J. R.: Sc.D. Thesis, Metallurgy Dept., M.I.T. (1960).

23. Grimble, M., R. G. Ward and D. J. Williams: The Kinetics of Silica Reduction by Carbon Saturated Iron. Part I. Electro-Chemical Contribution to Transfer. JISI <u>203</u>, 264 (1965).

24. Simkovich, A., Kun Li and C. L. McCabe: Kinetics of Dissolution of Solid Oxides in Liquid Iron. To be published in Trans. A.I.M.E.

25. Tiberg, L.: The Dissolution of Oxides in Carbon Steel Melts Under Vacuum. Jernkont. Ann. <u>144</u>, 771 (1960).

26. Grimble, M.: Ph.D. Thesis, Department of Metallurgy, Sheffield University 1962.

27. Fuwa, T., and J. Chipman: The Carbon-Oxygen Equilibria in Liquid Iron. Trans. A.I.M.E. <u>218</u>, 887 (1960).

28. Thermochemistry for Steelmaking Vol. II. J. F. Elliott, Molly Gleiser and V. Ramakrisha Ed., Addison-Wesley Publishing Co., Inc. Reading, Mass. 1964.

29. Taylor, J.: Silica Reduction Reaction in the Blast Furnace. JISI <u>202</u>, 420 (1964).

30. Gokcen, N. A. and J. Chipman: Silicon-Oxygen Equilibrium in Liquid Iron. Trans. A.I.M.E. <u>194</u>, 171 (1952).

31. Taylor, H. S.: The Temperature Variation of Diffusion Processes. J. Chem. Phys. <u>6</u>, 331 (1938).

32. Saito, T., Y. Kawai, K. Maruya and M. Maki: Diffusion of Some Alloying Elements in Liquid Iron, in Physical Chemistry of Process Metallurgy, Part I. G.R.St. Pierre Ed. p. 523, Interscience Publishers, New York (1961).

33. Basic Open-Hearth Steelmaking: G. Derge Ed., Chapters 15 and 16, Published by A.I.M.E. 1964 Edition.

34. King, T. B. and S. Ramachandran: Electrochemical Nature of Sulphur Transfer in the System Carbon-Saturated-Iron-Slag, in the Physical Chemistry of Steelmaking, J. F. Elliott, Ed., p. 125, Technology Press and Wiley 1958.

35. Bodsworth, C.: Physical Chemistry of Iron and Steel Manufacture, Longmans, Green & Co. Ltd. London 1963.

36. Mickley, H. S., T. K. Sherwood, and C. E. Reed: Applied Mathematics in Chemical Engineering, p. 53-57, McGraw-Hill Book Co., Inc., New York 1957.

37. A.S.T.M. Methods for Chemical Analysis of Metals (A.S.T.M. 1961).

38. Lucas, L. D.: Density of Liquid Iron-Carbon Alloys. Compt. Rend. 248, 2336 (1959).

39. Young, H. D.: Statistical Treatment of Experimental Data, McGraw-Hill Book Co., Inc. New York 1962.

APPENDIX I

(A) Calculation of Equilibrium Constant K_{Si}

In Chapter II, the silica dissociation reaction was expressed as

$$SiO_2(\beta\text{-Crist.}) = \underline{Si} + 2\underline{O} \qquad (1)$$

where the reference state for silicon and oxygen adopted, is the infinitely dilute solution in liquid iron.

The free energy change ΔG_1^o, for above reaction is calculated from the following data.

$$Si(l) + O_2(g) = SiO_2\ (\beta\text{-Crist.}) \qquad (2)$$

$$\Delta G_2^o = -226500 + 47.5\ T \qquad \text{(Ref. 28)}$$

$$Si(l) = \underline{Si}\ \text{(1\% solution, hypothetical)} \qquad (3)$$

$$\Delta G_3^o = -28500 - 6.74\ T \qquad \text{(Ref. 29)}$$

$$\frac{1}{2}\ O_2(g) = \underline{O}\ (\%) \qquad (4)$$

$$\Delta G_4^o = -28000 - 0.69\ T$$

Hence $\Delta G_1^o = -\Delta G_2^o + \Delta G_3^o + 2\Delta G_4^o$

or $\Delta G_1^o = 142000 - 55.62\ T \qquad (5)$

The equilibrium constant K_{Si}, for reaction (1) is given by

$$\Delta G_1^o = -RT \ln K_{Si}$$

or
$$\log K_{Si} = \frac{31000}{T} - 12.157 \qquad (6)$$

At 1600°C, $K_{Si} = 4.046 \times 10^{-5}$

and $K_{Si}^{1/2} = 6.36 \times 10^{-3}$.

(B) Formation of Silicon Monoxide.

In presence of CO, silica could be reduced to form silicon monoxide according to reaction

$$SiO_2(\beta\text{-Crist.}) + CO(g) = SiO(g) + CO_2(g) \qquad (7)$$

The standard free energy change for this reaction is computed from the following data available in reference (28).

$$Si(l) + \frac{1}{2} O_2(g) = SiO(g) \qquad (8)$$

$$\Delta G_8^o = -36000 - 11.7\ T$$

$$Si(l) + O_2(g) = SiO_2(\beta\text{-Crist.}) \qquad (9)$$

$$\Delta G_9^o = -226500 + 47.5\ T$$

$$CO\,(g) + \frac{1}{2}\,O_2(g) \;=\; CO_2(g) \qquad (10)$$

$$\Delta G^o_{10} \;=\; -66555 + 20.36\,T$$

Combining these equations, the standard free energy change for reaction (7) is obtained as,

$$\Delta G^o_7 \;=\; +\,123945 - 38.84\,T \qquad (11)$$

Hence the equilibrium constant K_7, is given by

$$\log K_7 \;=\; -\frac{27100}{T} + 8.50 \qquad (12)$$

At 1600°C, $K_7 \;=\; 1.08 \times 10^{-6}$

Since $K_7 \;=\; \dfrac{p_{SiO}\,p_{CO_2}}{a_{SiO_2}\,p_{CO}}$,

$$p_{SiO}\,p_{CO_2} \;\approx\; 10^{-6} \quad \text{as} \quad a_{SiO_2} \;=\; 1 \quad \text{and} \quad p_{CO} \;\approx\; 1 \text{ atm.}$$

Hence at 1600°C, SiO may be formed to a small extent only.

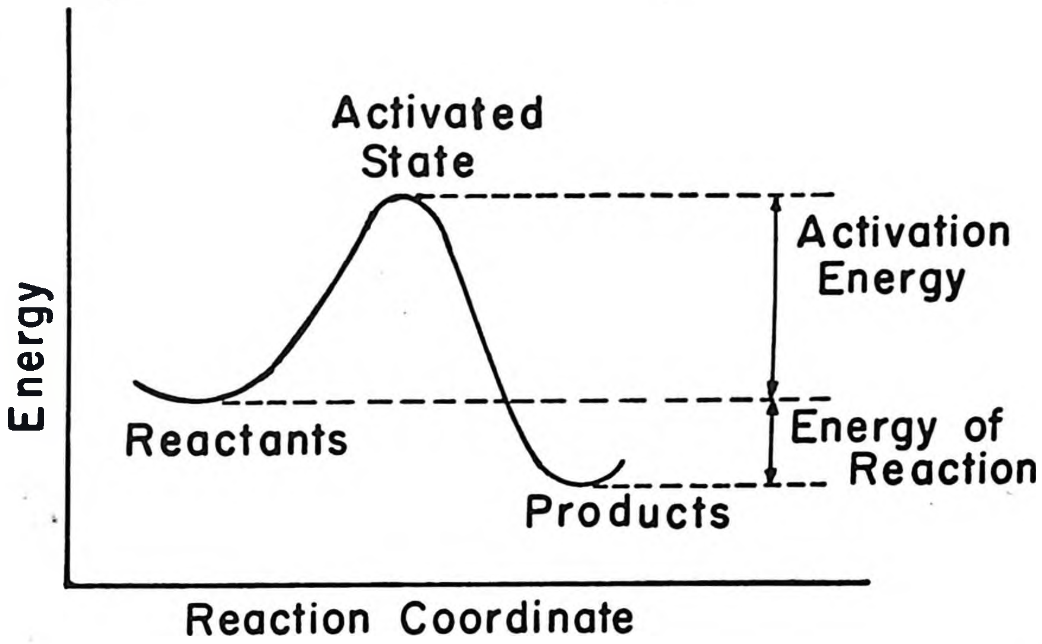

Figure 1 Schematic Representation of Energy Change in a Reaction.

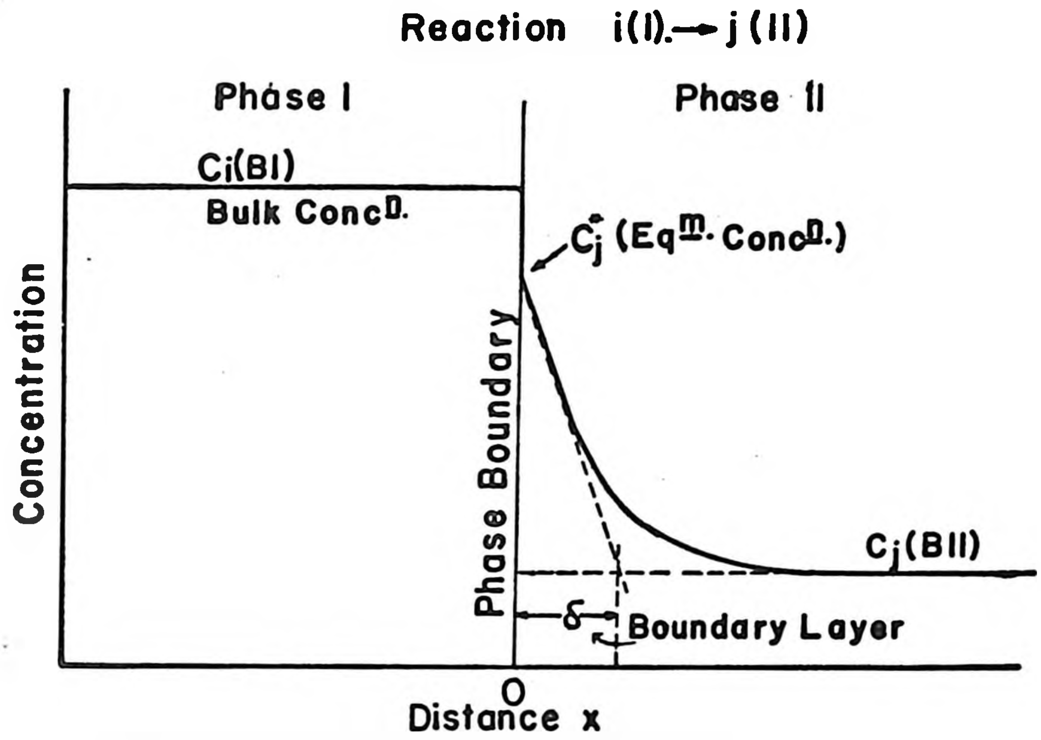

(a) Transport Control in Phase II

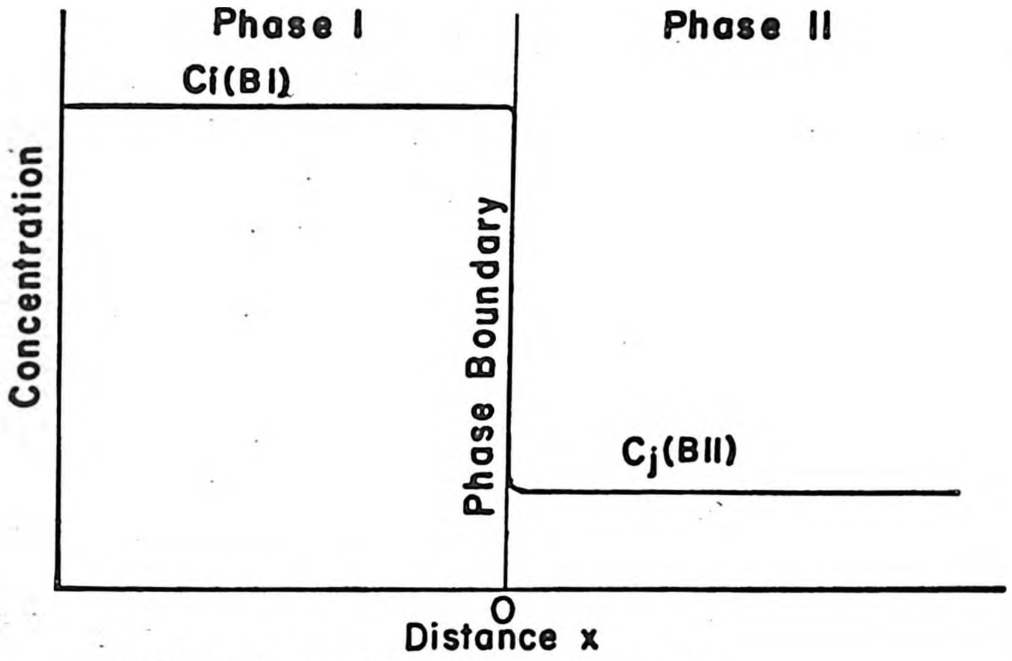

(b) Chemical Reaction Control

Figure 2 Schematic Representation of Transport and Chemically Controlled Processes.

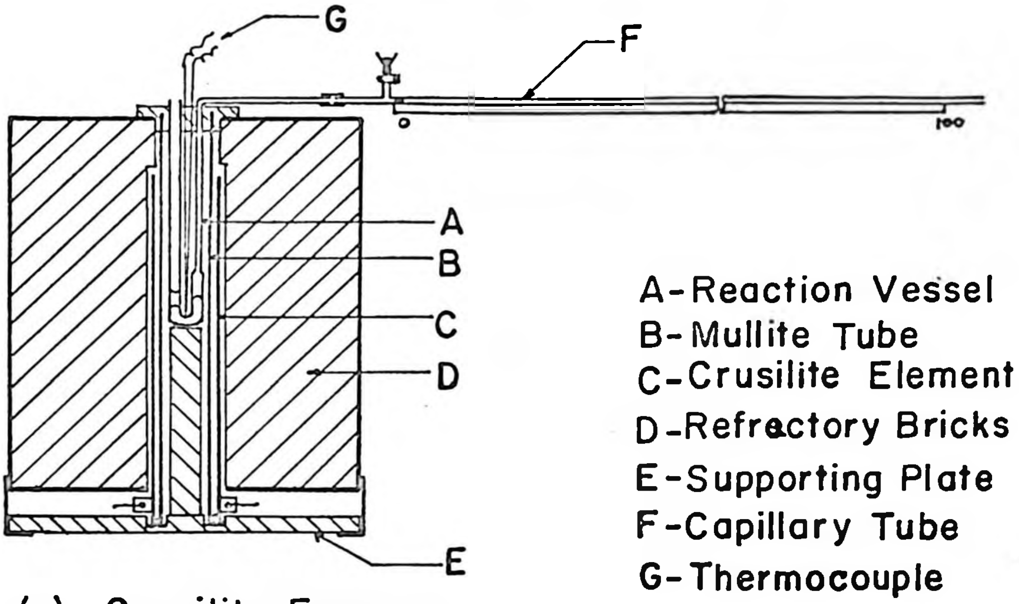

(a) Crusilite Furnace

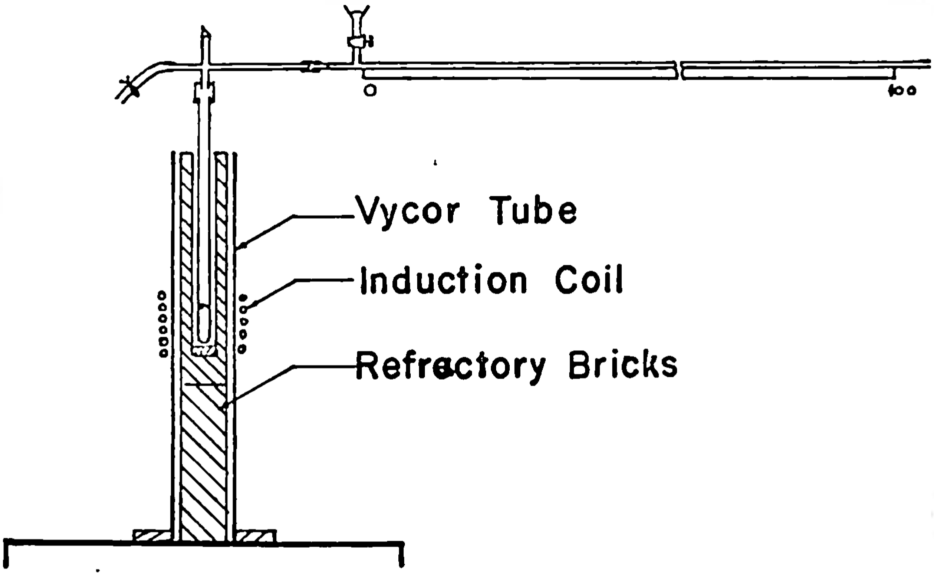

(b) Induction Furnace

Figure 3. Schematic Arrangement of Apparatus.

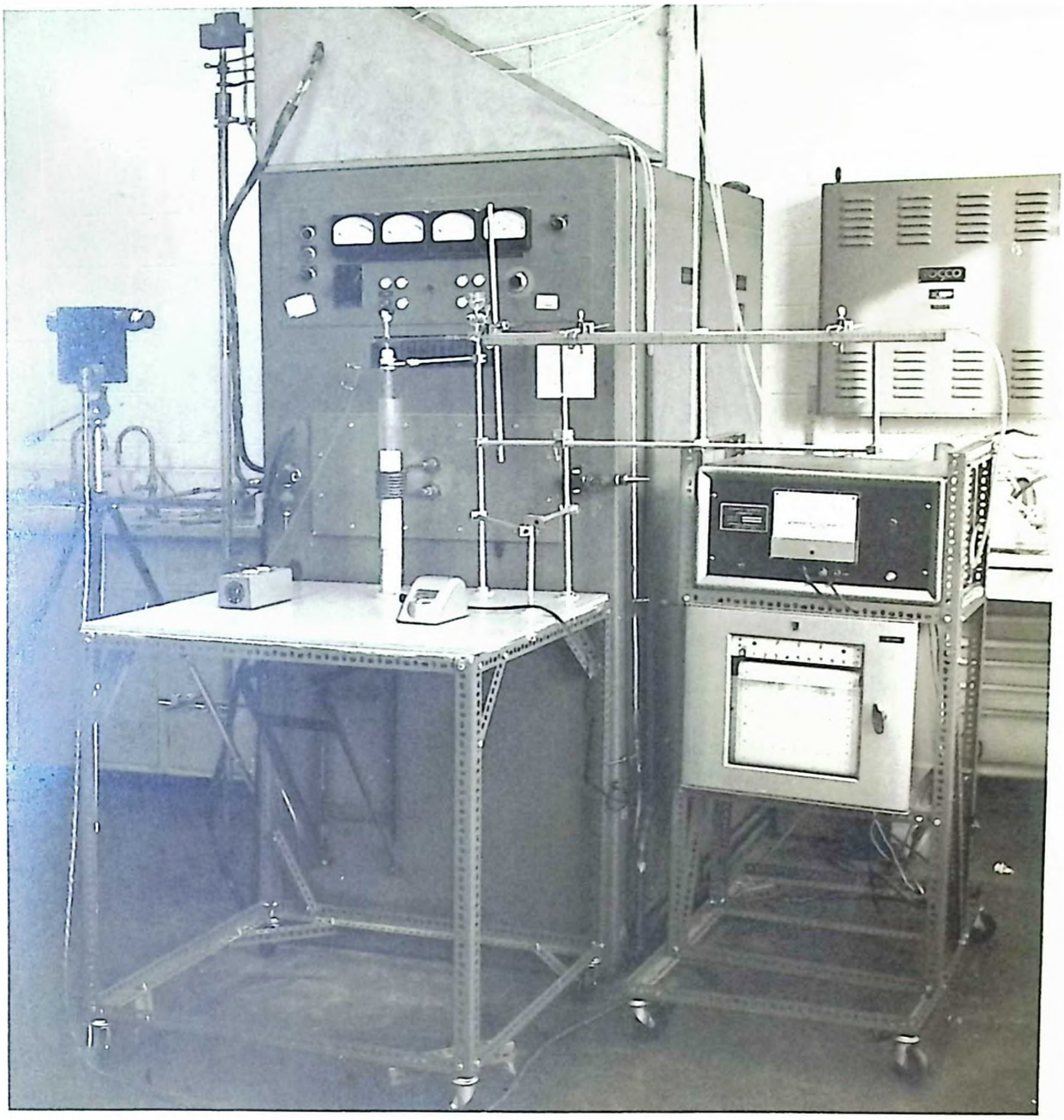

Figure 4. Photograph of Apparatus

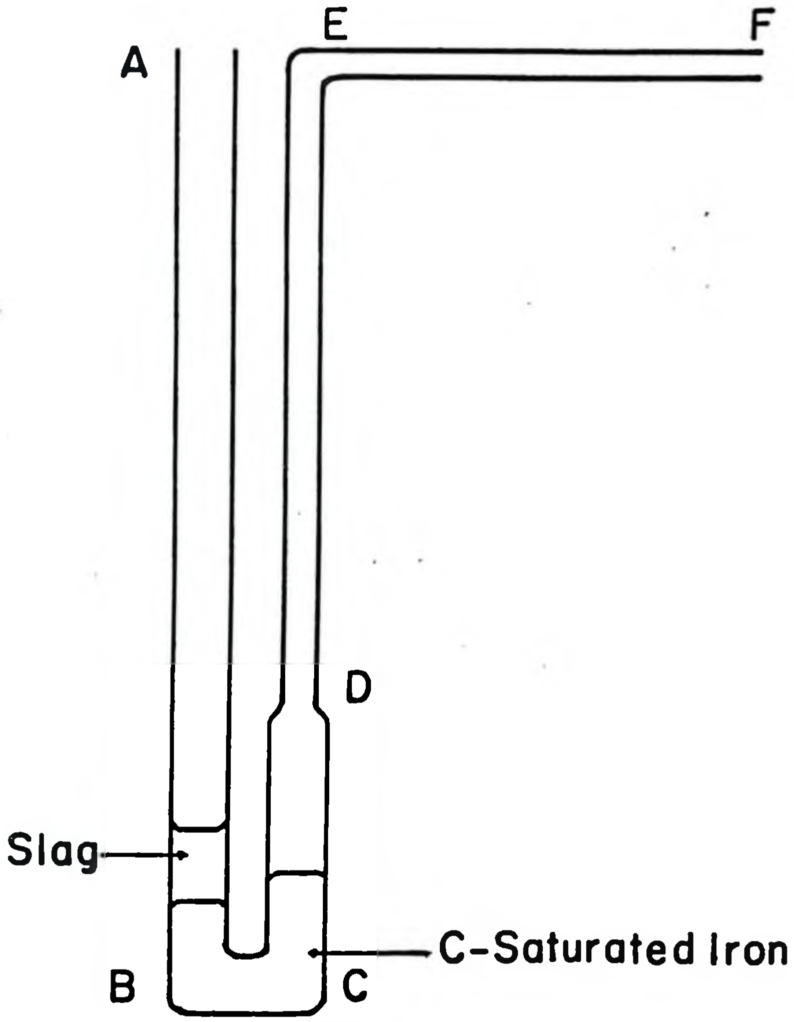

Figure 5(a) "U" Shaped Reaction Vessel

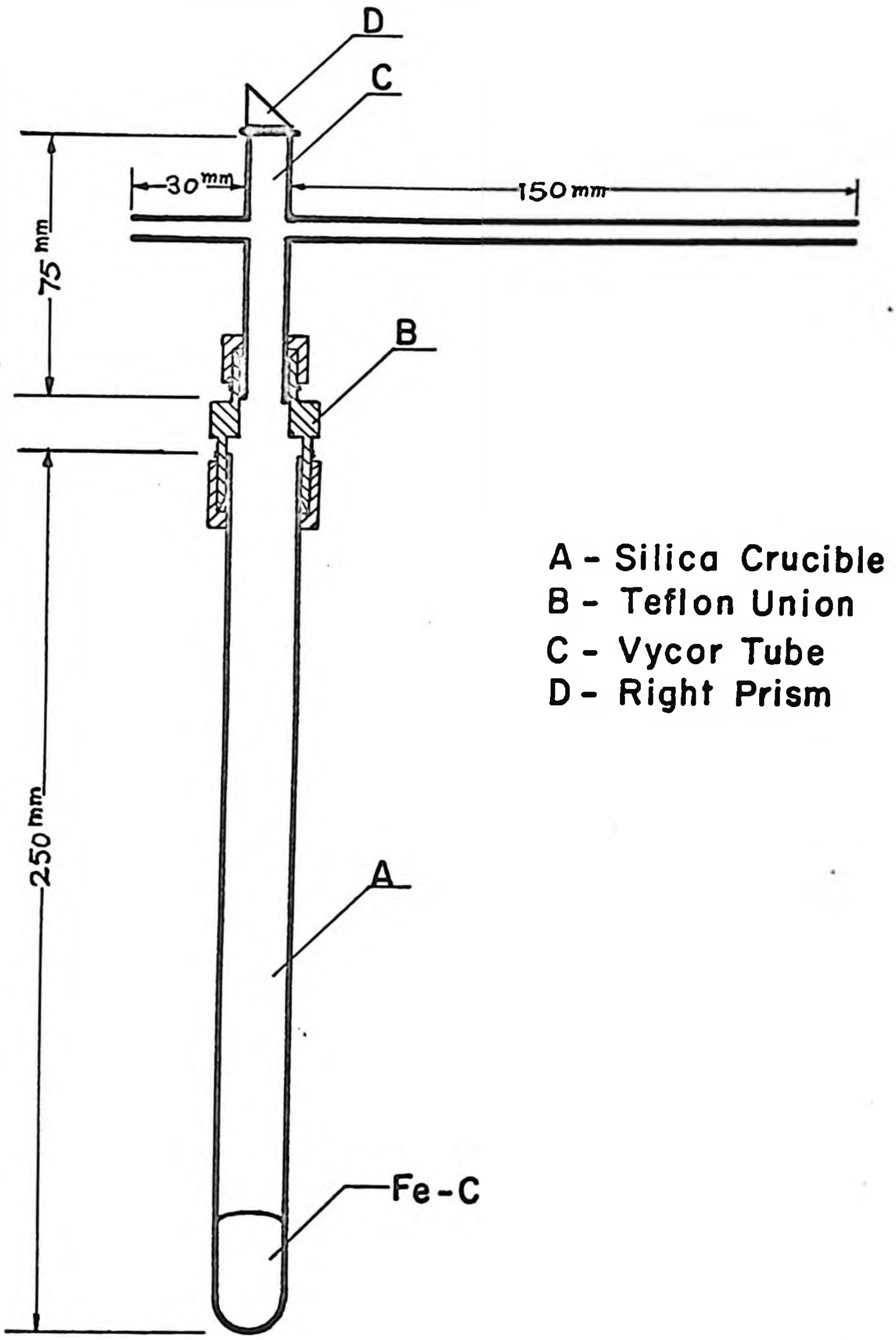

Figure 5(b) Modified Reaction Vessel

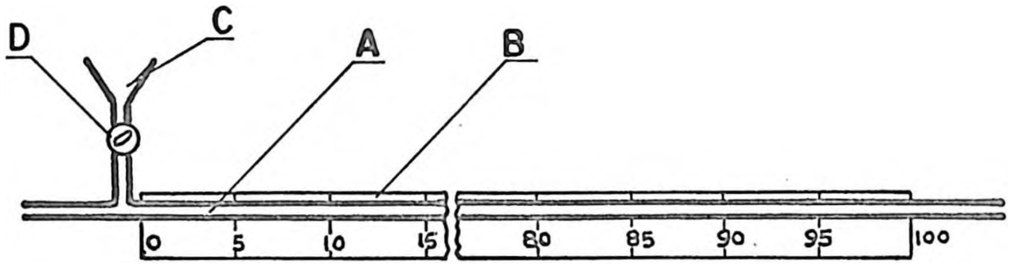

A 2 mm Bore Capillary Tube
B Meter Scale
C Mercury Reservoir
D Stop Cock

Figure 6– Schematic Diagram of Capillary Tube

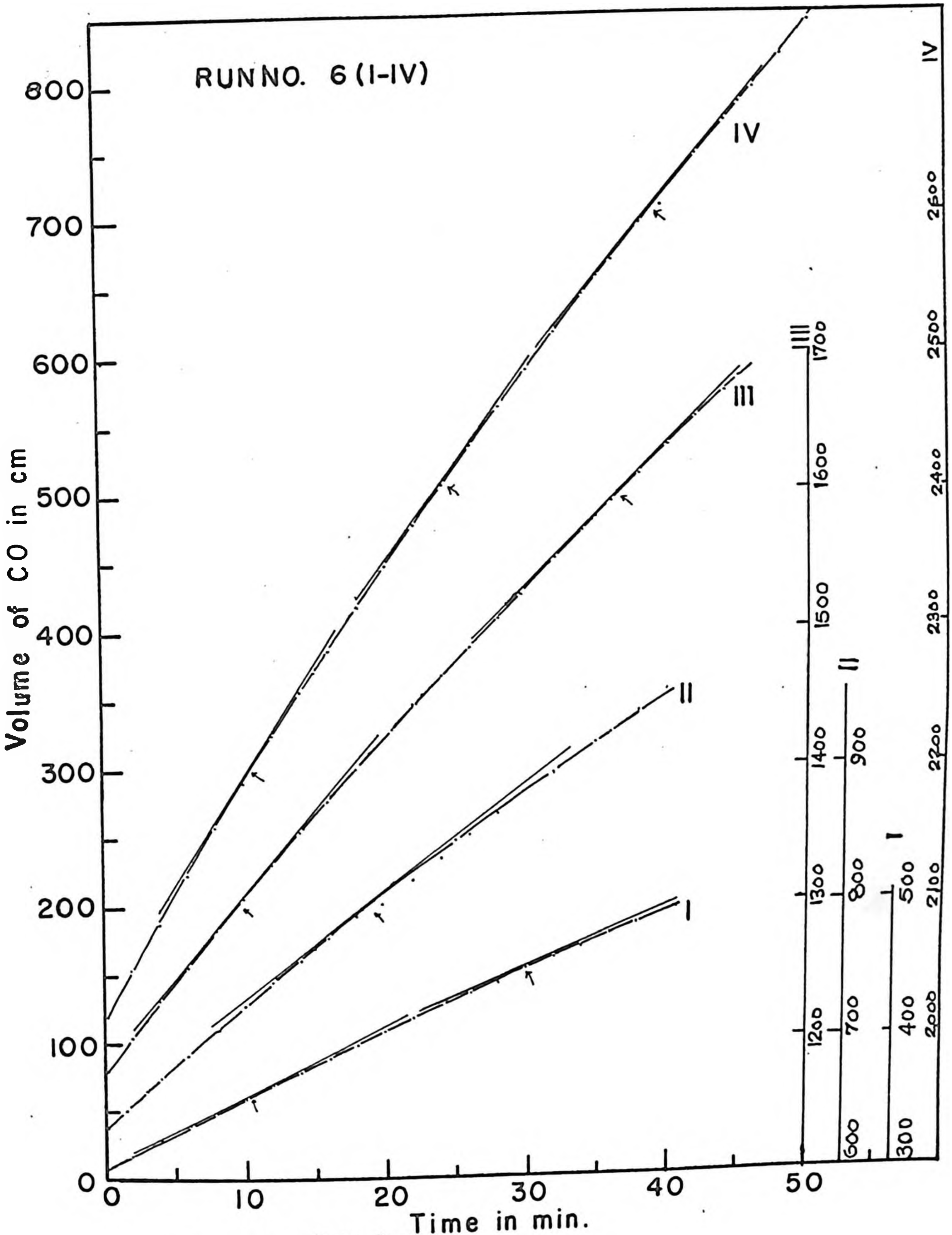

Figure 7 Rate Curves

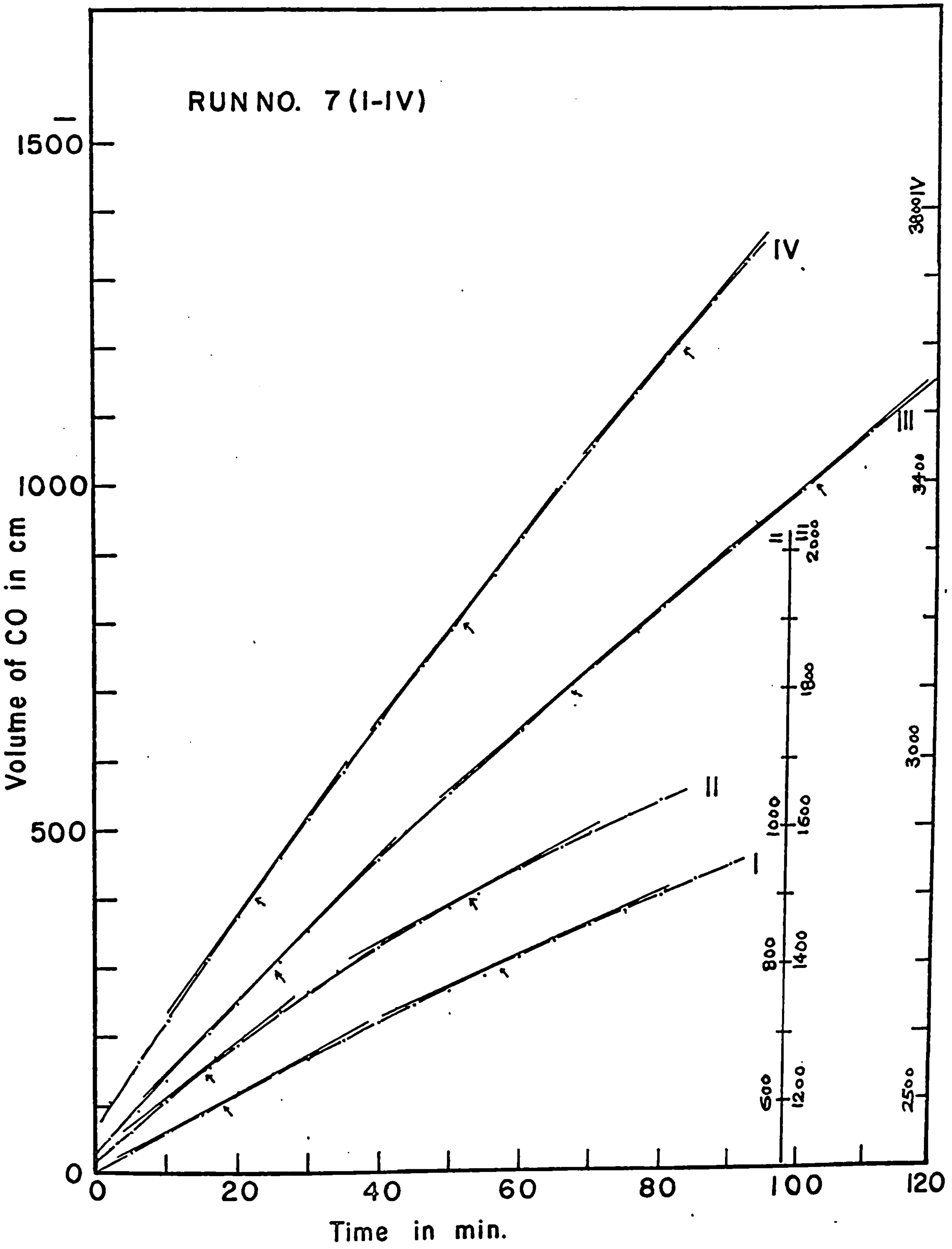

Figure 8 Rate Curves

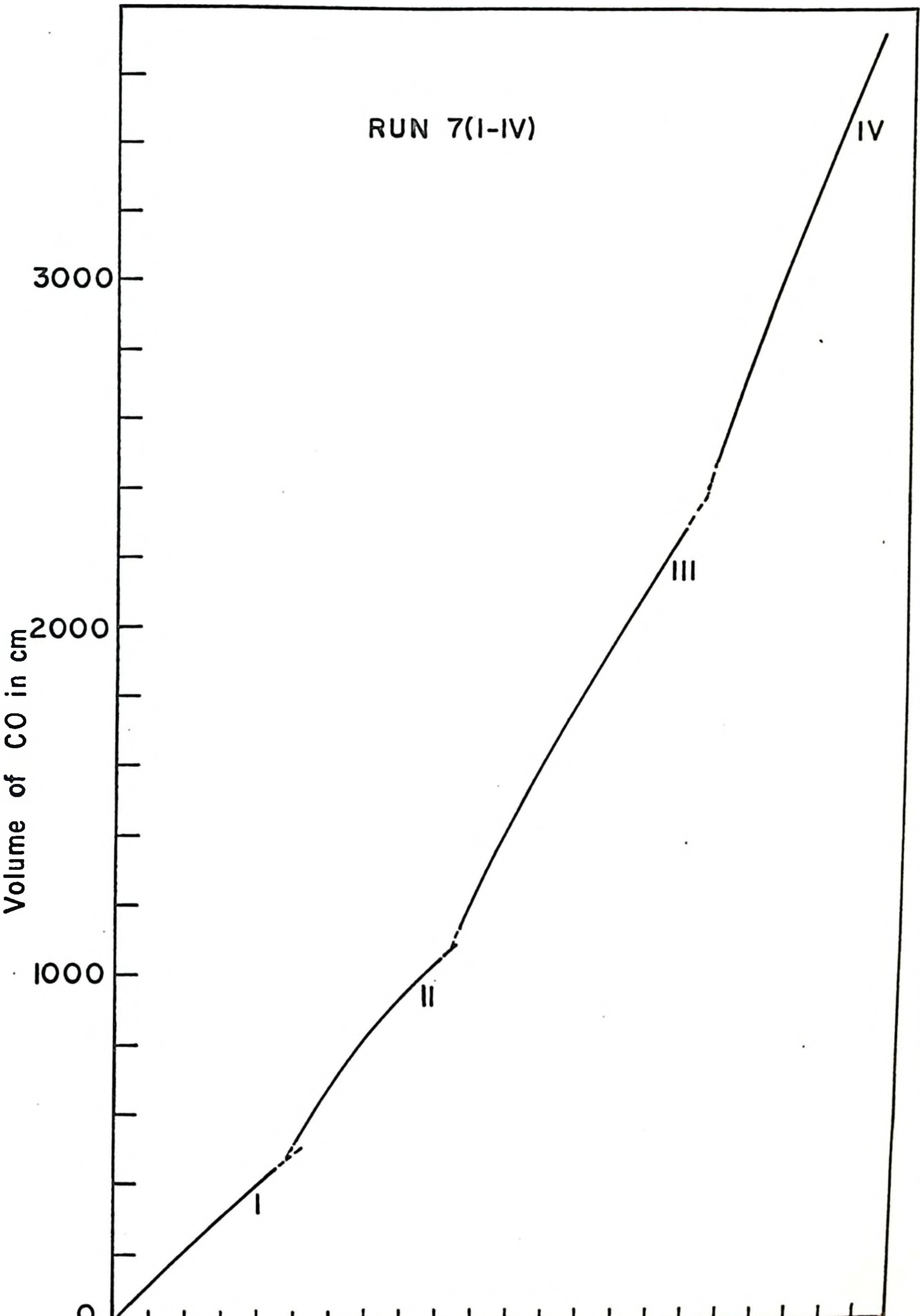

Figure 9 Rate Curves

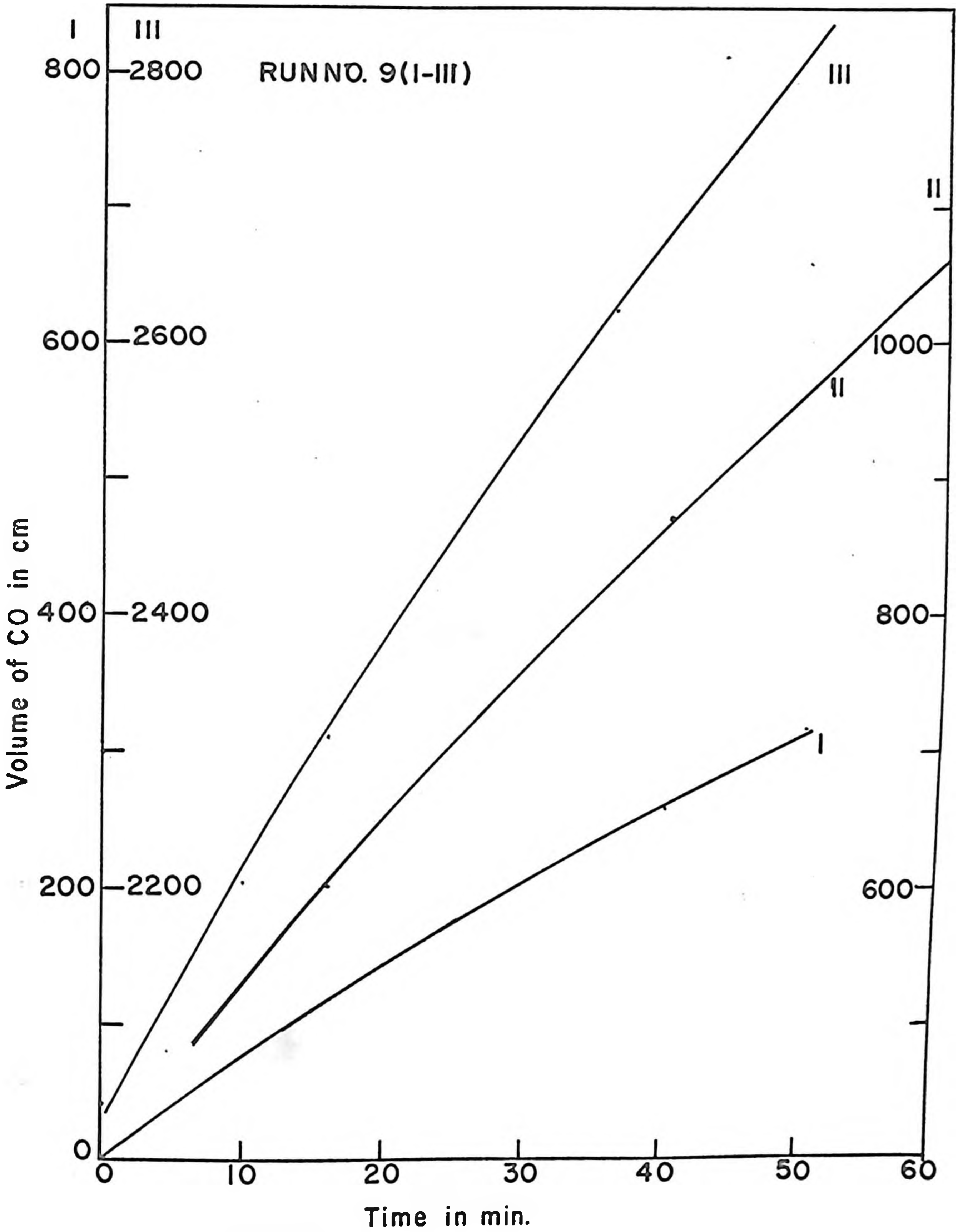

Figure 10 Rate Curves

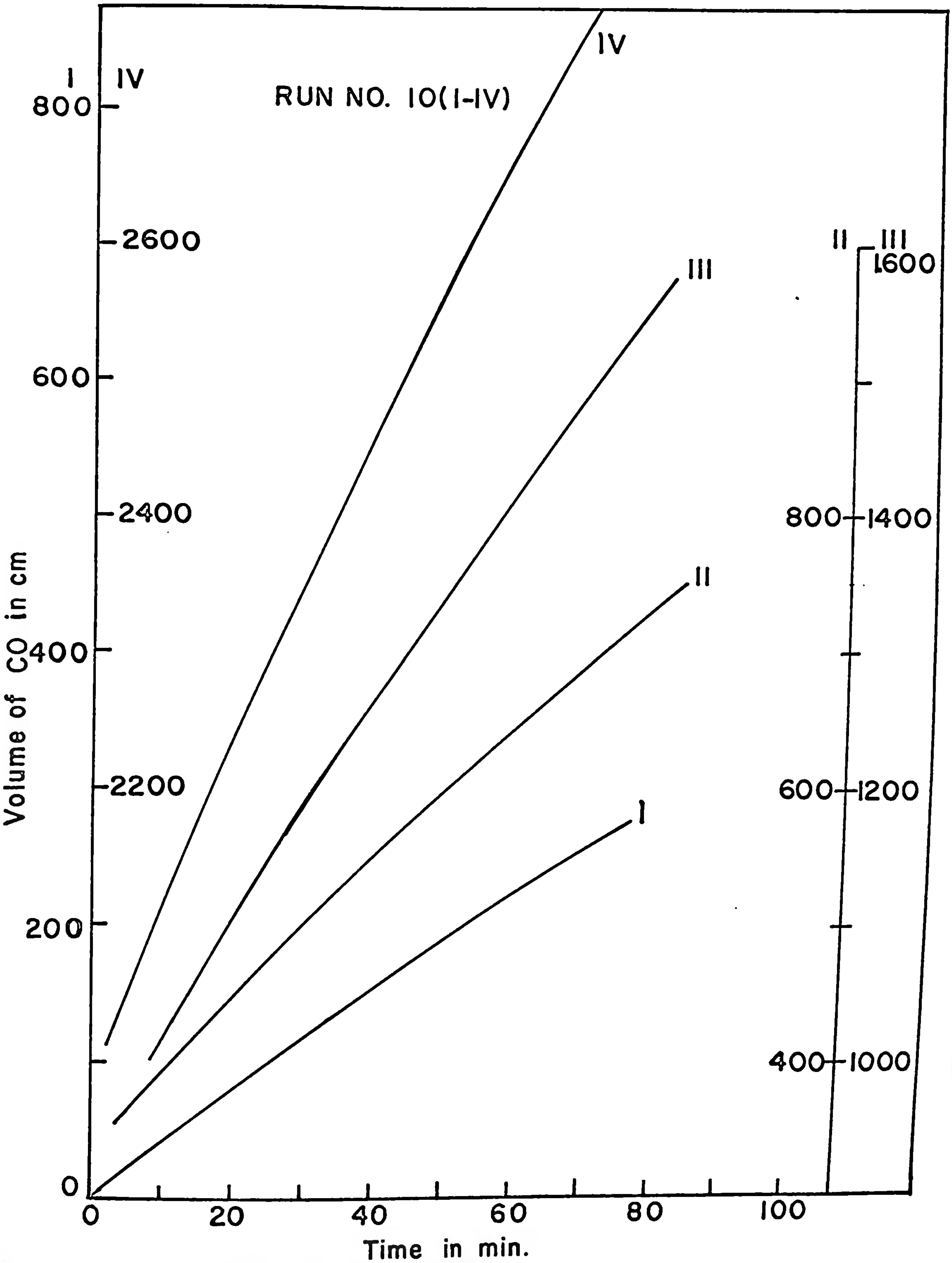

Figure II Rate Curves

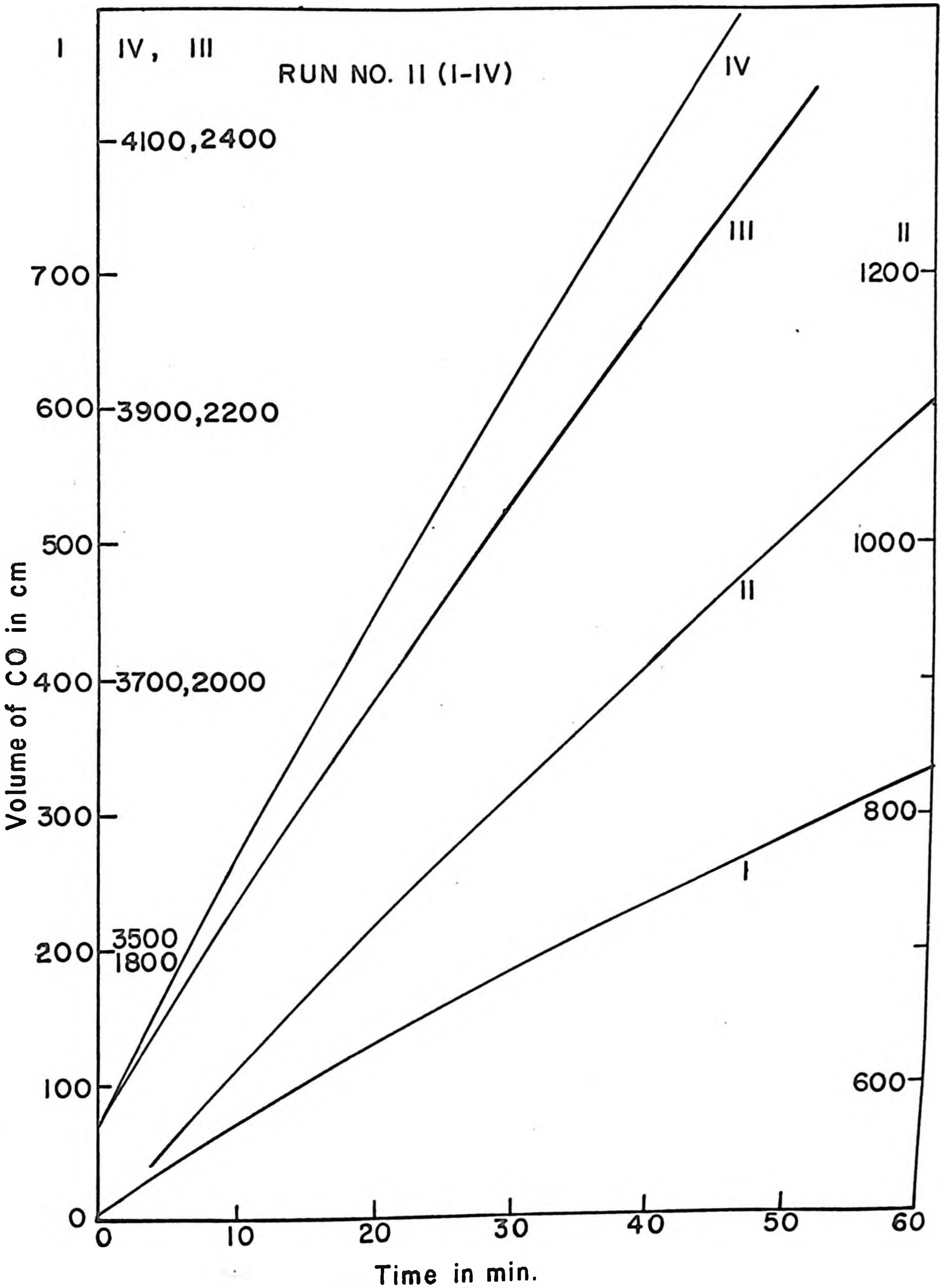

Figure 12 Rate Curves

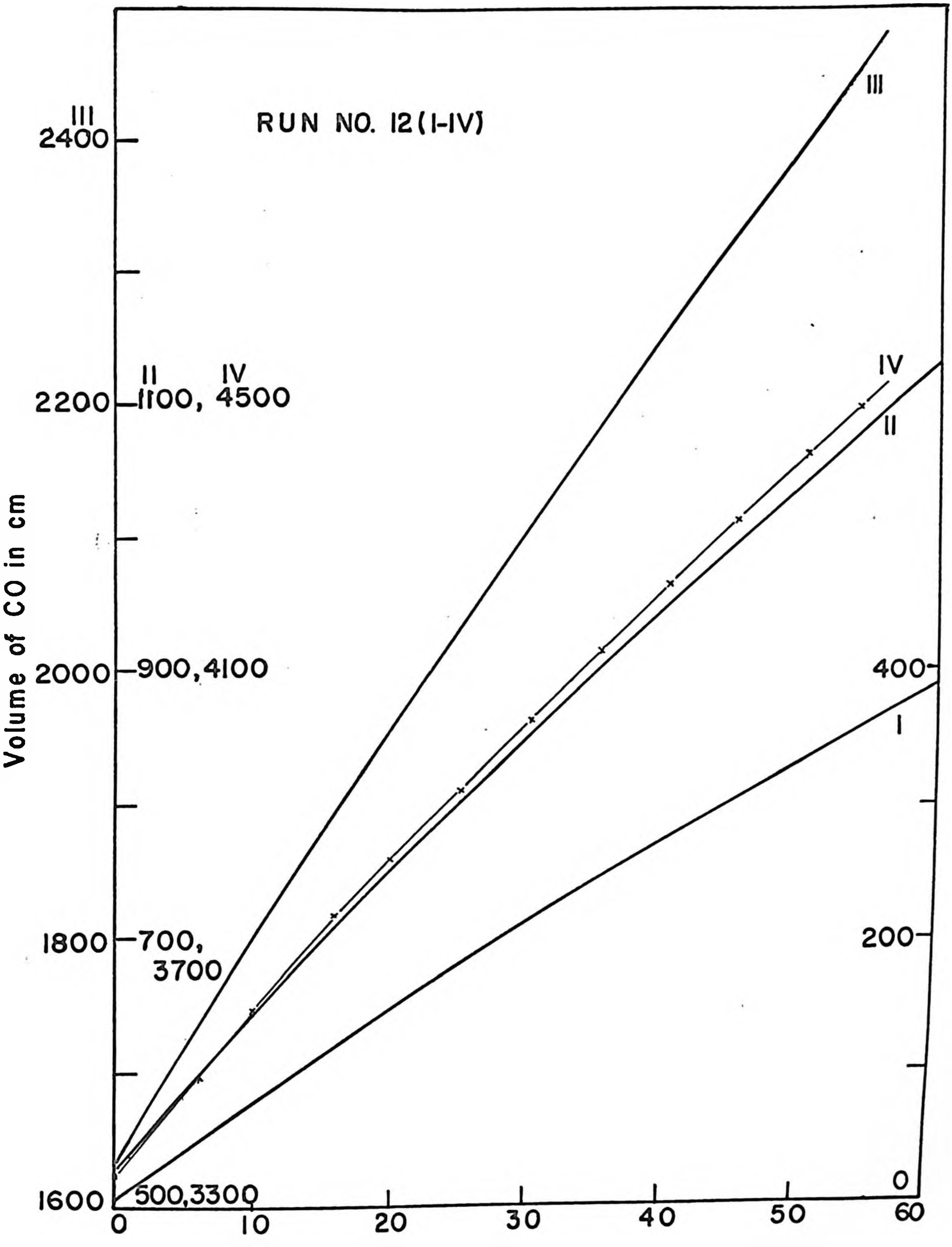

Figure 13 Rate Curves

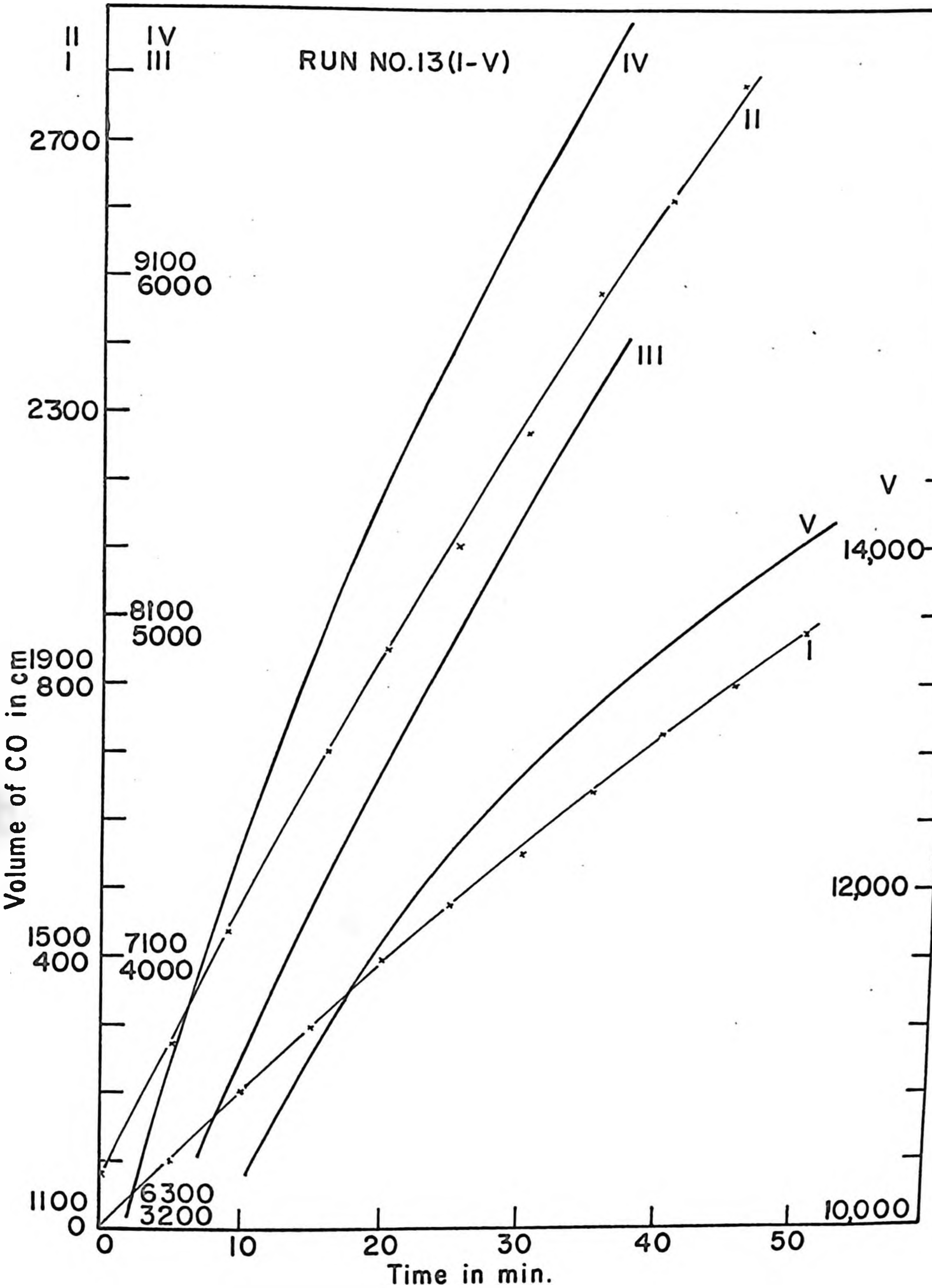

Figure 14 Rate Curves

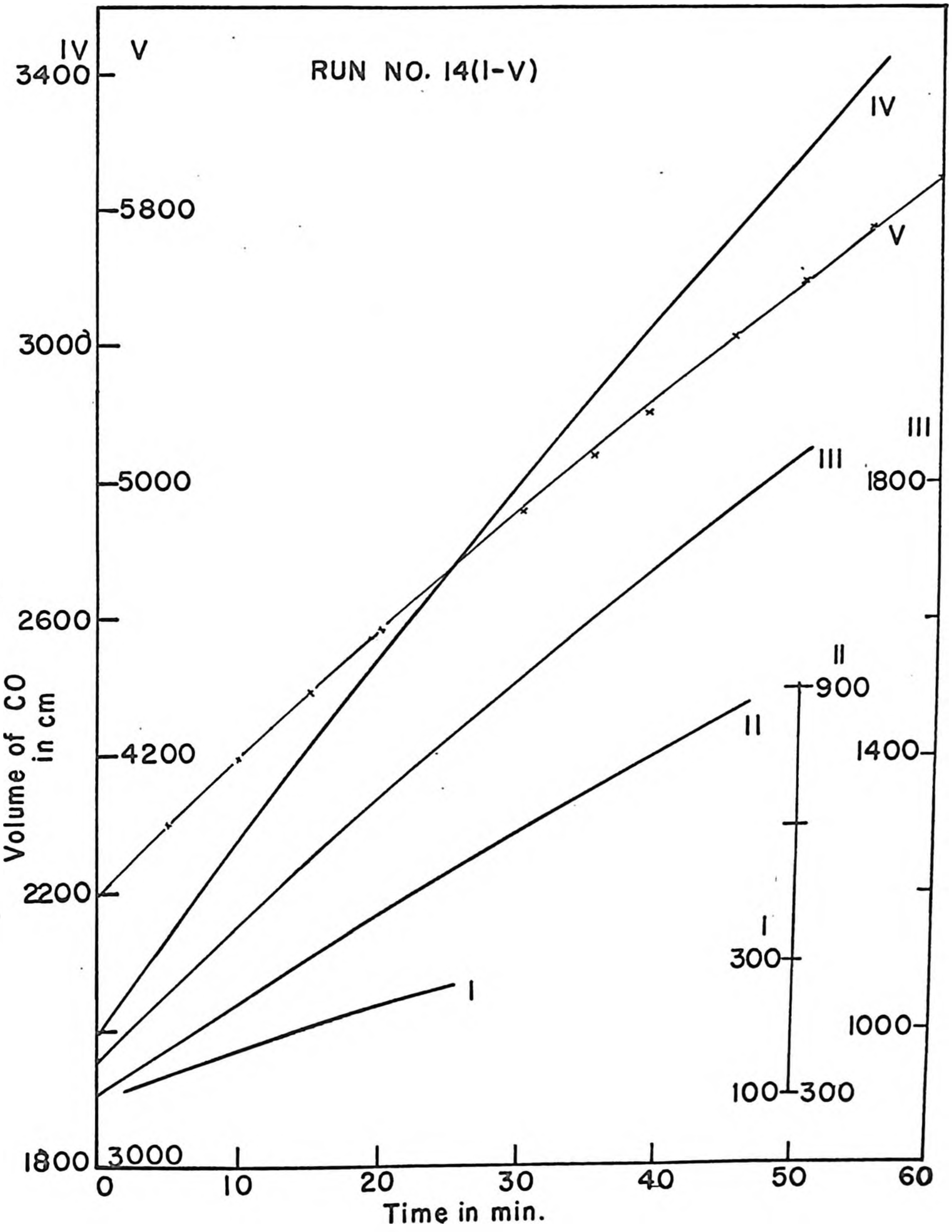

Figure 15 Rate Curves

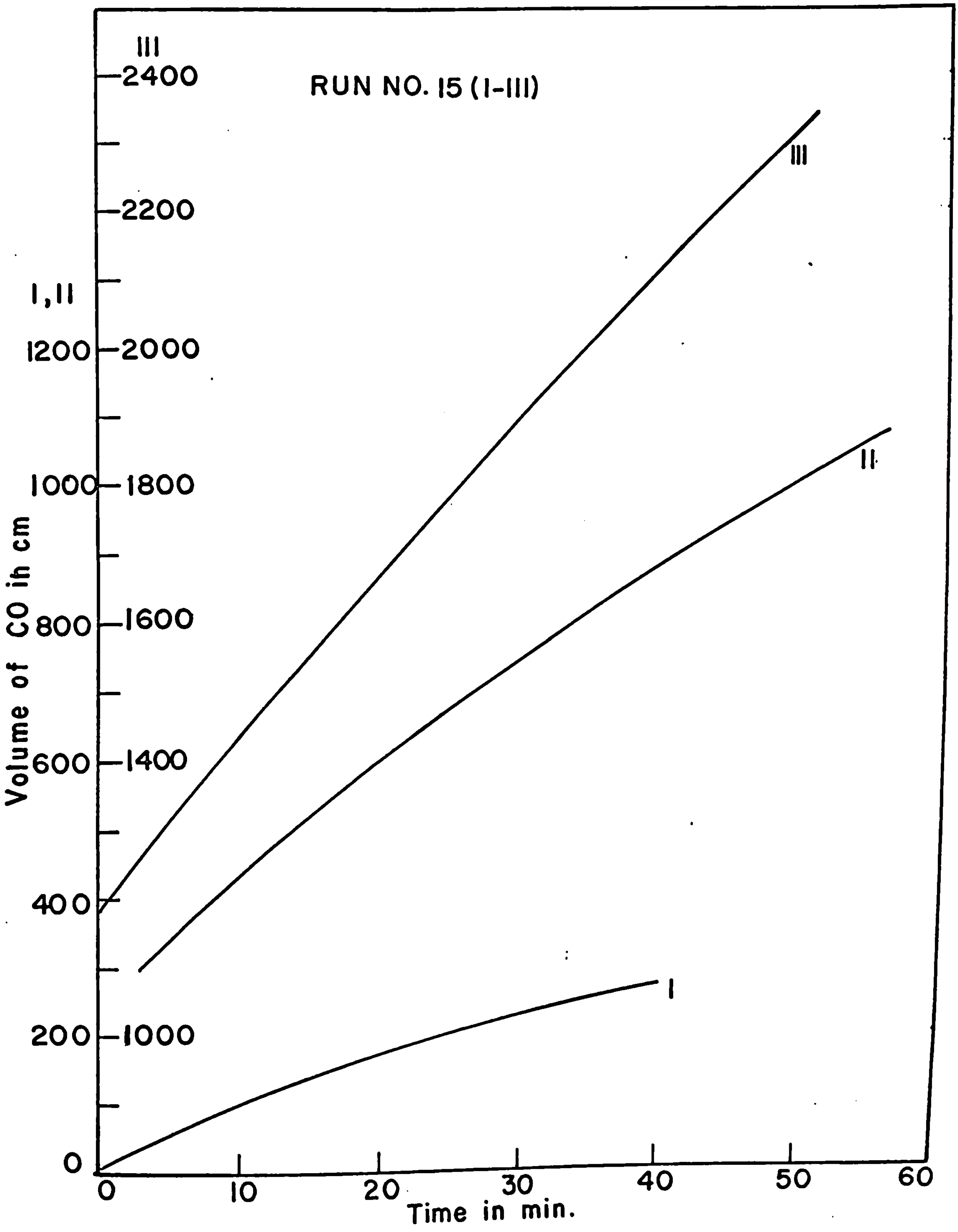

Figure 16(a) Rate Curves

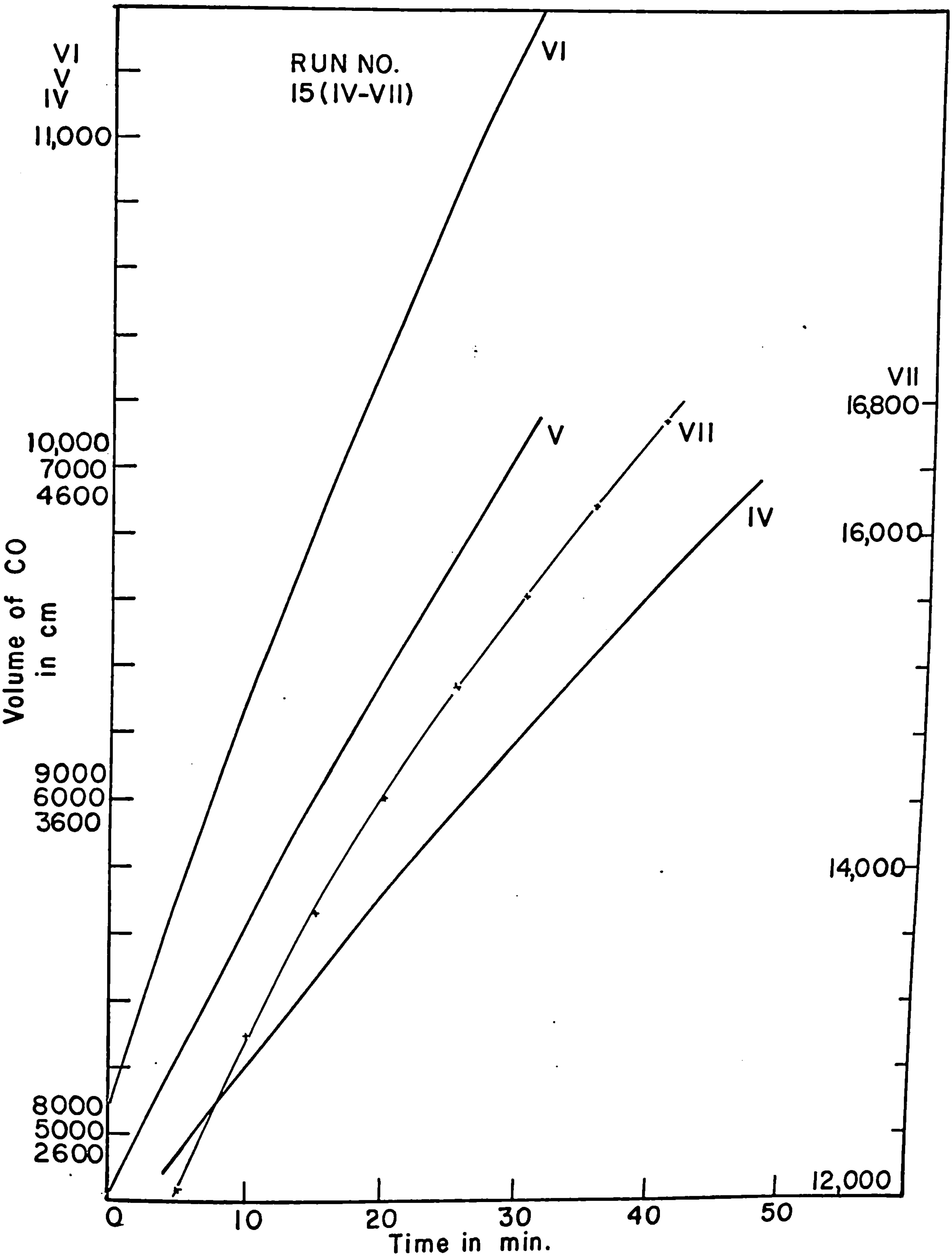

Figure 16(b) Rate Curves

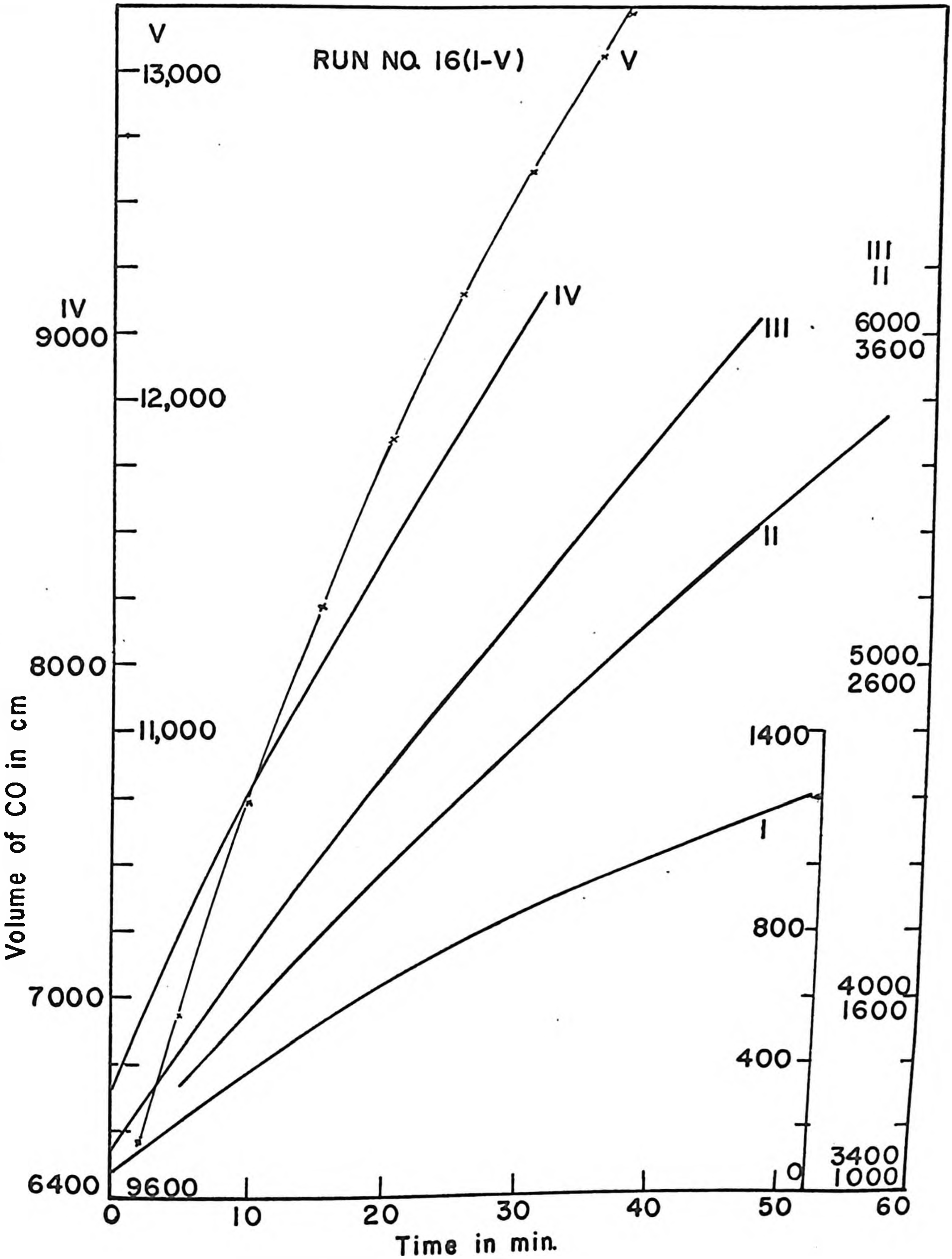

Figure 17 Rate Curves

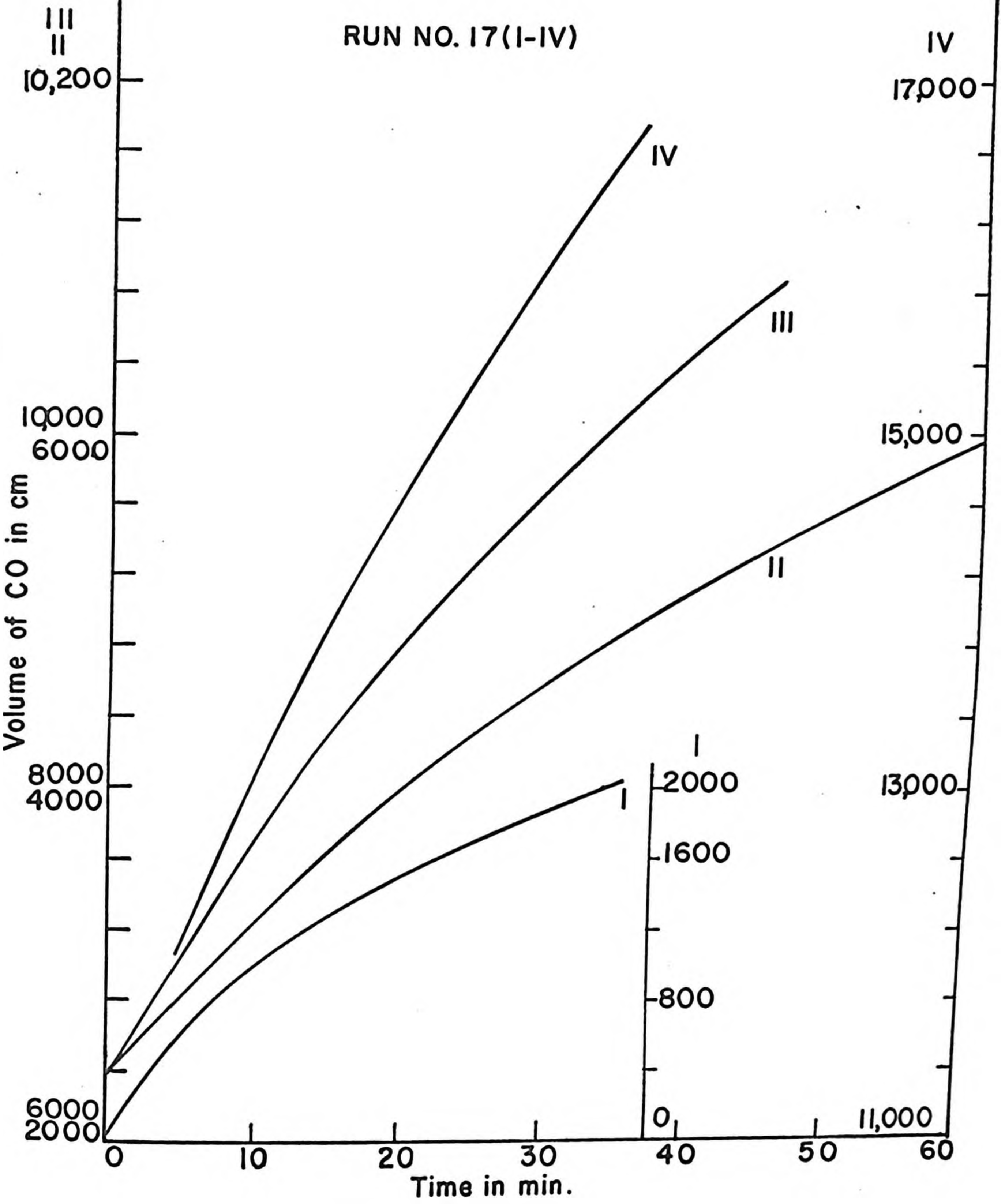

Figure 18 Rate Curves

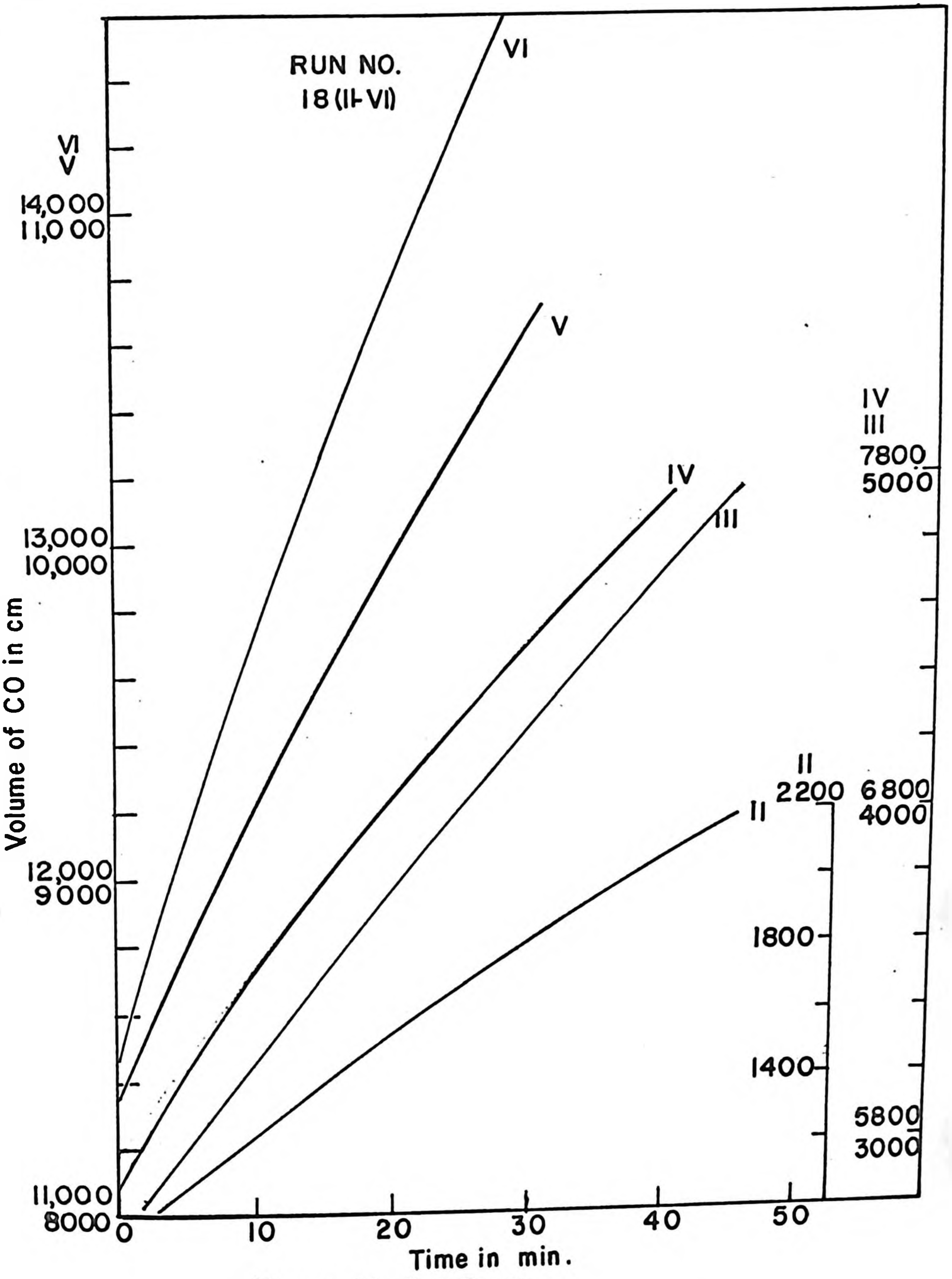

Figure 19 Rate Curves

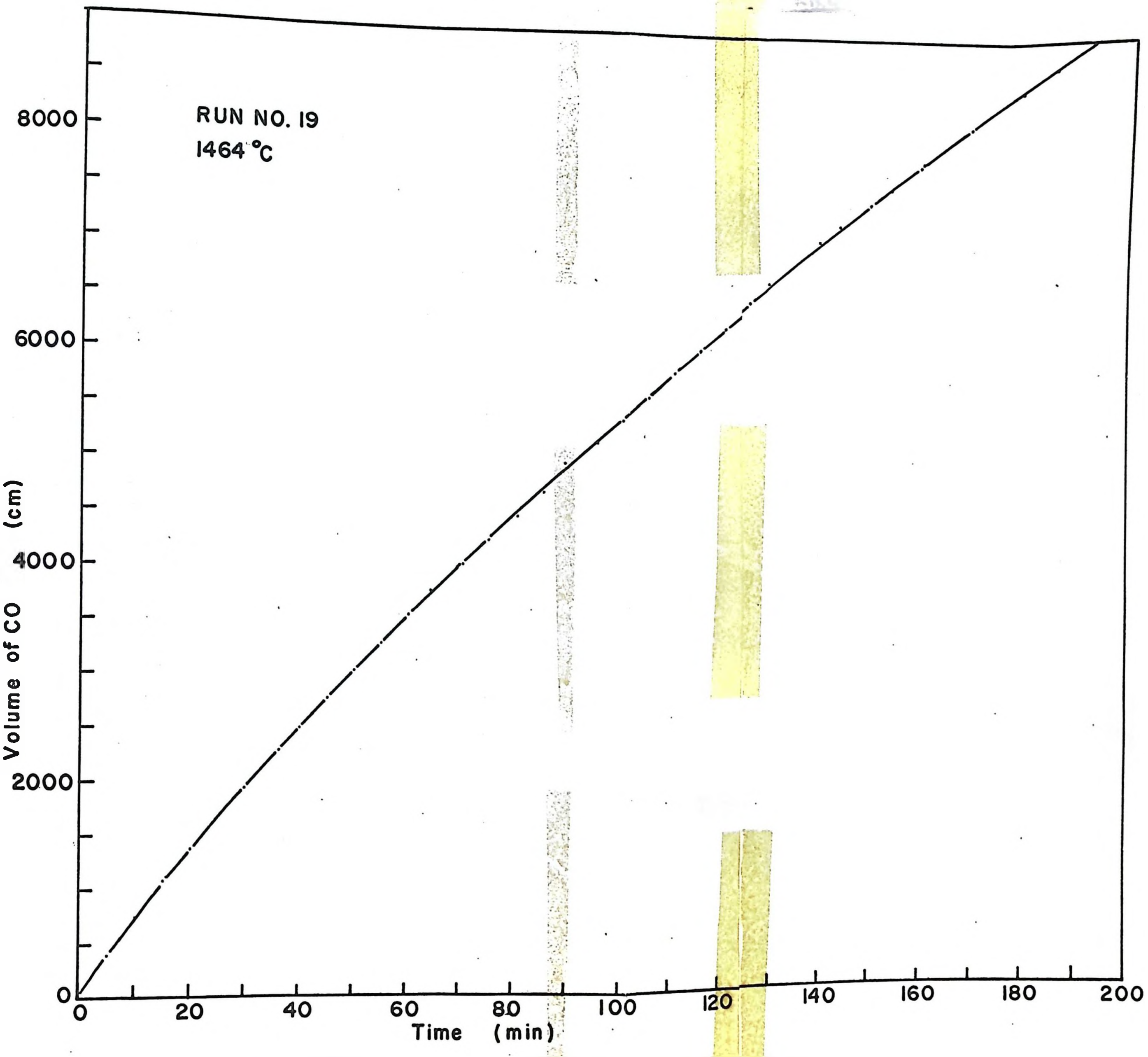

Figure 20 Rate Curves

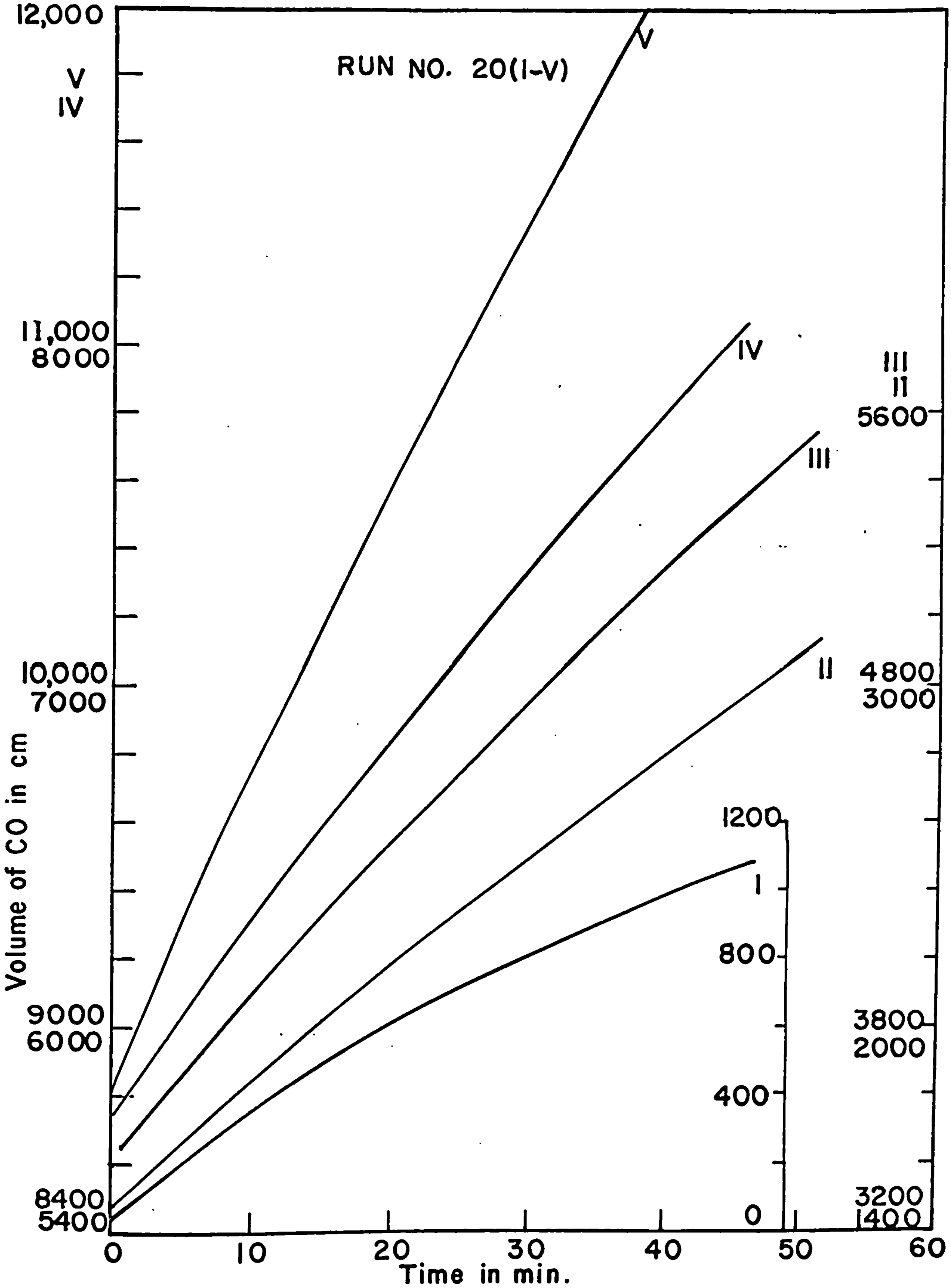

Figure 21 Rate Curves

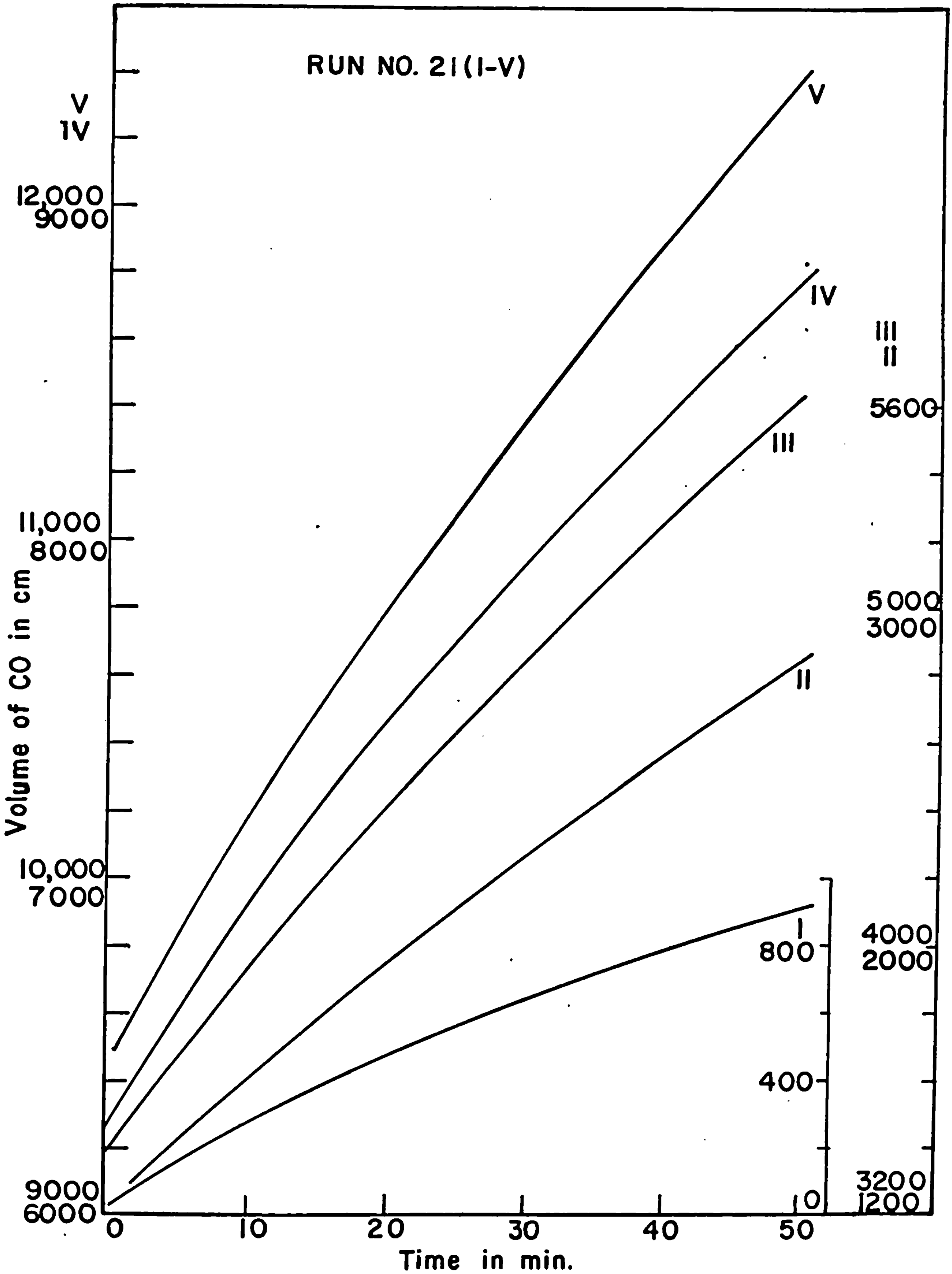

Figure 22 Rate Curves

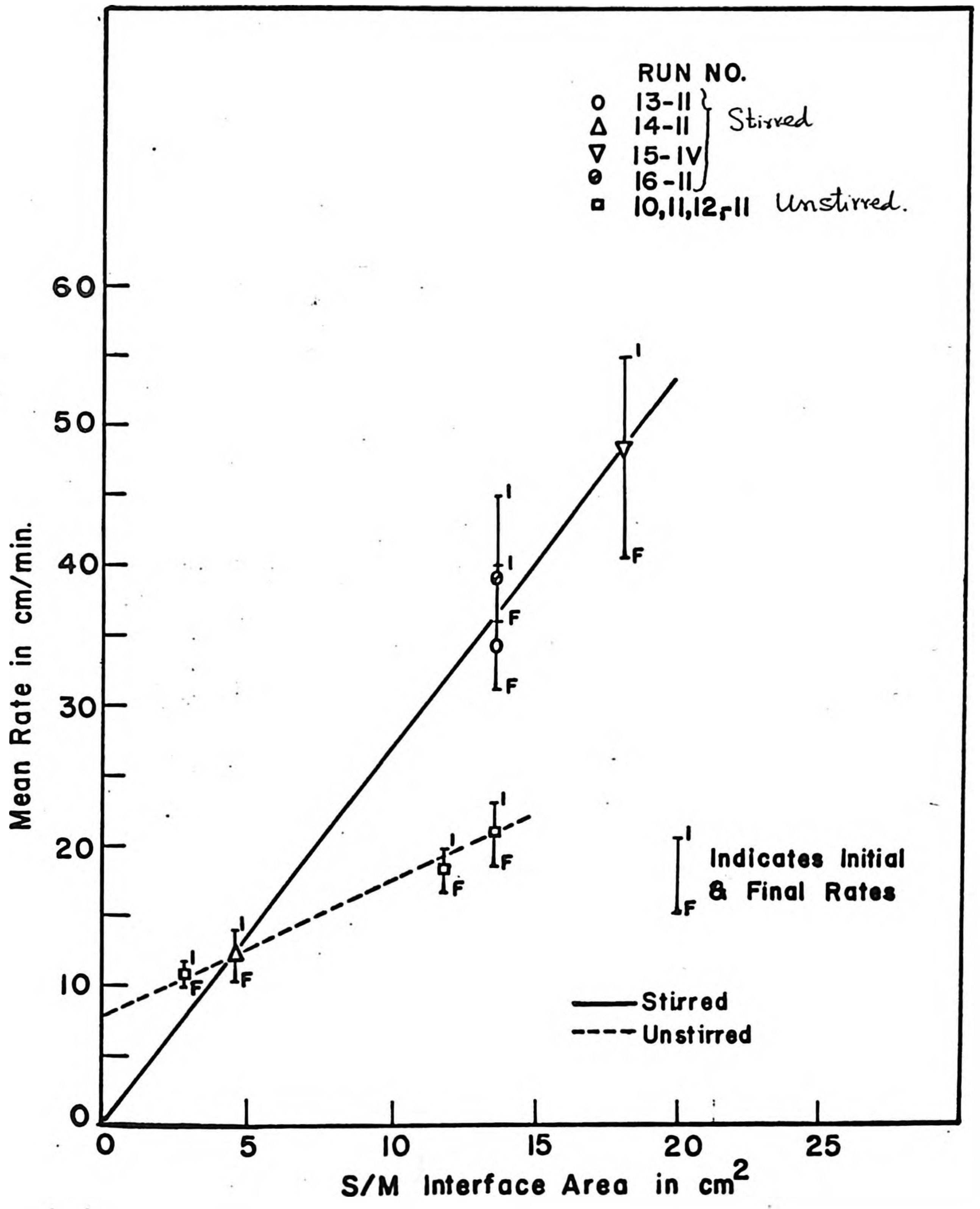

Figure 23 Rate-Area Plot

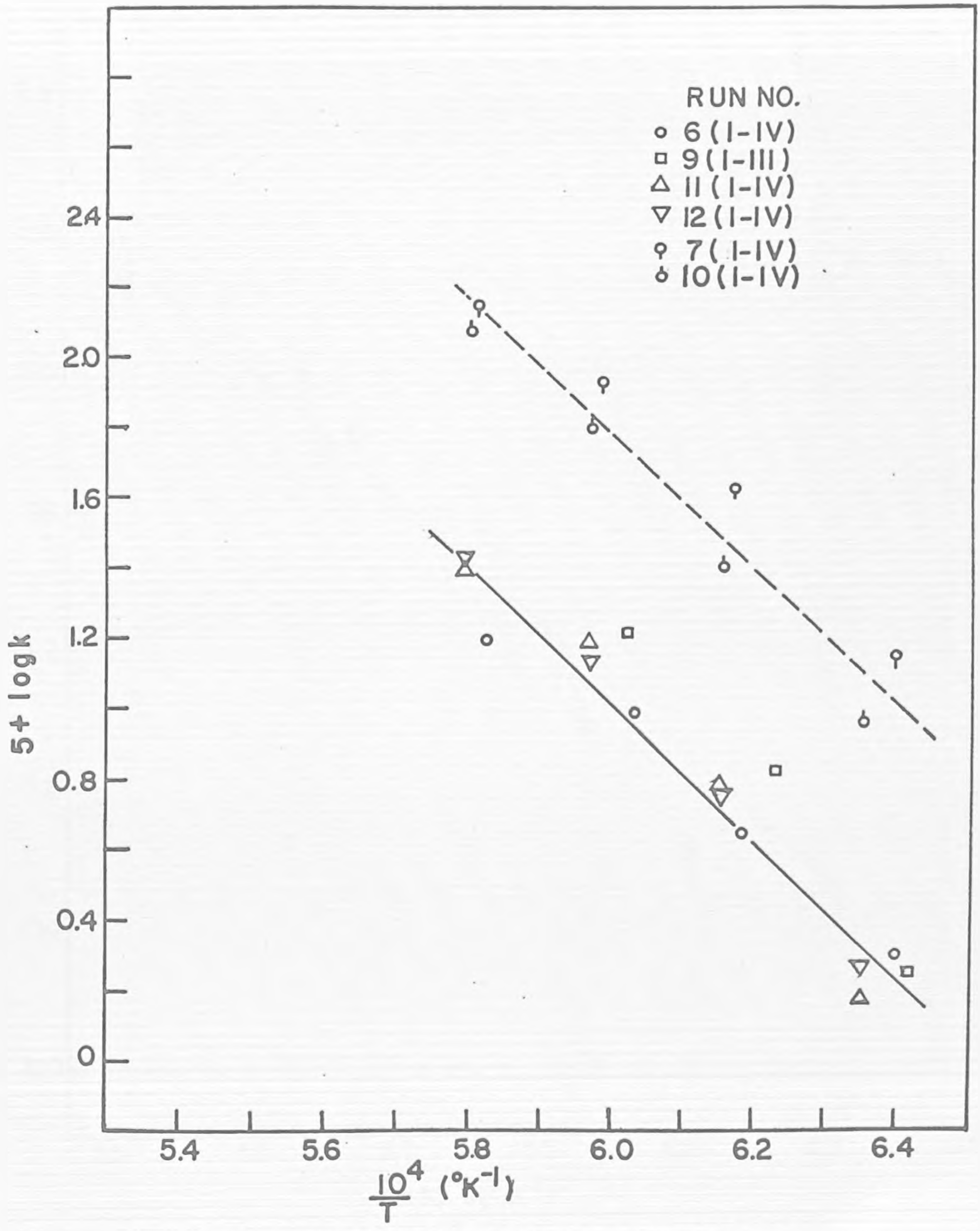

Figure 24 Specific Rate Constant vs. Temperature

(Unstirred Melts)

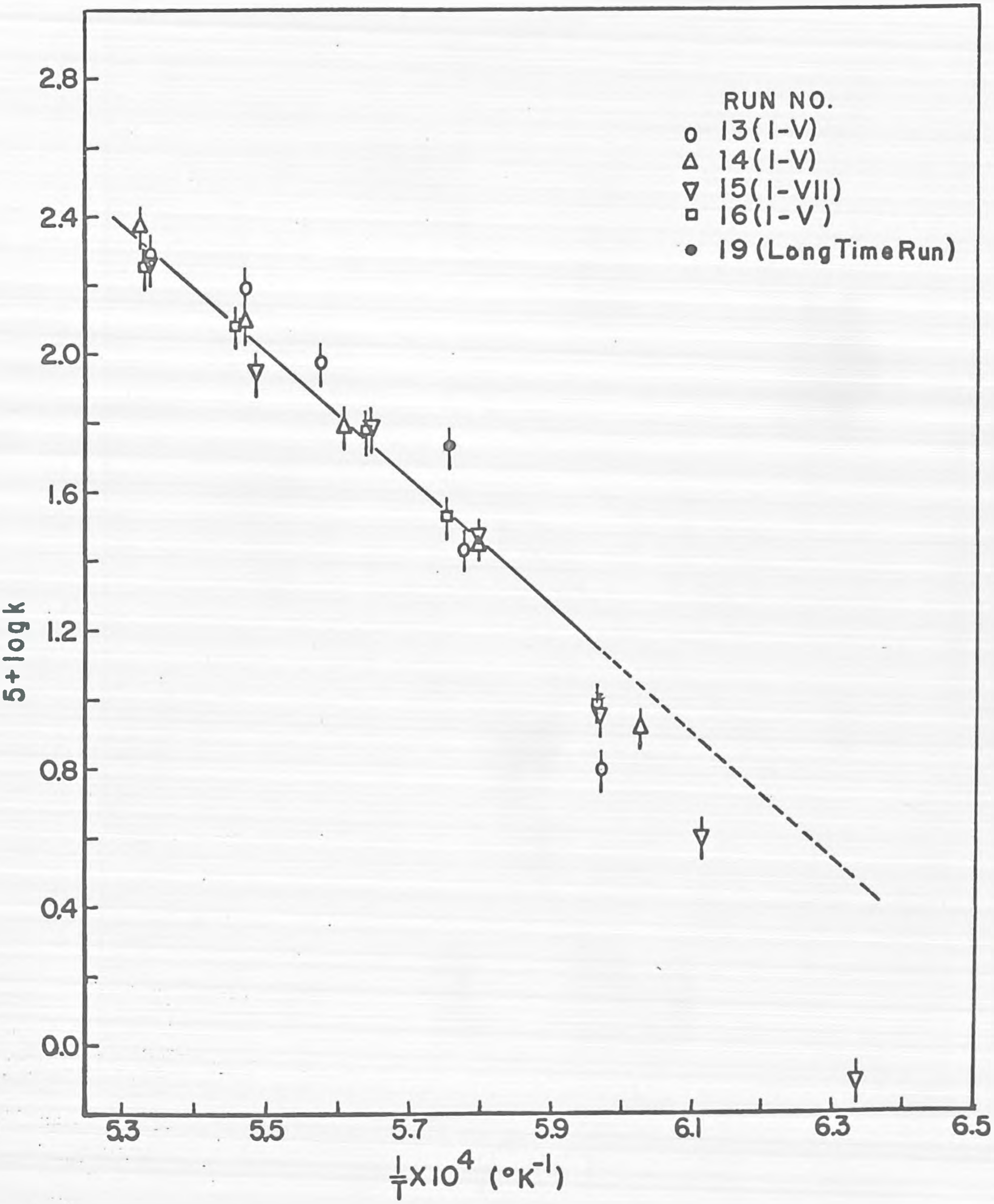

Figure 25 Specific Rate Constant vs. Temperature

(Stirred Melts)

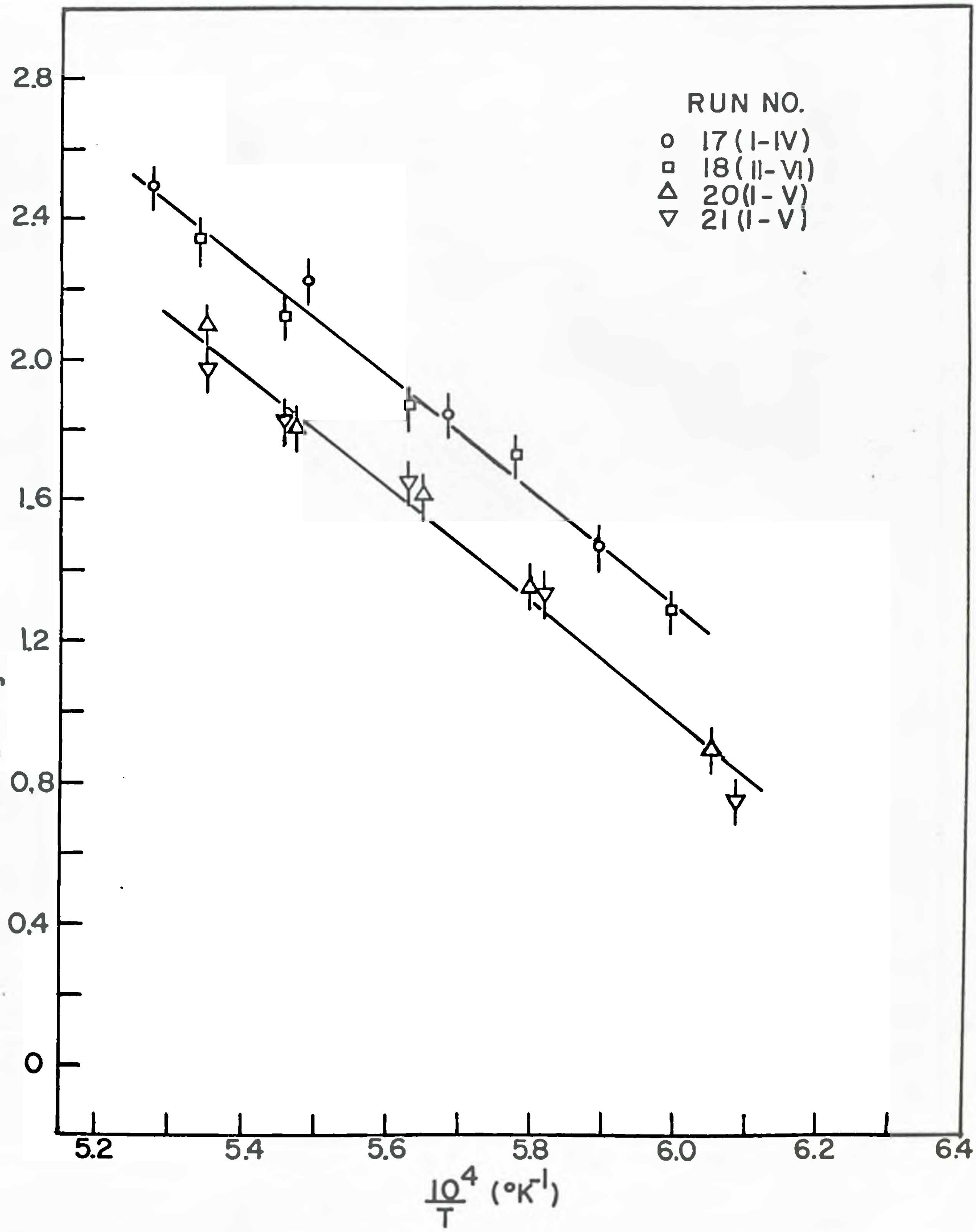

Figure 26 Specific Rate Constant vs Temperature (Carbon Saturated Melts)

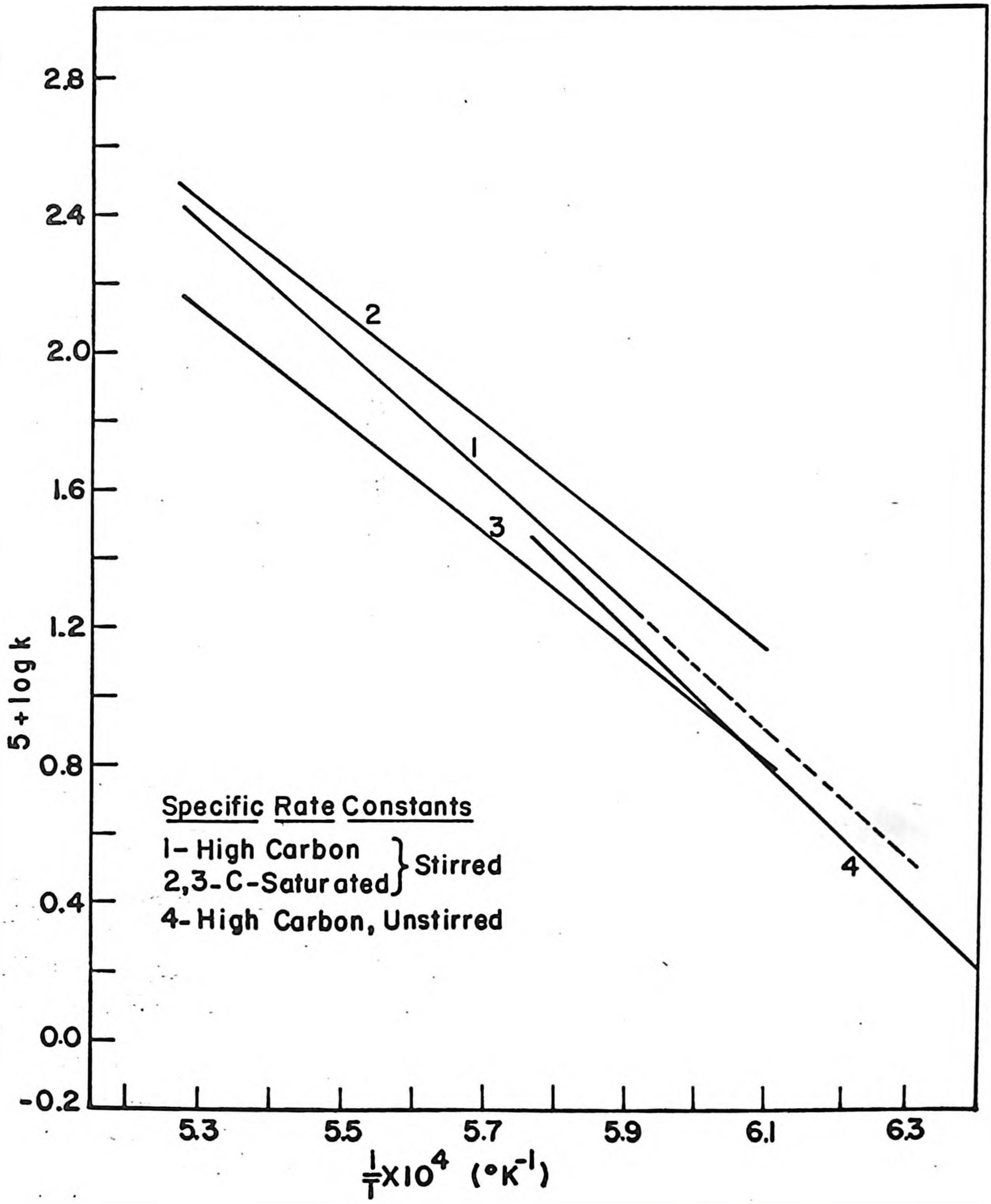

Figure 27 Specific Rate Constant vs. Temperature

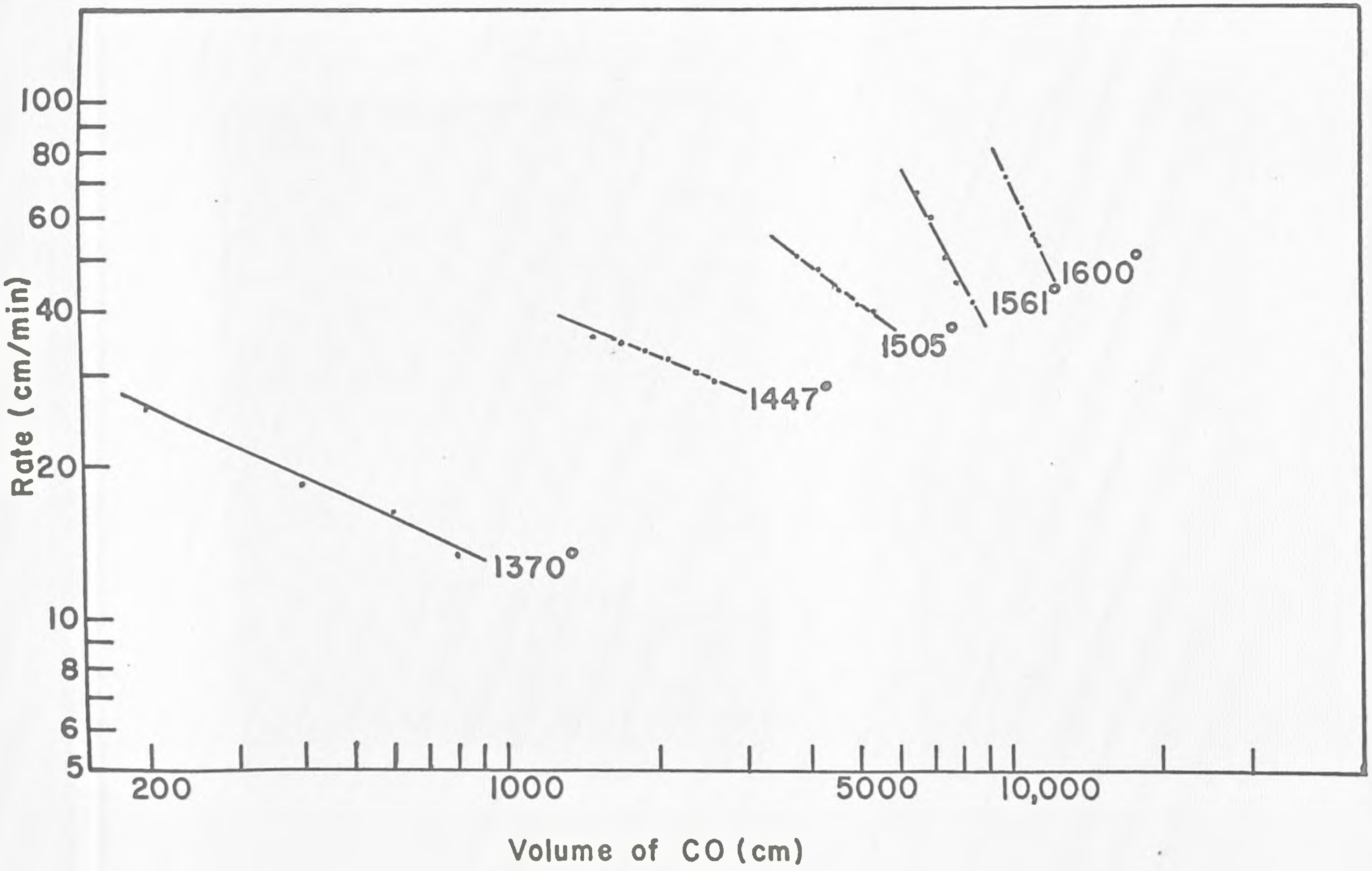

Figure 28 Rate vs Volume of CO Plot

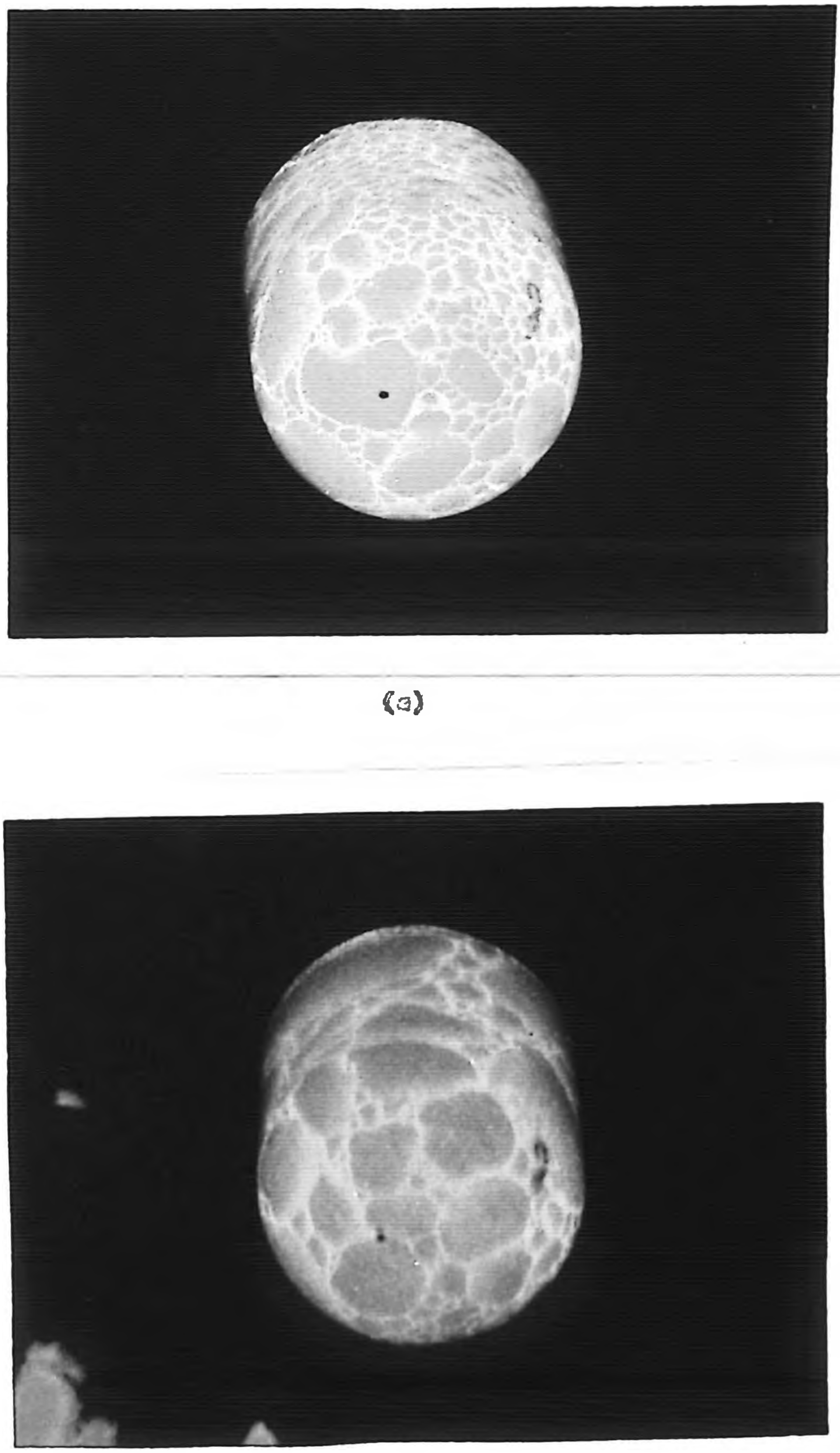

(a)

(b)

Figure 29. Photographs showing CO Bubbles on the Silica Crucible

Figure 30. Movie Photographs of CO Bubbles

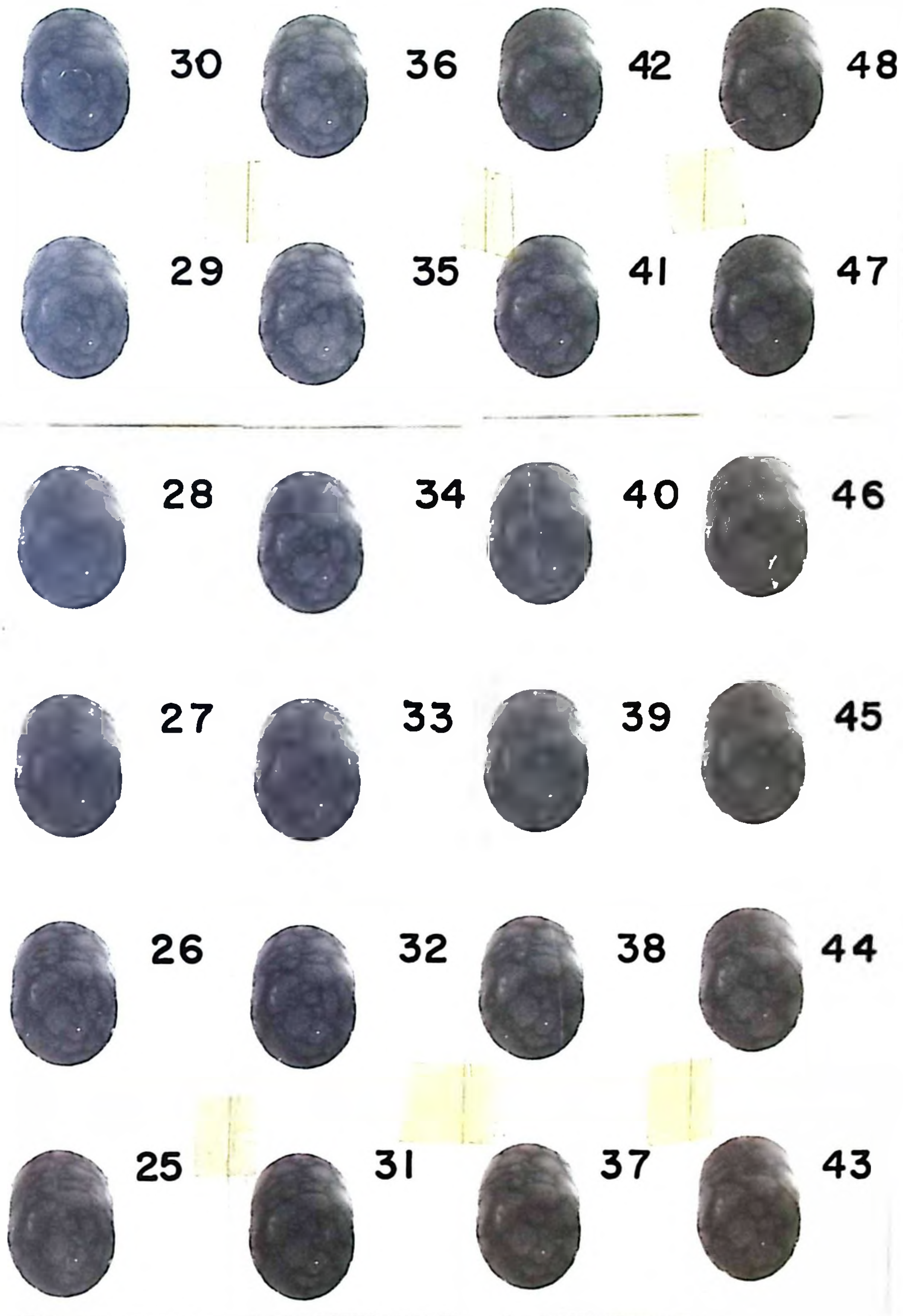

Figure 30 (continued)

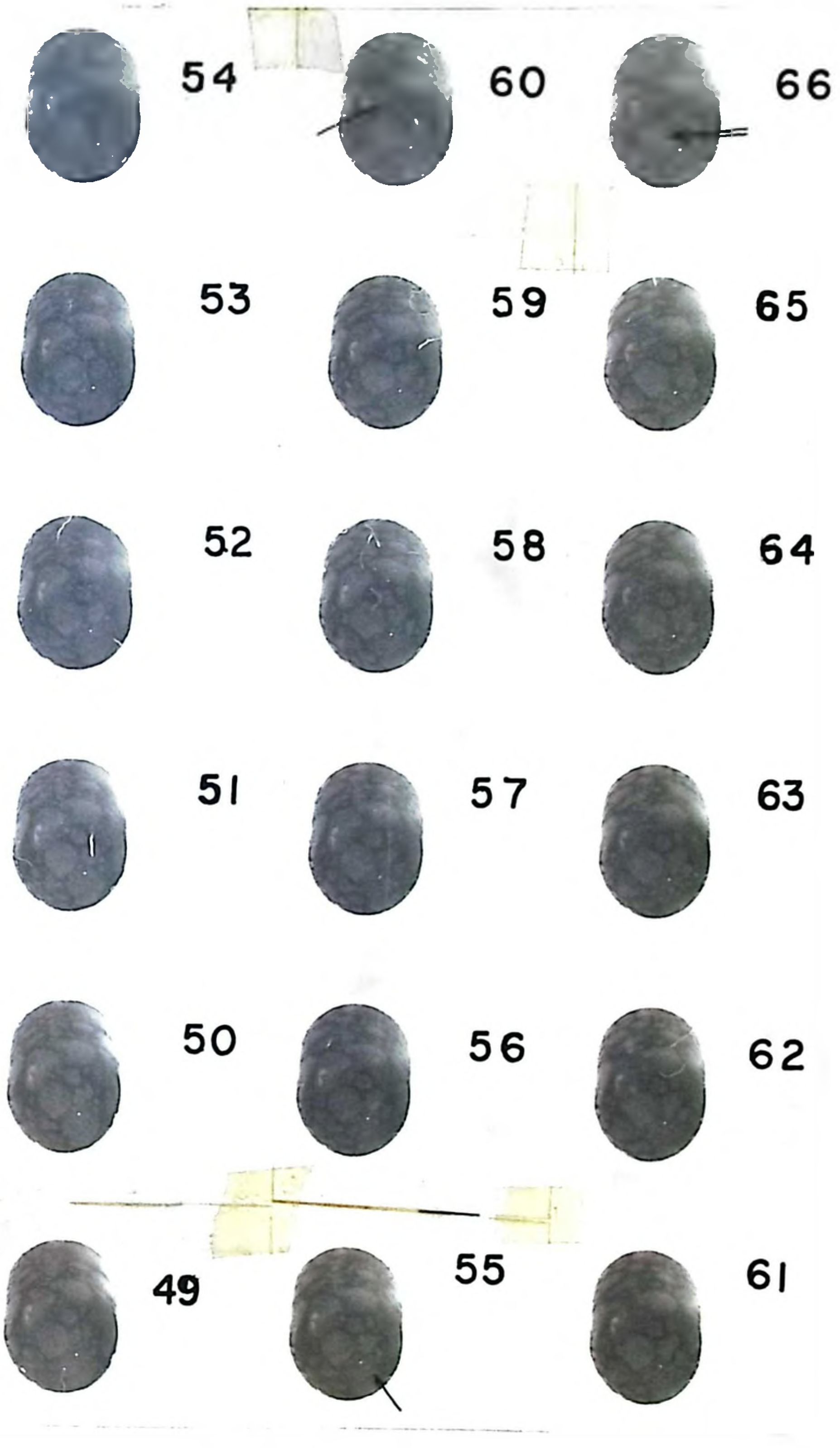

Figure 30 (continued)